

# Impacts of Ionospheric Ions on Magnetic Reconnection and Earth's Magnetosphere Dynamics

S. Toledo-Redondo, M. André, N. Aunai, C. Chappell, J. Dargent, S. Fuselier, A. Glocer, D. Graham, S. Haaland, M. Hesse, et al.

▶ **To cite this version:**

S. Toledo-Redondo, M. André, N. Aunai, C. Chappell, J. Dargent, et al.. Impacts of Ionospheric Ions on Magnetic Reconnection and Earth's Magnetosphere Dynamics. Reviews of Geophysics, 2021, 59 (3), 10.1029/2020RG000707 . hal-03841344

**HAL Id: hal-03841344**
**https://cnrs.hal.science/hal-03841344**

Submitted on 7 Nov 2022

**HAL** is a multi-disciplinary open access archive for the deposit and dissemination of scientific research documents, whether they are published or not. The documents may come from teaching and research institutions in France or abroad, or from public or private research centers.

L'archive ouverte pluridisciplinaire **HAL**, est destinée au dépôt et à la diffusion de documents scientifiques de niveau recherche, publiés ou non, émanant des établissements d'enseignement et de recherche français ou étrangers, des laboratoires publics ou privés.

Check for updates

AGU ADVANCING EARTH AND SPACE SCIENCE

Reviews of Geophysics



REVIEW ARTICLE
10.1029/2020RG000707

**Key Points:**

- Ionospheric plasma contributes a significant part of the magnetospheric density in the regions where magnetic reconnection is most frequent
- Cold and heavy ions of ionospheric origin reduce magnetic reconnection efficiency and modify energy conversion mechanisms
- The presence of ionospheric ions and their effects on reconnection and magnetospheric dynamics are enhanced during geomagnetic storms

**Correspondence to:**
S. Toledo-Redondo,
Sergio.Toledo@um.es

**Citation:**
Toledo-Redondo, S., André, M., Aunai, N., Chappell, C. R., Dargent, J., Fuselier, S. A., et al. (2021). Impacts of ionospheric ions on magnetic reconnection and Earth's magnetosphere dynamics. *Reviews of Geophysics*, *59*, e2020RG000707. https://doi.org/10.1029/2020RG000707

Received 23 DEC 2020
Accepted 26 MAY 2021

© 2021. The Authors.
This is an open access article under the terms of the Creative Commons Attribution License, which permits use, distribution and reproduction in any medium, provided the original work is properly cited.

# Impacts of Ionospheric Ions on Magnetic Reconnection and Earth's Magnetosphere Dynamics

**S. Toledo-Redondo[1,2], M. André[3], N. Aunai[4], C. R. Chappell[5], J. Dargent[6], S. A. Fuselier[7,8], A. Glocer[9], D. B. Graham[3], S. Haaland[10,11,12], M. Hesse[13], L. M. Kistler[14], B. Lavraud[2,15], W. Li[16], T. E. Moore[8], P. Tenfjord[11], and S. K. Vines[17]**

[1]Department of Electromagnetism and Electronics, University of Murcia, Murcia, Spain, [2]Institut de Recherche en Astrophysique et Planétologie, Université de Toulouse, CNRS, UPS, CNES, Toulouse, France, [3]Swedish Institute of Space Physics, Uppsala, Sweden, [4]Laboratoire de Physique des Plasmas, Paris, France, [5]Physics and Astronomy Department, Vanderbilt University, Nashville, TN, USA, [6]Physics Department E. Fermi, University of Pisa, Pisa, Italy, [7]Southwest Research Institute, San Antonio, TX, USA, [8]Department of Physics and Astronomy, University of Texas at San Antonio, San Antonio, TX, USA, [9]NASA Goddard Space Flight Center, Greenbelt, MD, USA, [10]Max-Planck Institute for Solar Systems Research, Göttingen, Germany, [11]Space Plasma Physics Group, University of Bergen, Bergen, Norway, [12]The University Centre in Svalbard, Longyearbyen, Norway, [13]Science Directorate, NASA Ames Research Center, Moffett Field, CA, USA, [14]Institute for the Study of Earth Oceans and Space, University of New Hampshire, Durham, NH, USA, [15]Laboratoire d'Astrophysique de Bordeaux, Univ. Bordeaux, CNRS, Pessac, France, [16]State Key Laboratory of Space Weather, National Space Science Center, Beijing, China, [17]Johns Hopkins University Applied Physics Laboratory, Laurel, MD, USA

**Abstract** Ionospheric ions (mainly $H^+$, $He^+$, and $O^+$) escape from the ionosphere and populate the Earth's magnetosphere. Their thermal energies are usually low when they first escape the ionosphere, typically a few electron volt to tens of electron volt, but they are energized in their journey through the magnetosphere. The ionospheric population is variable, and it makes significant contributions to the magnetospheric mass density in key regions where magnetic reconnection is at work. Solar wind—magnetosphere coupling occurs primarily via magnetic reconnection, a key plasma process that enables transfer of mass and energy into the near-Earth space environment. Reconnection leads to the triggering of magnetospheric storms, auroras, energetic particle precipitation and a host of other magnetospheric phenomena. Several works in the last decades have attempted to statistically quantify the amount of ionospheric plasma supplied to the magnetosphere, including the two key regions where magnetic reconnection occurs: the dayside magnetopause and the magnetotail. Recent in situ observations by the Magnetospheric Multiscale spacecraft and associated modeling have advanced our current understanding of how ionospheric ions alter the magnetic reconnection process, including its onset and efficiency. This article compiles the current understanding of the ionospheric plasma supply to the magnetosphere. It reviews both the quantification of these sources and their effects on the process of magnetic reconnection. It also provides a global description of how the ionospheric ion contribution modifies the way the solar wind couples to the Earth's magnetosphere and how these ions modify the global dynamics of the near-Earth space environment.

**Plain Language Summary** Above the neutral atmosphere, space is filled with charged particles, which are tied to the Earth's magnetic field. The particles come from two sources, the solar wind and the Earth's upper atmosphere. Most of the solar wind particles are deflected by the Earth´s magnetic field, but some can penetrate into near-Earth space. The ionized layer of the upper atmosphere is continuously ejecting particles into space, which have low energies and are difficult to measure. We investigate the relative importance of the two charged particle sources for the dynamics of plasma processes in near-Earth space. In particular, we consider the effects of these sources in magnetic reconnection. Magnetic reconnection allows initially separated plasma regions to become magnetically connected and mix, and converts magnetic energy to kinetic energy of charged particles. Magnetic reconnection is the main driver of geomagnetic activity in the near-Earth space, and is responsible for the release of energy that drives a variety of space weather effects. We highlight the fact that plasma from the ionized upper atmosphere contributes a significant part of the density in the key regions where magnetic reconnection is at work, and that this contribution is larger when the geomagnetic activity is high.



19449208, 2021, 3, Downloaded from https://agupubs.onlinelibrary.wiley.com/doi/10.1029/2020RG000707 by Cochrane France, Wiley Online Library on [07/11/2022]. See the Terms and Conditions (https://onlinelibrary.wiley.com/terms-and-conditions) on Wiley Online Library for rules of use; OA articles are governed by the applicable Creative Commons License

19449208, 2021, 3, Downloaded from https://agupubs.onlinelibrary.wiley.com/doi/10.1029/2020RG000707 by Cochrane France, Wiley Online Library on [07/11/2022]. See the Terms and Conditions (https://onlinelibrary.wiley.com/terms-and-conditions) on Wiley Online Library for rules of use; OA articles are governed by the applicable Creative Commons License

## 1. Introduction

Magnetospheric plasma composition and circulation, as well as the sources and sinks of plasma populations in the magnetosphere, have been extensively studied since the beginning of the space era in the late 1950s. Magnetospheric ions of ionospheric origin, or ionospheric-originating ions, however, are difficult to characterize. Their initial low thermal and kinetic energies prevent them from reaching the spacecraft, which are usually positively charged in the magnetosphere, and therefore they remain invisible until energized, usually far away from the ionosphere. Nevertheless, using various direct and indirect techniques, past and recent studies have demonstrated that these particles are important to the dynamics of the Earth's magnetosphere. These particles, $H^+$, along with heavy ions species such as $O^+$ and $He^+$, often dominate the magnetospheric mass-density. In the past years, several review works have addressed the current understanding of these ionospheric ions in the Earth's magnetosphere. Kronberg et al. (2014) reviewed the production and circulation of ionospheric heavy ions in the nightside and inner magnetosphere, highlighting their consequences for the plasma sheet, ring current and radiation belts. Chappell (2015) provided a historical review on the sources and transport of ionospheric ions toward the magnetosphere, highlighting their main role as a magnetospheric plasma source together with the solar wind. Welling et al. (2015) undertook a thorough review of the Earth's magnetosphere plasma sources, transport and losses. Kistler (2016) analyzed the effects of $O^+$ coming from the ionosphere in magnetotail dynamics. Yamauchi (2019) reviewed the terrestrial ion escape and circulation in space using knowledge gained from the Cluster space mission. Finally, Yau et al. (2020) and André et al. (2020) briefly reviewed the escape of ionospheric ions in the polar regions and their impact on magnetic reconnection.

In this work, we discuss the implications of ionospheric ions for magnetic reconnection occurring in the magnetosphere. We focus on the two main regions where magnetic reconnection plays a major role: the dayside magnetopause and the Earth's magnetotail. In Section 2 we present a summary of the plasma sources and the transport mechanisms that are responsible for bringing ionospheric plasma to these outer magnetospheric regions where magnetic reconnection operates. Section 2 is written at introductory level and it is of particular interest for early career scientists and scientists coming from different disciplines. Space physicists may opt to go directly to Section 3, which presents a review of observational works that attempted to quantify the amount of ionospheric ions that are present near the reconnecting regions. Section 4 focuses on how these changes in magnetospheric composition and plasma properties affect magnetic reconnection, both on the dayside and at the tail. In this section, we review the most relevant numerical simulations and spacecraft observations of magnetic reconnection. In Section 5, we discuss the implications of having the ionospheric source of plasma in the magnetosphere, and compile a list of open questions on the subject. Finally, in Section 6, we summarize and highlight the main points of this review.

## 2. Sources and Transport of Ionospheric Ions to the Main Reconnection Regions

### 2.1. The Ionosphere as a Source of Plasma

Ionization of the upper atmosphere (Figure 1) occurs through photoionization by solar EUV emission and other radiation, and sometimes also by precipitating charged particles, such as accelerated electrons that generate auroras. At the altitudes where collisions with neutrals in the atmosphere dominate, the energy of charged particles in the ionosphere is of the order 0.1 eV (Kelley, 2009).

At higher altitudes (a few hundred kilometers), the density is lower and the plasma becomes essentially collisionless. Here low-mass electrons can move to even higher altitudes and create an ambipolar electric field, pulling positive ions upward (cyan arrows in Figure 1). The ambipolar electric field makes the ions flow upward along the geomagnetic field. While the heavier ions, $O^+$, $N^+$, $NO^+$ typically do not reach escape velocity and return to the ionosphere because of the gravitational force, light ions, $H^+$ and $He^+$ can escape upward into the magnetosphere and have been called the “classical” polar wind (Axford, 1968; Banks & Holzer, 1968; Banks, et al., 1971; Schunk et al., 1975). The polar wind occurs from midlatitudes (above ~50° latitude) all the way to the magnetic poles. Therefore, it supplies plasma to the plasmasphere, the outer magnetosphere and the plasma sheet (see Figure 1). Ionospheric ions, including heavy ions, are also energized by other mechanisms than an ambipolar electric field, such as waves, which can also make them escape

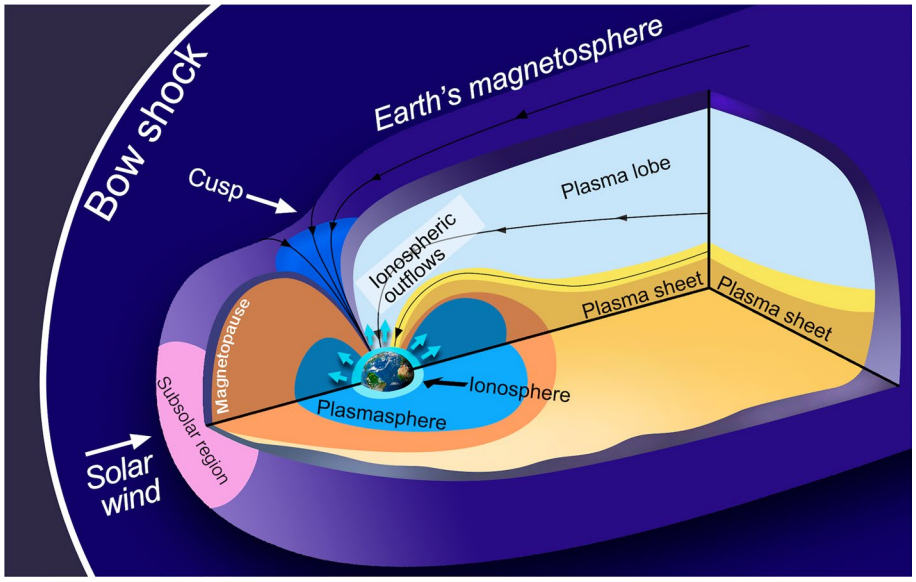



**Figure 1.** Main regions of the Earth's magnetosphere. Ionospheric ions are continuously escaping along magnetic field lines, and end up in different magnetospheric regions depending on their initial geomagnetic location. Credit: J. M. Domínguez, adapted from Pollock et al. (2003).

upward into the magnetosphere, constituting what is often called "nonclassical" polar wind or energetic polar wind. In contrast to the escape of a few neutral particles in the upper atmosphere, a major part of the mass outflow from the Earth's atmosphere is in the form of charged particles.

What happens to each individual ion depends strongly on its initial latitude and local time, and the magnetospheric conditions at the time (e.g., Huddleston et al., 2005). Due to the configuration of the Earth's magnetic field, it is convenient to separately discuss high latitudes and mid latitudes, that is, roughly above or below the auroral zone (see Figure 2). At high latitudes (Section 2.1.1), magnetic field lines are open, that is, connected to the interplanetary magnetic field (IMF) originating from the Sun. The source region, that is, the location where the ions leave the ionosphere, and transport along the continuously changing open magnetic field, determines where the ions go, how much they get energized, and where they contribute to the magnetospheric particle populations. At midlatitudes (Section 2.1.2), where the geomagnetic field lines close back to Earth, the ionospheric ions accumulate and form the plasmasphere, see Figure 1.

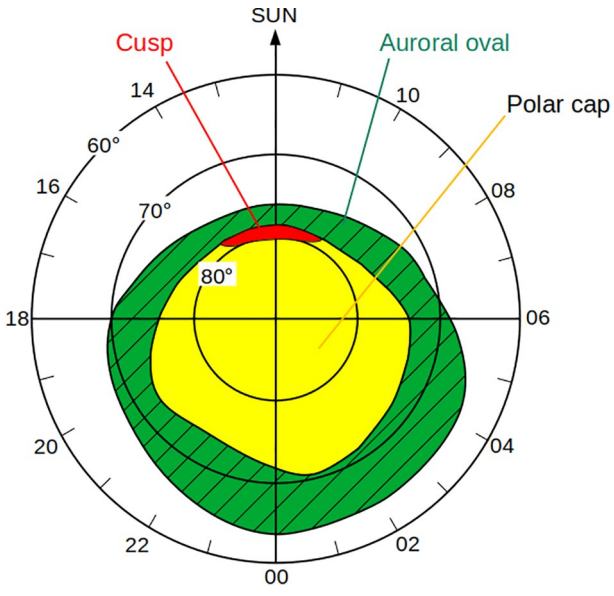



**Figure 2.** Top view of the Earth's ionosphere in geomagnetic latitude and local magnetic time coordinates, indicating typical locations of the auroral oval (green color), the cusp (red) and the polar cap (yellow). Poleward of the auroral oval, magnetic field lines are open, with the polar cap mapping to the tail lobes, and the cusp mapping to the dayside. Adapted from Akasofu (2015).

### 2.1.1. High-Latitude Outflow

In the polar cap region, where magnetic field lines are open and connected to the IMF (see Figures 1 and 2), an ambipolar electric field starts the upflow of ions, above the H-O crossover height (~800–1,200 km). This upflow is the basis for the aforementioned "classical" polar wind at high latitudes (Axford, 1968; Banks & Holzer, 1968). These ions can be further energized by centrifugal acceleration at higher altitudes, due to the drift caused by a large-scale convection electric field in the curved geomagnetic field (e.g., Cladis & Francis, 1992; Cladis et al., 2000; Huddleston et al., 2005; Nilsson et al., 2008, 2010). Waves and parallel electric fields in the auroral and cusp regions also energize the outflowing ions (e.g., André & Yau, 1997), and the mirror force provides parallel acceleration (e.g., Comfort, 1998). The ions are typically carried toward the magnetotail both by convection of magnetic field lines and the ion parallel motion along the magnetic field direction. The classical polar wind, or simply



19449208, 2021, 3, Downloaded from https://agupubs.onlinelibrary.wiley.com/doi/10.1029/2020RG000707 by Cochrane France, Wiley Online Library on [07/11/2022]. See the Terms and Conditions (https://onlinelibrary.wiley.com/terms-and-conditions) on Wiley Online Library for rules of use; OA articles are governed by the applicable Creative Commons License

19449208, 2021, 3, Downloaded from https://agupubs.onlinelibrary.wiley.com/doi/10.1029/2020RG000707 by Cochrane France, Wiley Online Library on [07/11/2022]. See the Terms and Conditions (https://onlinelibrary.wiley.com/terms-and-conditions) on Wiley Online Library for rules of use; OA articles are governed by the applicable Creative Commons License

polar wind, consists of the lighter $H^+$ and $He^+$ ions and electrons. A large fraction of these ions has low energies, less than tens of electron volt, up to altitudes of several Earth radii ($R_E$ = 6,371 km).

The auroral oval and the cusp constitute the regions at the boundary between open and closed magnetic field lines. As in the polar cap, ion upflow can be initiated by an ambipolar electric field within the dayside cusp and auroral oval. Here additional mechanisms like friction between the neutral atmosphere and charged particles affected by a convection electric field in the collisional ionosphere also initiate ion heating and upflow (e.g., Schunk, 2007). In these regions, upflowing ions typically reach higher energies than those ions originating from the polar cap. At higher altitudes, collisions are negligible, and electric fields in the form of waves or quasi-static structures can energize the ions. The energy required to energize the ions can come in the form of waves (often Alfvén waves) generated far away from the local upflowing ion population, or can be carried by particles locally producing waves (e.g., lower-hybrid waves). The mass composition and energy of the outflow depends highly on the ionospheric and magnetospheric conditions. Major ion species comprising ion outflow from the dayside cusp and nightside auroral oval are typically $H^+$, $He^+$ and $O^+$, but with contributions also from $N^+$, $N^{++}$, $O^{++}$, and $NO^+$ (e.g., Craven et al., 1985; Hoffman et al., 1974; Ilie & Liemohn, 2016; Yau et al., 1993). These outflows are often referred to as "energetic outflows" and were the first indicators of an ionospheric source of plasma in the magnetosphere (Shelley et al., 1972).

In the dayside cusp, energy often comes from waves or accelerated particles originating from magnetic reconnection or other processes at the dayside magnetopause. Wave-particle interactions seen in this region of the ionosphere, particularly interaction with Alfvén waves, often result in ion heating in the direction perpendicular to the geomagnetic field. Together with ion motion in a diverging magnetic field, this interaction also provides a parallel velocity component, forming so-called conics in ion velocity space. These energetic outflows typically move across the polar cap and the lobes of the magnetotail via convection during southward IMF periods, with velocities depending on solar wind conditions. Sometimes these ions are hard to distinguish from ions originating in the polar cap. Many of these ions reach energies of at least one hundred electron volt at altitudes of several $R_E$.

In the nightside auroral region, energy can also come from waves or impinging particles originating at higher altitudes. Similar to the dayside cusp region, wave-particle interactions often cause outflowing ion conics. In addition, quasi-static parallel electric fields are common at altitudes of about one $R_E$, accelerating auroral electrons downward toward the Earth and ion beams upward. These energetic outflows are typically transported to the inner plasma sheet and the ring current region. Many of these outflowing ions reach keV energies at higher altitudes.

Ion energization and outflow mechanisms are discussed in several studies; for example, the polar wind is discussed by Barakat and Schunk (2006) and Yau et al. (2007), and the dayside cusp and nightside auroral region by, for example, André and Yau (1997), Strangeway et al. (2005), and Moore and Horwitz (2007). For the purpose of this review, estimates of typical ion outflow rates are needed, as discussed in several papers (e.g., André et al., 2015, 2020; Cully et al., 2003; Peterson et al., 2006, 2008; Slapak, Hamrin, et al., 2017; Slapak, Schillings, et al., 2017; Su et al., 1998; Yau & André, 1997; Yau et al., 2017, 2020). Overall, a typical outflow rate from the high-latitude region is $10^{26}$ ions/s, including $H^+$ and heavier ions such as $O^+$. Rates vary by at least one order of magnitude, typically increasing with higher solar EUV and geophysical activity. This trend is even more pronounced for heavier ions.

### 2.1.2. Mid-Latitude Outflow: The Plasmasphere

The Earth's plasmasphere is a torus of cold (<1 eV), dense (10–1,000s $cm^{-3}$) plasma that occupies the inner magnetosphere, typically <3–6 $R_E$ from the Earth, that is, at magnetic latitudes up to ~60° (up to L-shells 4–5), confined within the near-Earth closed geomagnetic field lines. It is composed primarily of $H^+$, with a substantial (1%–10%) amount of $He^+$ and typically much less $O^+$ (Berube et al., 2005), in addition to electrons, originating from the low- to mid-latitude ionosphere. Mechanisms such as the ion outflows described above are applicable as the source of plasma escape from the ionosphere toward the plasmasphere. The low energy plasma of the plasmasphere approximately co-rotates around the Earth on closed plasma drift paths. The outer edge of the plasmasphere, known as the plasmapause, separates closed and open drift paths. At low energies, the convection paths set up a condition whereby the plasmasphere has an elongation or bulge on the duskside (e.g., Carpenter et al., 1993). The convection path in Figure 3 that separates open drift paths

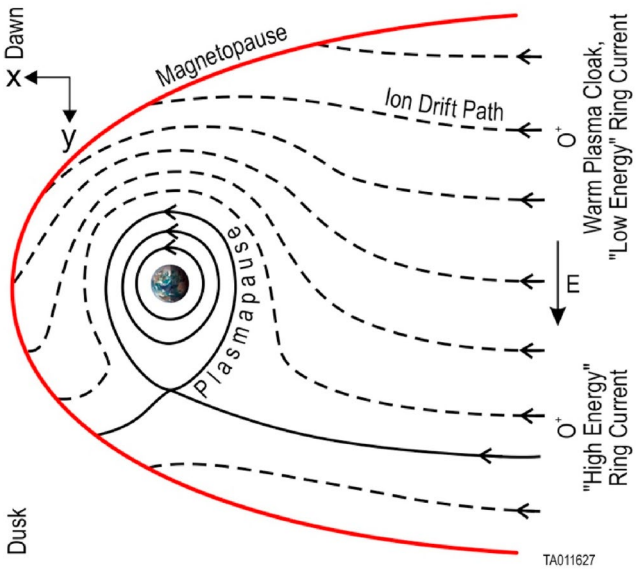



**Figure 3.** Schematic of the open and closed drift paths in the magnetosphere. The cross-tail electric field and the gradient and curvature drifts set up energy dependent, open drift paths to the dayside magnetopause. The plasmapause is the boundary that separates these open drift paths from closed drift paths in the plasmasphere. The Alfvén layer is the solid line that originates in the tail, connects to the plasmapause, and extends to the dayside magnetopause. This layer separates open drift paths around the dawnside from those on the duskside and indicates the location of the drainage region in the dayside magnetopause.

(dashed lines that intersect the magnetopause) from closed drift paths (solid lines in the plasmasphere) is called the plasmapause.

## 2.2. Transport of Ionospheric Plasma in the Earth's Magnetosphere

### 2.2.1. Plasmaspheric Erosion, Trough, and Wind (Midlatitude Outflows)

The diagram in Figure 3 illustrates the conditions for relatively quiet and quasi-static magnetospheric conditions. These conditions rarely occur. Geomagnetic activity is typically either increasing or decreasing as the coupling changes between the Earth's magnetosphere and the highly variable solar wind. When geomagnetic activity increases, the plasmasphere contracts, a combined process that includes earthward flow on the nightside with erosion of the outer plasmasphere on the duskside. This is because, as it contracts, plasmaspheric plasma initially located on closed drift paths suddenly finds itself on open drift paths so that the plasma may drain along the newly open drift paths toward the magnetopause on the dayside (e.g., Moldwin et al., 2016). The plasma convects sunward approximately along the plasmapause boundary at a rate of the order of 20 km/s (e.g., Denton et al., 2019). This sunward convection carries the eroded plasmasphere material toward the dayside magnetopause. This erosion often produces high-density (>few $cm^{-3}$) clouds of plasma in the outer magnetosphere (Chappell, 1972), typically referred to as plasmaspheric plumes or simply plumes. The azimuthal extent of this eroded plasma can be quite thin (<1 $R_E$) or very thick (many $R_E$) (Borovsky & Denton, 2008). The thickness depends on the time history of the plasmaspheric erosion and the location and motion of the magnetopause. Typically, the plasmaspheric plasma encounters the magnetopause on the duskside and late pre-noon sectors. This region is commonly referred as the plasmaspheric drainage region.

The original plasmaspheric composition does not change as the plasma convects to the magnetopause and observations at the magnetopause confirm the dominant $H^+$ component, with lower amounts of $He^+$ and $O^+$(Fuselier et al., 2017). However, as the exiting plasmaspheric material propagates toward the magnetopause, the magnetic flux tubes originating in and filled with plasma from the plasmasphere expand and their density decreases. The magnitude of the decrease in density depends on the convection path and the location of the magnetopause. The plasmaspheric plasma is also heated as it expands in the magnetosphere (e.g., Genestreti et al., 2017), although the degree of heating is variable and there are certainly times when very cold plasmaspheric material is observed at the magnetopause. Finally, the density within the plasmaspheric material is quite variable. Detailed density measurements across plumes show variations of an order of magnitude (e.g., Borovsky & Denton, 2008; Chappell, 1974; Goldstein et al., 2004). These blobs, fingers, and striations align along the line that separates drift paths around the dawnside from those on the duskside in Figure 3, that is, the drainage region.

In addition to plasmasphere erosion by magnetospheric convection, there are other mechanisms that facilitate ion escape from the plasmasphere to the outer magnetosphere: the plasmaspheric trough (Chappell et al., 1971) and the plasmaspheric wind (Dandouras, 2013). The plasmaspheric trough corresponds to the regions just outside the plasmasphere (e.g., Ober et al., 1997; Sheeley et al., 2001). The classical polar wind lifts light ions ($H^+$ and $He^+$) and electrons in the same way as inside the plasmasphere, but this plasma is located at open drift paths (see Figure 3), outside the corotating plasmasphere. Typical densities of the plasmaspheric trough are ~10 $cm^{-3}$ at L-shell = 4 (Chappell et al., 1971), which drop to a few tenths of $cm^{-3}$ when they reach the magnetopause at L-shells of 10–12, due to radial expansion. The plasmaspheric wind is believed to continuously eject material in the radially outward direction, from the plasmasphere to the outer magnetosphere, at all local times, as a consequence of diffusion occurring at the plasmapause due to the sharp density gradient. This continuous wind was predicted by Lemaire and Schunk (1992), and occurs



19449208, 2021, 3, Downloaded from https://agupubs.onlinelibrary.wiley.com/doi/10.1029/2020RG000707 by Cochrane France, Wiley Online Library on [07/11/2022]. See the Terms and Conditions (https://onlinelibrary.wiley.com/terms-and-conditions) on Wiley Online Library for rules of use; OA articles are governed by the applicable Creative Commons License

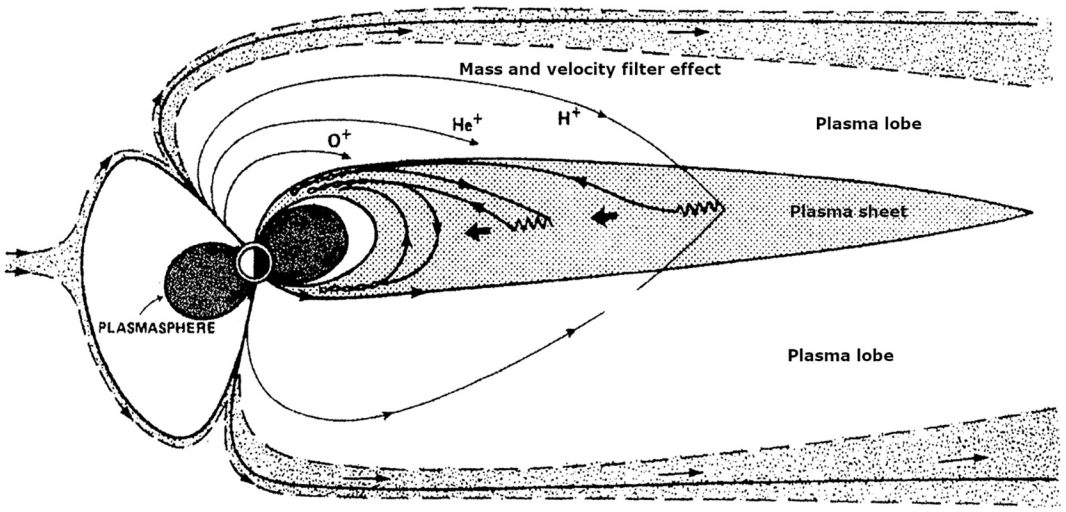



**Figure 4.** Schematic illustration of transport paths for ions escaping from the polar cap regions. Owing to magnetospheric convection, outflowing ions with the same energy will follow distinct paths depending on their mass. In a similar way, outflowing ions of the same species will follow different paths depending on their parallel velocity (energy). This is known as a velocity filter effect. Adapted from Chappell et al. (1987).

as the result of instabilities at high latitudes that drive plasma outwards. However, there is no evidence that the contribution of the plasmaspheric wind to plasmasphere erosion is significant.

### 2.2.2. Convection of High-Latitude Outflows and Filter Effects

The magnetic flux tubes connected to high latitudes move across the polar cap from the dayside to the nightside plasma sheet, due to the interaction between the solar wind and the magnetosphere at the dayside magnetopause, as described in the Dungey cycle (Dungey, 1963). The effective transport of outflowing ions to the magnetosphere is thus the result of the combination of magnetic field-aligned outflow and convection. For northward IMF, that is, when magnetospheric convection becomes negligible, the motion of magnetic field lines becomes erratic and quasi-stagnant, and escaping ions from the dayside ionosphere can travel along reconnected field lines directly to the dayside boundary layer (e.g., Fuselier, 2020; Fuselier et al., 1989; Fuselier, Trattner, et al., 2019; Kasahara et al., 2008) or escape along open field lines in the cusps (e.g., Lavraud et al., 2002). When magnetospheric convection is at work (typically for southward IMF), both dayside and nightside ionospheric outflows are convected toward the magnetotail. In situ observations have shown that the $O^+$ content of the ring current increases during geomagnetic storms (e.g., Grande et al., 2003; Hamilton et al., 1988; Moore et al., 2001). Kistler (2020) shows that the ionospheric contribution to the near-Earth plasma sheet increases strongly when *Dst* drops during the storm main phase.

For the same amount of parallel energization, lighter ions have larger parallel velocities than heavy ions, while the transport perpendicular to **B** due to magnetospheric convection acts in the same way for all species. As a consequence, a mass filter effect arises when magnetospheric convection is non-negligible: lighter ions escaping the polar cap region or nightside auroral zone travel further along the magnetic field line before reaching the plasma sheet in the magnetotail than heavier ions (Figure 4). A velocity filter effect also applies within a single species: the slowest, that is, less energetic, ions being deposited close to Earth, and faster, that is, more energetic, ions further tailward.

Some of the fast ions from these source regions will escape directly into the solar wind and plasma mantle (Krcelic et al., 2019; Schillings et al., 2019; Slapak et al., 2015; Slapak, Hamrin, et al., 2017; Slapak, Schillings, et al., 2017; Westerberg, 2019) and do not contribute to the ionospheric plasma supply of the Earth's magnetosphere. For the ions escaping into the lobes, their fate partly depends on the location at which they enter the magnetotail plasma sheet. The magnetotail neutral line is located at around 100 $R_E$ downstream from Earth (Birn et al., 1992; Daly, 1986; Nishida et al., 1996). A fraction of escaping ions is able to travel very far down the magnetotail before the containing flux tube closes via magnetic reconnection near the neutral line, resulting in the plasma being lost downtail (Haaland, Eriksson, et al., 2012). Other ions starting



19449208, 2021, 3, Downloaded from https://agupubs.onlinelibrary.wiley.com/doi/10.1029/2020RG000707 by Cochrane France, Wiley Online Library on [07/11/2022]. See the Terms and Conditions (https://onlinelibrary.wiley.com/terms-and-conditions) on Wiley Online Library for rules of use; OA articles are governed by the applicable Creative Commons License

19449208, 2021, 3, Downloaded from https://agupubs.onlinelibrary.wiley.com/doi/10.1029/2020RG000707 by Cochrane France, Wiley Online Library on [07/11/2022]. See the Terms and Conditions (https://onlinelibrary.wiley.com/terms-and-conditions) on Wiley Online Library for rules of use; OA articles are governed by the applicable Creative Commons License

from the same location, but with a lower parallel velocity, will not reach as far before the flux tube is convected to the equatorial plasma sheet, resulting in the ions being deposited in the magnetotail closer to the Earth, where magnetotail magnetic reconnection can take place. During quiet conditions, typically associated with a northward IMF, escaping ions from the nightside travel along open field lines that are more or less stagnant (e.g., Haaland, Eriksson, et al., 2012), due to the low magnetospheric convection. These ions are more likely to be lost in the distant magnetotail region or escape directly into the solar wind than during disturbed conditions. Interestingly, this scenario means that ions from the high latitude ionosphere are deposited far downtail during quiet conditions, and therefore will spend more time in the plasma sheet, where additional heating and acceleration can take place.

In summary, the upward flowing ions from the high-latitude regions are subject to energization along their individual trajectories. These trajectories depend on the magnetic latitude and local time of their initial escape from the ionosphere, their initial energy and pitch angle, that is, angle between their velocity and the magnetic field direction, and any energization along their path of travel. The energization along the trajectory depends on waves and parallel electric fields the particles may encounter, on the changing shape of the magnetosphere, as well as the variable cross tail convection electric field that is caused by coupling to the solar wind (Huddleston et al., 2005).

### 2.2.3. Warm Plasma Cloak

Satellite observations made in the 1970s through the 2000s, for example, the International Sun-Earth Explorer (ISEE), Dynamics Explorer (DE), Polar, and Cluster missions, measured the characteristics of a plasma population extending from the nightside through dawn up to the noon sector outside of the plasmasphere that appeared unrelated to the known magnetospheric plasma populations in the radiation belts, plasmasphere, magnetotail plasma sheet, and inner magnetospheric ring current. This plasma population had energies of tens of electron volt to a few kiloelectron volt and was made up of both $H^+$ and $O^+$, suggesting an ionospheric source (e.g., Jahn et al., 2017). These energies indicated that this population was not a direct ionospheric upflow originating from the classical polar wind. Because the cross-tail convection electric field causes particles to flow from the tail in a sunward direction, and because lower energy ions drift dawnward, the new region comprising this plasma population was called the warm plasma cloak (WPC), as the plasma was being "blown" sunward through the dawn sector to the magnetopause (Chappell et al., 2008).

Extensive modeling of ion trajectories has been done by for example, Delcourt et al. (1989, 1993) and Huddleston et al. (2005). This modeling shows how the original low energy ionospheric origin ions can move through the various regions of the Earth's magnetosphere, having their energy and pitch angle changed as they travel. The energization may be caused by centrifugal acceleration in the polar cap, initially, followed by the energy-changing effects of curvature and gradient drift in the presence of the cross-tail convection electric field, which corresponds to potential drops of 50–100 kV across the magnetospheric tail (e.g., Stern, 1977). The statistical results of trajectory calculations suggest that these upflowing ions are energized to 100 eV, 1 keV, 20 keV as they move through the lobes and tail plasma sheet. The study did not include acceleration by waves and parallel electric fields, which would add more energization to ions originating from the cusps and auroral regions. The net effect of the combination of these different upflowing ions is to create both densities and energies that are actually observed in these different regions, indicating that the ion outflows constitute a primary source of plasma for the Earth's magnetosphere, see Figure 5. It was shown that the source of the warm plasma cloak was indeed the ionosphere. However, unlike the ionospheric supply to the plasmasphere, where ionospheric ions with energies of a few eV move directly up the magnetic field line to fill flux tubes, the warm plasma cloak ions come from the ionosphere as polar wind and polar cusp outflows but follow different trajectories across the polar cap and into the near-Earth dawnside of the magnetotail where the ions are energized from tens of electron volt up to a few keV (Chappell et al., 2008). It was also shown that the ultimate energy of an ionospheric particle that flows up into the magnetosphere is determined by where it enters the center plane of the magnetotail. The farther a particle travels down the tail, the more the magnetic field lines are distended in the center plane of the tail and the more curvature drift the particle will encounter when it enters this region. Particles which become the warm plasma cloak enter the tail earthward of those which become the plasma sheet and subsequently the ring current.

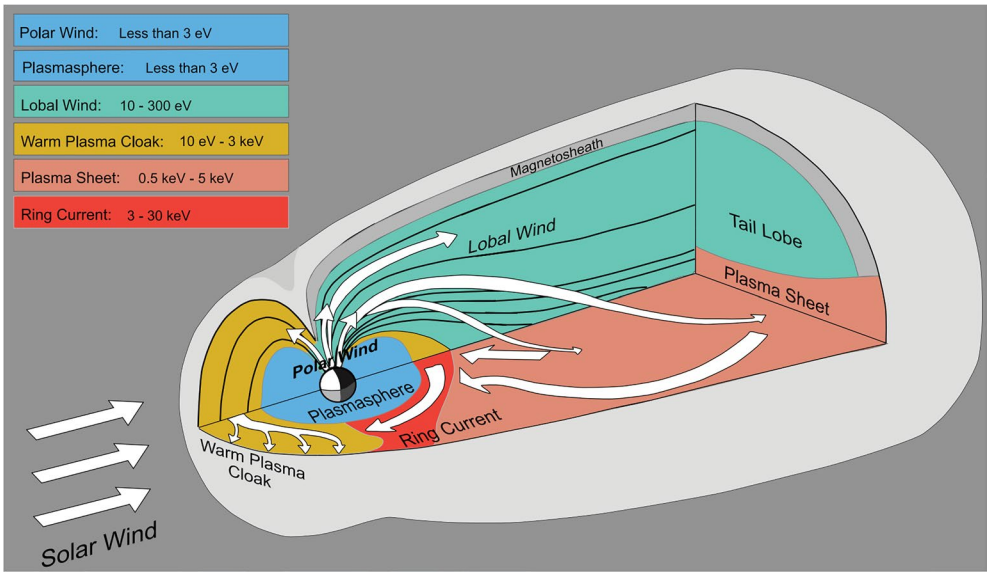



**Figure 5.** Schematic summarizing the particle tracing results from Delcourt et al. (1993) and Huddleston et al. (2005). The ions of ionospheric origin are energized as they travel in the Earth's magnetosphere. Adapted from Chappell et al. (2008).

In summary, the flow of ionization from the ionosphere through the lobes to the central plane of the magnetosphere affects two different areas of reconnection, initially the neutral sheet area of the tail and potentially, through the sunward flow of the warm plasma cloak to the dayside magnetopause.

### 2.3. The Ionospheric Plasma Source From a Global Modeling Perspective

While the magnetosphere is known to have two sources of plasma, the solar wind and the ionosphere, global magnetospheric models have for many years only included the solar wind source. The first models to include an explicit source of ionospheric plasma appeared more than 20 years ago (e.g., Winglee, 1998), but the regular inclusion of ionospheric outflows into global models is a relatively recent innovation. There are multiple approaches to modeling the source and impacts of ionospheric plasma in the magnetosphere implemented in different studies, but these disparate approaches all demonstrate that ion outflows can have a profound effect on the near-Earth space environment.

Tracking ionospheric plasma as it flows through the magnetosphere requires two critical components: (a) a model capable of following disparate plasma populations, and (b) a specification of the ionospheric source of plasma. One method of tracking the flow of ionospheric plasma through the magnetosphere involves tracking large numbers of test particles, launched from the ionosphere, through either static or dynamic fields using MHD (e.g., Moore et al., 2005; Peroomian et al., 2007). Such an approach has the advantage of allowing for kinetic effects and non-Maxwellian particle distributions as the full equation of motion is evolved for many particles. This test-particle method has the disadvantage that the particles and fields do not evolve self-consistently. An alternative approach that has been more actively pursued in recent years is to track each source of plasma separately in its own fluid in a multi-fluid MHD model of the magnetosphere (e.g., Glocer et al., 2009, 2018, 2020; Wiltberger et al., 2010; Winglee et al., 2002). While this methodology does not allow for non-Maxwellian distributions, it does allow for the self-consistent evolution of both plasma and electromagnetic fields.

In terms of specification of the ionospheric source, three methods are commonly used. The simplest method is to specify an ionospheric boundary density which acts as a reservoir from which diffusion and MHD forces effectively pull ionospheric plasma into the magnetospheric simulation domain. This approach was studied extensively by Welling and Liemohn (2014) and found to roughly approximate the observed statistical pattern of ionospheric outflow. A more causally regulated method for representing the outflow is to apply a statistical relationship connecting magnetospheric energy inputs with escaping plasma developed from the



19449208, 2021, 3, Downloaded from https://agupubs.onlinelibrary.wiley.com/doi/10.1029/2020RG000707 by Cochrane France, Wiley Online Library on [07/11/2022]. See the Terms and Conditions (https://onlinelibrary.wiley.com/terms-and-conditions) on Wiley Online Library for rules of use; OA articles are governed by the applicable Creative Commons License

19449208, 2021, 3, Downloaded from https://agupubs.onlinelibrary.wiley.com/doi/10.1029/2020RG000707 by Cochrane France, Wiley Online Library on [07/11/2022]. See the Terms and Conditions (https://onlinelibrary.wiley.com/terms-and-conditions) on Wiley Online Library for rules of use; OA articles are governed by the applicable Creative Commons License

FAST (Strangeway et al., 2005) or Polar (Zheng et al., 2005) spacecraft mission data. This approach has been applied in both test particle and multi-fluid MHD models (e.g., Brambles et al., 2010; Moore et al., 2005). The applicability and uncertainties inherent in the underlying statistical models of outflow has led in recent years to the incorporation of physics-based first principles models of ion escape in to magnetospheric models to represent the ionospheric source (Glocer et al., 2009; Varney et al., 2016a; Welling et al., 2016).

Although the approaches to studying the influence of ionospheric plasma on magnetosphere dynamics differ, they have demonstrated that ion outflow has wide ranging influences on the broader space environment. Moore and Delcourt (1995) introduced the concept of the geopause as boundary inside of which the plasma is primarily of ionospheric origin. The location of the geopause is found to depend heavily on the solar wind IMF orientation (Winglee, 1998) and may have significant North-South asymmetries (Li et al., 2000). The different transport paths to the magnetosphere taken by disparate plasma sources are found to have a major influence on the ring current. For example, polar wind protons and solar wind protons contribute similarly to the ring current during a geomagnetic storm, but the solar wind-originating protons have a higher mean energy due to a longer inward travel path from the tail (Moore et al., 2005). The different plasma trajectories through the magnetosphere also result in local time-dependent injections of plasma of different species into the ring current (Welling et al., 2011).

In simulations, ion outflows are also found to have large-scale consequences for the magnetosphere. Indeed, simulations that include outflow often have a lower cross polar cap potential, and hence reduced global convection (Glocer et al., 2009; Welling & Zaharia, 2012; Wiltberger et al., 2010). Simulations that include ionospheric outflow with self-consistent feedback between the particles and fields are better able to reproduce observed magnetic fields (Glocer et al., 2009). Intriguingly, simulations by Brambles et al. (2010) suggest a potential connection between the escape of ionospheric outflow and periodic sawtooth oscillations (one particular manifestation of geomagnetic activity). These simulations were later reproduced with a more physically realistic simulation (Varney et al., 2016b), but the proposed mechanism remains an actively debated topic in the magnetospheric and ionospheric communities (e.g., Liao et al., 2014; Lund et al., 2018). In addition to sawtooth events, $O^+$ from the ionosphere is found to have a significant influence on dynamics in the magnetotail, such as bursty bulk flows (Garcia et al., 2010; Garcia-Sage et al., 2015). Glocer et al. (2020) modeled separate $H^+$ fluids from the ionosphere and the solar wind and showed a significant contribution of ionospheric $H^+$ to both the plasma sheet and the ring current regions during times of southward IMF. The model also showed that the ring current contains both ionospheric $O^+$ and $H^+$ making the ionospheric contribution dominant over the solar wind $H^+$ and $He^{++}$.

### 2.4. Final Considerations on the Role of the Ionosphere as a Source of Magnetospheric Plasma

In the early years of magnetospheric physics, an important role for the ionosphere was recognized, but mainly as a region that was responding to the inflow of particle and wave energy from the energetic particle populations above. While the link between the plasma sheet and ring current regions to the auroral oval with particles, electromagnetic fields, and currents was accepted and studied, the role of the ionosphere as a source of the more energetic particles was neither fully realized nor understood (Chappell, 2015).

Advances in instrumentation that could measure the low (eV), medium (100 eV–1s keV) and higher energy (10–100 keV) particles combined with the ability to separate masses were a critical new contribution. In the 1970s, 1980s, and 1990s this improved instrumentation enabled the observation of a significant upflow of ions from the ionosphere out into the magnetosphere (ISEE, Akebono, DE, Cluster, Polar). Early estimates of the contributions of these initially low energy particles showed that they were sufficient in terms of density to create the major observed plasma regions of the magnetosphere (Chappell, 1988; Chappell et al., 1987). Later ion trajectory studies of these upflowing cold ions showed that they not only moved through the different magnetospheric regions, but in so doing were energized to match the observed energies in these regions (Delcourt et al., 1993; Howarth & Yau, 2008; Huddleston et al., 2005; Peroomian & Ashour-Abdalla, 1995). In addition, more recent studies show that the changing low energy plasma of the inner magnetosphere can have a significant effect on changing wave generation and propagation which can affect the creation and loss of the very energetic radiation belt electrons and ions (e.g., Thorne, 2010).

19449208, 2021, 3, Downloaded from https://agupubs.onlinelibrary.wiley.com/doi/10.1029/2020RG000707 by Cochrane France, Wiley Online Library on [07/11/2022]. See the Terms and Conditions (https://onlinelibrary.wiley.com/terms-and-conditions) on Wiley Online Library for rules of use; OA articles are governed by the applicable Creative Commons License

As discussed above, for the outflowing ions in the polar cap and lobes, the distance that they travel down the tail is controlled continuously by the changing solar wind - magnetosphere coupling (e.g., Haaland, Li, et al., 2012; Liemohn et al., 2007). The entry point of the ions from the lobe into the central plane of the magnetotail determines their subsequent trajectories and how much they will be energized (see also Figure 4). Huddleston et al. (2005) used data from the Thermal Ion Dynamics Experiment (TIDE) on the Polar spacecraft combined with ion trajectories based on the work of Delcourt et al. (1993). Using TIDE measurement of the outflowing ions (2–400 eV) above the ionosphere as input to the trajectory models, Huddleston et al. (2005) showed that the sum of the outflowing ionospheric-originating ions, combining the outflowing polar cusp ions and some nightside auroral zone upflowing ions, gives enough flux to fill the plasma sheet to the densities that are observed.

One further consideration is the timing required for the two sources, solar wind and ionosphere, to add plasma to the plasma sheet. Sorathia et al. (2019) used particle tracing from the solar wind at the bow shock into the magnetosphere during northward IMF, which is the favorable condition to convect solar wind ions into the plasma sheet region by the Kelvin-Helmholtz instability between the magnetosheath (shocked solar wind) and the flank magnetosphere. The solar wind ion access takes about 3 h to move from the bow shock to the outer plasma sheet and add the particles. In contrast, when the IMF shifts to southward, the outflowing ions already in the tail lobes can be convected into the center of the plasma sheet in a matter of tens of minutes to an hour depending on their location in the lobe.

Finally, we want to emphasize an important consideration about basic nomenclature. For upflowing ionospheric ions, cold ions and ionospheric ions are not necessarily synonymous. There are instances, particularly in the plasmasphere region where the outflowing ionospheric ions are not energized as they fill up the dipolar flux tubes that are corotating, hence cold and ionospheric are the same. At higher L-shells, however, where the ions are carried into the tail, their energies can be significantly changed during transport, hence the ions are still from an ionospheric source but can have total energies >1,000 eV (bulk acceleration plus thermalization). The extension of this realization is that in the reconnection regions, there can be instances where lower energy cold ions can enter the reconnection region, but it is also the case that the hotter plasmas that are involved in the reconnection process are often ionosphere-originated.

## 3. Quantification of Ionospheric Plasma Near the Reconnecting Regions

As described in Section 2, the escape and transport of ionospheric ions into the various regions of the magnetosphere depends on multiple interrelated processes, including for instance energy deposition in the ionosphere and magnetospheric convection. This section compiles all the statistical work that has quantified the contributions of the ionospheric plasma source to the regions where magnetic reconnection, the primary mechanism for coupling with the solar wind and driving energy in the Earth's magnetosphere, occurs.

There have been recent global modeling efforts including the ionospheric source, which clearly indicate their relevance for populating the Earth's magnetosphere, as discussed in Section 2.3. The main challenge of these models is that they need to couple many different physical processes occurring at very different spatial scales and plasma regimes, from the highly collisional ionosphere, including chemical processes to assess the plasma density and composition, to the collisionless magnetosphere and convection of the magnetic field lines.

In the following subsections, we first describe the techniques for detecting cold ions (up to ~10 eV), corresponding to the initial energy of ionospheric ions when they escape to the magnetosphere. Then, we review all the available statistical in situ and remote ion observations near the two main reconnection regions in the Earth's magnetosphere: the dayside magnetopause and the magnetotail. We describe and put together the statistics of observations of ionospheric-originating ions in these two key regions. As mentioned in Section 2, not all ions of ionospheric origin are cold when they reach the reconnection regions. However, from an observational perspective, it is not possible to distinguish the origin of hot (keV) protons. The cold ions discussed in this section correspond to the young ionospheric plasma supply, in the sense that they have not yet been energized significantly, and correspond unequivocally to the ionospheric source.

19449208, 2021, 3, Downloaded from https://agupubs.onlinelibrary.wiley.com/doi/10.1029/2020RG000707 by Cochrane France, Wiley Online Library on [07/11/2022]. See the Terms and Conditions (https://onlinelibrary.wiley.com/terms-and-conditions) on Wiley Online Library for rules of use; OA articles are governed by the applicable Creative Commons License

### 3.1. Techniques for Cold Ion Measurements

While ionospheric-originating ions are very important for understanding magnetospheric dynamics and the coupling of the solar wind and magnetosphere to the ionosphere and underlying atmosphere, ions with energies of less than ~10 eV, such as those directly originating from ionospheric outflow and the plasmasphere, are often hard to detect in space plasmas. A main source of this difficulty arises from the fact that a sunlit spacecraft in a low-density plasma becomes positively charged up to tens of volts (Grard, 1973; Garrett, 1981; Whipple, 1981). Hence, positively charged ions at very low energies will not reach the spacecraft and cannot be directly detected. Various techniques have been developed to overcome this challenge (André & Cully, 2012).

Remote sensing can be used to detect plasmas of both low and high energy. For example, actively transmitting ground-based ionosondes and topside sounding from a spacecraft have been used to determine the plasma density at a specific altitude (Benson, 2010). With both ground-based incoherent and coherent scatter radars, several plasma parameters of the ionospheric plasma populations can be estimated (e.g., Foster et al., 2002; Ogawa et al., 2009). In the magnetosphere, passive remote sensing with instruments on spacecraft detect EUV solar photons resonantly scattered from $He^+$ ions (Spasojevic & Sandel, 2010). Another passive, remote sensing technique for inferring the plasma density is field line resonance, based on measuring the properties of resonant ultralow frequency (1 mHz–1 Hz) waves, which depend on mass density along the field line (e.g., Denton et al., 2002; Goldstein et al., 2001; Takahashi et al., 2004). This technique is of particular interest for characterizing the plasmasphere and inner magnetosphere. Also, energetic neutral atoms (ENAs) produced by charge-exchange between magnetospheric ions and hydrogen atoms in the exosphere travel in line-of-sight paths to a spacecraft and are detected at energies at least down to tens of electron volt (Fuselier, Dayeh, et al., 2020; Sandel et al., 2003), allowing for inference of the low-energy plasma populations in certain regions.

Observing plasma in situ with detectors onboard a spacecraft allows for direct measurements of local plasma properties, but adds uncertainties in the observations caused by interaction of the spacecraft itself with the plasma. In the source region of ionospheric outflow, the plasma density can be so high that the spacecraft potential becomes zero or slightly negative, due to many impacting electrons on the spacecraft surface, allowing for low-energy populations to be measured. At altitudes of a few hundred kilometers, ion detectors are used to study positive ions at low energies (e.g., Shen et al., 2018). Additionally, Langmuir probes are used to determine electron density and temperature in dense plasmas (e.g., Brace, 2013; Knudsen et al., 2017).

At higher altitudes in a low-density plasma, low-energy ions are still able to be observed in situ, for instance when a satellite is in eclipse (i.e., in the Earth's shadow) during short periods, and hence becomes negatively charged (Seki et al., 2003). When a spacecraft is positively charged, an indirect method for measuring the cold ion density is to estimate the total plasma density from observations of electromagnetic wave emission at the electron plasma frequency or upper hybrid frequency, and subtract the ion density deduced from particle detectors (Fuselier, Haaland, et al., 2020; Jahn et al., 2020; Lee et al., 2012; Sauvaud et al., 2001). In addition, the total plasma density is estimated from the spacecraft potential. This potential depends on the density and the electron temperature but can in many magnetospheric plasmas be calibrated and used to estimate the total density (e.g., Grard, 1973; Jahn et al., 2020; Laakso & Pedersen, 1998; Lybekk et al., 2012). To obtain particle distribution functions in velocity space, the positive charging of the spacecraft that repels the positive ions must be reduced. One method is to use a negatively charged aperture plane around the ion detector entrance, as was used for the RIMS instrument on Dynamics Explorer (Chappell et al., 1980). An alternative approach is to negatively bias the entire instrument or a large part of the spacecraft as done for the Magnetospheric Plasma Analyzers (MPAs) on certain geosynchronous spacecraft (Borovsky et al., 1998). Yet another alternative approach used by some missions is to reduce the charging of the whole spacecraft by emitting a plasma cloud (Moore et al., 1997; Su et al., 1998) or a beam of positive ions (Torkar et al., 2016), but often a spacecraft potential of a few volts remains. We note that several studies concentrate on initially cold ions that have been heated (i.e., larger thermal velocity than expected given the plasmaspheric or ionospheric source) or are drifting, for example, due to $\mathbf{E} \times \mathbf{B}$ motion, that is, large enough bulk velocity to overcome the spacecraft charging (e.g., Lee & Angelopoulos, 2014). In these situations, ion detectors on a positively charged spacecraft are still effective (e.g., Lavraud et al., 2005; Sauvaud et al., 2001), and accurate

19449208, 2021, 3, Downloaded from https://agupubs.onlinelibrary.wiley.com/doi/10.1029/2020RG000707 by Cochrane France, Wiley Online Library on [07/11/2022]. See the Terms and Conditions (https://onlinelibrary.wiley.com/terms-and-conditions) on Wiley Online Library for rules of use; OA articles are governed by the applicable Creative Commons License

estimations of the densities of these cold populations require moment calculations that properly account for the spacecraft potential (e.g., Lavraud & Larson, 2016).

An alternative method for determining the presence and properties of a cold ion population utilizes the fact that a supersonic flow of cold positive ions can create a large enhanced wake behind a positively charged spacecraft. The wake will be filled with electrons with a thermal energy that is higher than the ram kinetic energy, in contrast to that of the ions. This creates a local electric field which can be observed and then used to detect the presence of cold ions. Using multiple instruments to measure the geophysical electric field, magnetic field, and spacecraft potential in order to estimate the total plasma density, the cold ion flux can be deduced (Engwall et al., 2009). This method requires one technique to determine the local electric field, such as detecting the potential difference between probes on wire booms in the spin-plane of a spinning spacecraft, and another to characterize the essentially unperturbed geophysical electric field, such as detecting the drift of artificially emitted keV electrons gyrating back to the spacecraft, as is done with an instrument onboard the Cluster and Magnetospheric Multiscale (MMS) missions. Such observations from the Cluster satellites have been used for statistical studies covering a major part of the solar cycle (André et al., 2015). In addition, observations from the MMS spacecraft have been used to show that charging of the individual wire booms affects observations, but can also be used to obtain information on cold ions (Toledo-Redondo et al., 2019).

### 3.2. Quantification of Ionospheric-Originating Ions at the Dayside Magnetopause

In this subsection, we summarize the findings of the statistical studies found in the literature which attempted to infer the properties of ions of ionospheric origin present at the dayside magnetopause, that is, the region where the magnetosphere couples to the solar wind via magnetic reconnection. Most of these studies are based on in situ observations, which are local in nature and orbit dependent. Inferring the global properties of the ionospheric component at the dayside magnetosphere by means of in situ observations can only be done from a statistical perspective, using from months to years of spacecraft observations. Different missions have different orbits, including equatorial versus polar orbits, and different or even varying apogee and perigee distances. In addition, the dayside magnetopause location is dynamic, most of the time being located between 8 and 12 $R_E$ from Earth. Another important difference between studies is the instruments and associated techniques they use for inferring the plasma properties, in particular density, composition and temperature. We decided to group the studies by the main technique they use for cold ion detection. Since the studies reviewed in this section use different spacecraft, different techniques, and even different definitions of ionospheric plasma, one needs to be careful when comparing their results. We tried to enunciate the main points to consider for each of these studies when discussed together. At the end of this sub-section, we provide a table with the main findings, compare the results of each of these studies and draw conclusions from putting all these observations together.

#### 3.2.1. Studies Based on In Situ Ion Detectors

The most straightforward technique to infer the properties of cold ions in space plasmas is by using the low-energy range (up to a few tens or a few hundred electron volt) of ion detectors onboard spacecraft. The main problem of this approach is that any ion with total energy (bulk drift energy plus thermal energy) lower than the spacecraft potential will not be detected, cf. Section 3.1. While this is not a problem for detecting the WPC (typical thermal energies of few hundred electron volt), it poses a serious challenge for detecting plasmaspheric material (typical thermal energies in the eV range).

Chappell (1974) performed a statistical analysis of the plasmaspheric plume properties using OGO 5 satellite (equatorial orbit). He reported 73 cases (orbits) of observations of exiting plasmasphere material in the dayside magnetosphere, at L-shells >4. He reported only peak densities and found an average peak density of ~65 $cm^{-3}$, with the observations being concentrated in the 9:00–21:00 Local Time (LT) sector, that is, mainly in the drainage region.

Chen and Moore (2006) used 3.5 years (January 2000–June 2003) of the Polar spacecraft (polar orbit) data to infer the statistical probability of observing thermal ions (cold ions at eV temperature and any drift velocity) as a function of local time in the dayside magnetosphere. This method allowed for detection of the plasmaspheric material but disregarded WPC events, which are often not so cold. Thermal ions were detected 50%

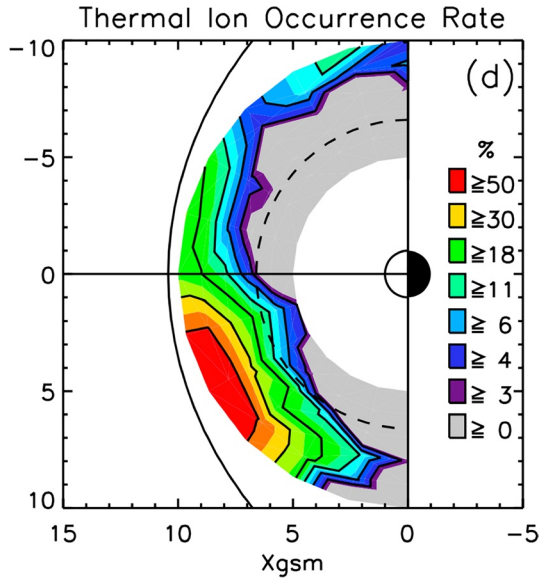



**Figure 6.** Occurrence probability of thermal ions, based on 3.5 years of POLAR spacecraft observations. Adapted from Chen and Moore (2006).

of the time near the dusk side magnetopause, while the occurrence near the dawn-side magnetopause was 30% (see Figure 6), considering as detection any flux above the noise level of the instrument at the low energy range. Their occurrence probabilities are higher for larger L-shells, and this is because the ion detector requires that the bulk plasma velocity has higher energies than the equivalent spacecraft potential energy (typically a few to several V). This occurs preferentially near the magnetopause, where local motions of the boundary and ULF waves accelerate the cold plasma to energies above the spacecraft potential. The dawn-dusk asymmetry is explained by the location of the drainage region, which is predominantly in the dusk sector. Finally, they also compared the statistical occurrence of thermal ions with the orientation of the IMF. They found a larger occurrence probability of thermal ions during southward IMF periods, consistent with the picture of enhanced magnetic reconnection and magnetospheric convection that facilitates erosion of the plasmasphere, including plume formation.

Borovsky and Denton (2008) used 210 plasmaspheric plume events during geomagnetic storms, observed at geosynchronous orbit (6.6 $R_E$) by the Magnetospheric Plasma Analyzer (MPA) onboard Los Alamos satellites (McComas et al., 1993). They found that plasmaspheric plumes are a persistent feature of geomagnetic storms, and that they last for ∼4 days. Their flux is roughly $2 \times 10^{26}$ ions/s when they are young and it decreases with age, the average mass released per event being $\sim 3.3 \times 10^4$ kg. These numbers indicate that plumes constitute a primary escaping path of plasma. The plume plasma density, flow velocity and width all decrease with the plume age. However, these observations are taken far away from the Earth's magnetopause, which is typically situated at ∼10 $R_E$. Assuming an effective area of the drainage plume region at the magnetopause of $\sim 9 \times 12$ $R_E$, as in André and Cully (2012), and an average outflow velocity of ∼15 km/s (Borovsky & Denton, 2008), the resulting ionospheric average density at the magnetopause in the drainage region corresponds to ∼3 $cm^{-3}$ during storm times.

The previous studies discussed the presence of plasmaspheric material in the outer, dayside magnetosphere. Another important population that brings ionospheric-originating ions to the dayside magnetopause is the WPC (cf. Section 2.2.3). Nagai et al. (1983) analyzed ISEE-1 (equatorial orbit, 30° inclination) data (June 1978–December 1980) and searched for field-aligned bidirectional ion jets in the energy range of 10–100 eV, and found occurrences larger than 50% at the dawn side magnetopause (L-shells ∼10, see Figure 7a). Their search criteria match with the properties of the WPC. Similar results are obtained by Chappell et al. (2008), who analyzed 1 year (March 2001–March 2002) of Polar spacecraft data (polar orbit) searching for the WPC population. Their criteria were to find bidirectional, field aligned ions in the energy range of 10–400 eV within a 1 L-shell portion of the orbit. They did not impose a minimum density threshold for the bidirectional jets. They found, for L-shells of 10–12, that is, the region where the magnetopause is located, WPC detections of 30%–50% in the dusk side and >70% in the dawn side (see Figure 7b), with larger occurrence for latitudes <30°.

Lee et al. (2016) used Cluster data in the 2007–2009 period, to infer the occurrence and density of both the plasmaspheric plume and the WPC near the magnetopause. They looked individually at each of the 442 magnetopause crossings of Cluster 3 spacecraft, and searched for fluxes $>10^5$ keV/($cm^2$ s sr keV) lasting at least 2 min, in the energy range of 10–1,000 eV. Plasmaspheric plume occurrence may be underestimated in Lee et al. (2016), as in Chen and Moore (2006), because it often has energies below 10 eV, the instrument threshold. They distinguish between the two populations based on the pitch angle of the ions. The WPC typically exhibits field-aligned bidirectional jets, while the plasmaspheric material is observed at pitch angles perpendicular to the magnetic field (owing to the drift motion). Plasmaspheric material was found in the dusk sector near the magnetopause for 41 events out of 221 crossings, that is, 19%. This number is lower than for other studies probably due to non-detections of cases with total energies below 10 eV. With regards to the WPC, they find for the dawn sector 17 events out 221 featuring bidirectional jets for more than 2 min,



19449208, 2021, 3, Downloaded from https://agupubs.onlinelibrary.wiley.com/doi/10.1029/2020RG000707 by Cochrane France, Wiley Online Library on [07/11/2022]. See the Terms and Conditions (https://onlinelibrary.wiley.com/terms-and-conditions) on Wiley Online Library for rules of use; OA articles are governed by the applicable Creative Commons License

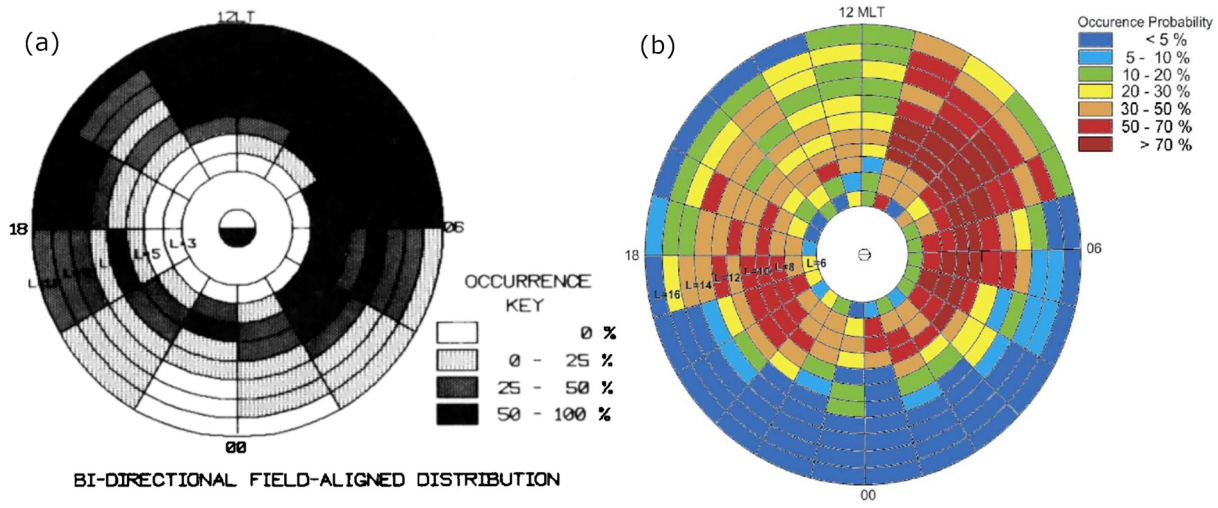



**Figure 7.** (a) Statistical occurrence of warm plasma cloak observed from ISEE-1, June 1978–December 1980, in the 1–100 eV energy range. Adapted from Nagai et al. (1983). (b) Polar statistical (March 2001–March 2002) observations of the warm plasma cloak (bidirectional field aligned ion jets of less than 400 eV). The occurrence is larger than 70% in the dawn side, for L-Shells of 10–12, that is, the region where the magnetopause is located. Adapted from Chappell et al. (2008).

corresponding to 8% occurrence. This value is again lower than previous estimates by Nagai et al. (1983) and Chappell et al. (2008), and the reason is that their threshold requirements for density and duration for considering detection were more restrictive for this study. They estimate a median density of 5.4 $cm^{-3}$ for plasmasphere-originating ions, and a median density of 5.2 $cm^{-3}$ for the WPC, indicating that they captured only very dense events.

### 3.2.2. Studies Based on In Situ, Mass-Resolving, Ion Detectors

Some ion detectors measure the time of flight inside the instrument, allowing to discriminate their mass. Fuselier et al. (2017) and Fuselier, Mukherjee, et al. (2019) statistically analyzed the properties of the plasmaspheric material and the WPC in the dayside magnetosphere, using roughly 5 months of MMS data between September 2015 and March 2016. They distinguished the populations by the relative amounts of heavy ($He^+$ and $O^+$) ions as measured by the Hot Plasma Composition Analyzer (Young et al., 2016). In their approach, they looked for observations with $H^+$ density above 1.5 $cm^{-3}$ in the dayside magnetosphere (i.e., plasmaspheric plumes and dense WPC), at distances >7 $R_E$, and within 1.5 h in time from the magnetopause crossing. They excluded the magnetosheath and the low-latitude boundary layer by imposing the requirement that no significant $He^{++}$ is present. With these criteria, they found that most of the intervals had $n_{He+}/n_{O+} < 1$, and identified these intervals as WPC. Then, they removed the criterion on $He^{++}$ and searched for intervals that were not WPC and had $He^+$ density above 0.03 $cm^{-3}$. With these criteria, they found that most of the intervals had $n_{He+}/n_{O+} > 1$, and identified these intervals as plasmaspheric plume material. Outflow from the high-latitude ionosphere is dominated by $O^+$ with much less $He^+$ (e.g., Collin et al., 1988); thus, it stands to reason that the WPC is distinguishable from the plume by its $O^+$ content. Since their observations rely on particle instruments, they cannot measure populations with total energy below the spacecraft potential (several electron volt to few tens of electron volt). Most of the plume observations occurred in the Low Latitude Boundary Layer (LLBL), where the convection flows are large and the cold plume can reach energies above the spacecraft potential and be observed by HPCA. Overall, they found that ionospheric $H^+$ with number density >1.5 $cm^{-3}$ was detected by HPCA ~14% of the time in the magnetospheric side of the magnetopause, 10% for the WPC and 4% for the plume populations. Fuselier et al. (2017) and Fuselier, Mukherjee, et al. (2019) show the lowest occurrence percentages of all the studies considered in this review, with findings similar to those in Lee et al. (2016). Their lower occurrences may be explained by the threshold density imposed (WPC) and the hidden plume at energies below the spacecraft potential.



19449208, 2021, 3, Downloaded from https://agupubs.onlinelibrary.wiley.com/doi/10.1029/2020RG000707 by Cochrane France, Wiley Online Library on [07/11/2022]. See the Terms and Conditions (https://onlinelibrary.wiley.com/terms-and-conditions) on Wiley Online Library for rules of use; OA articles are governed by the applicable Creative Commons License

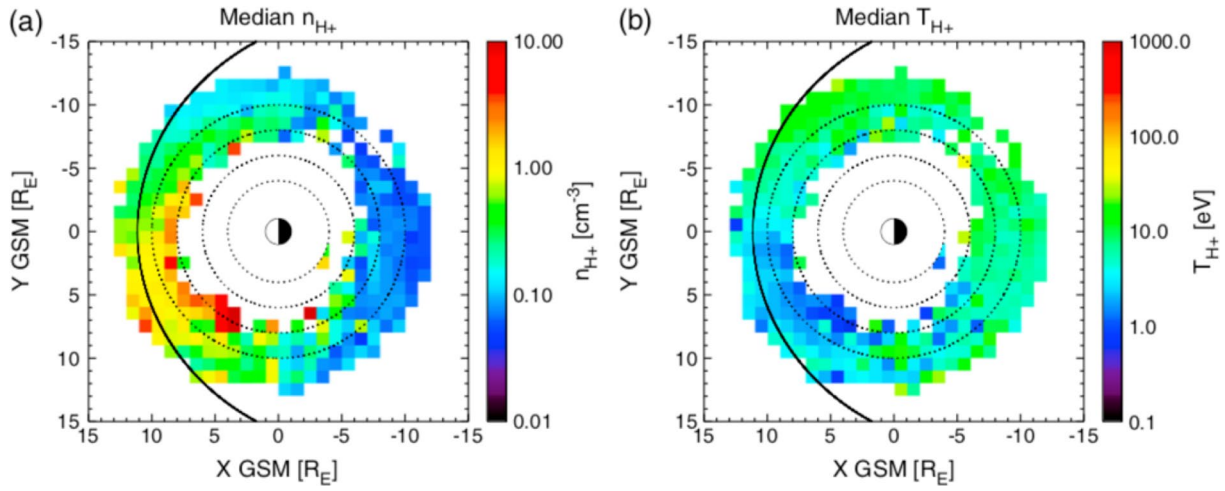



**Figure 8.** Median cold (<120 eV) $H^+$ (a) density and (b) temperature, obtained from 5 years of THEMIS data using 3 spacecraft. Adapted from Lee and Angelopoulos (2014).

### 3.2.3. Studies Using Specific Techniques Aimed for Cold Ion Detection

Walsh et al. (2013) examined all magnetopause crossings by the THEMIS constellation (equatorial orbit) during the years 2008–2010 and searched for dense plasmaspheric plumes on the magnetospheric side. Their criterium for selection was that the total density was larger than twice the plasmasphere density expected from a plasmaspheric model (Sheeley et al., 2001) inside the magnetosphere. The threshold for considering plume detection at 10 $R_E$ was 3.8 $cm^{-3}$ and therefore the study looked only for high-density plumes. The density was inferred from the average spacecraft potential, during 2 min of observations in the magnetosphere adjacent to the crossing. In principle, inferring the density from the spacecraft potential has the advantage of accounting for typically "hidden" low-energy ions, but this method has to be carefully calibrated by comparing with other observations (cf. Section 3.1). They found that 137 out of 520 crossings (26%) contained the high-density plasmaspheric plume adjacent to the magnetopause in the dusk sector, with most densities greater than 5 $cm^{-3}$ and up to more than 100 $cm^{-3}$.

Lee and Angelopoulos (2014) used ~5 years of data (January 2008–May 2013) from 3 spacecraft of the THEMIS constellation to infer the statistics of cold ions. Their observations are also based on the ion detector onboard the spacecraft, which cannot detect cold ions with total energy below the equivalent spacecraft potential energy (~10 eV). To account for that, they normalize their dwell times to the times when the bulk **E** x **B** drift energy exceeds the equivalent spacecraft potential energy. By using this normalization, they ensure that their occurrence rates are not biased by hidden, low-energy, plasmaspheric material. They search for ions in the 5–120 eV range, and impose that the number density measured by the ion detector and using the spacecraft potential match within a factor of 2. They find that cold ions are most frequently seen in the late morning and afternoon sector, that is, the drainage region, with relative occurrences of 60%–90%. They also found dependence with the *Kp* index, an index that accounts for the level of geomagnetic disturbance at the magnetosphere, with cold ions being more spread over all Magnetic Local Times (MLT) for $Kp < 1$, and more concentrated in the late morning to afternoon sector for $Kp > 1$. Figure 8 shows the median density and temperature of $H^+$. The densities are typically >1 $cm^{-3}$ in the drainage region and <1 $cm^{-3}$ in the other dayside regions. Typical temperatures are always below 50 eV. The ion instrument onboard the THEMIS spacecraft cannot directly resolve the mass of ions. However, if the ions experience flows, it is possible, under certain assumptions, to gain information on the multiple ion populations. For $He^+$, they found that the median number density ratio $n_{He+}/n_{H+} < 0.1$ in the dusk sector, and ~0.5 in the dawn sector. For $O^+$, they found roughly the same median ratios in the dayside, that is, $n_{O+}/n_{H+} < 0.1$ in the dusk sector, and ~0.5 in the dawn sector. In their heavy ion calculations, they exclude detections with total energies >1 keV.

André and Cully (2012) studied the statistical occurrence and characteristics of the cold ion component (below a few tens of eV) in various regions of the Earth's magnetosphere using data from the Cluster spacecraft (polar orbit), obtained during the period from November 2006 to July 2009. They combined various



19449208, 2021, 3, Downloaded from https://agupubs.onlinelibrary.wiley.com/doi/10.1029/2020RG000707 by Cochrane France, Wiley Online Library on [07/11/2022]. See the Terms and Conditions (https://onlinelibrary.wiley.com/terms-and-conditions) on Wiley Online Library for rules of use; OA articles are governed by the applicable Creative Commons License

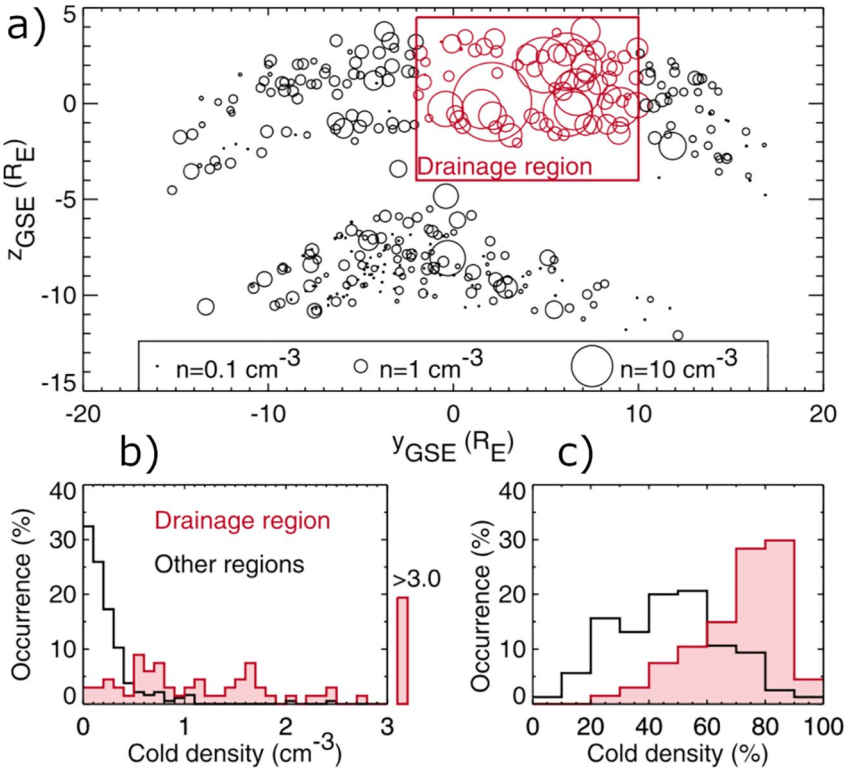



**Figure 9.** Statistics of cold ionospheric-originating ions at the magnetopause from Cluster data. (a) Cold ion density and location for each of the 370 magnetopause crossings identified during November 2006 to July 2009. The plasmaspheric drainage plume region is identified in red. (b) Histograms of cold ion density in the drainage region (red) and other regions (black) of the magnetopause. (c) Histograms of the fraction of the ion population not visible to the ion instrument in drainage (red) and other (black) regions. Low-energy ions contribute a significant fraction of the density nearly all of the time (>85%) in the drainage region, and 50%–70% of the time outside of that region. Adapted from André and Cully (2012).

techniques for assessing the occurrence and density of the cold ions: direct measurements by the ion detectors, inferred from the plasma frequency, inferred from the spacecraft potential, and using the wake method, cf. Section 3.1 (Engwall et al., 2009). Figure 9 summarizes their statistics on cold ion detections at the magnetopause. Panel a shows the location in the YZ GSE plane and the respective cold ion density for each of the 370 Cluster 3 magnetopause crossings analyzed. The drainage region (red) corresponds to the region where the plasmaspheric plumes are most likely to hit the magnetopause. Figure 9b indicates that inside the drainage region, ∼20% of the crossings showed cold ion densities higher than 3 $cm^{-3}$. Outside the drainage region, typical cold ion densities are usually below 1 $cm^{-3}$. These densities are obtained by subtracting the observed density by the ion detector (corresponding to hot ions) from the total electron density ($n$) inferred from the cutoff plasma frequency ($\omega_p = ne^2 / \varepsilon_0 m$), where $e$ and $m$ are the electron charge and mass, respectively. Finally, in Figure 9c a histogram of the relative occurrence of cold ions present in the magnetopause is shown. Cold ions contribute a significant fraction of the total number density (>40%) during more than 85% of the time inside the drainage region, and 50%–70% of the time in other regions of the dayside magnetopause.

### 3.2.4. Remote Imaging of $He^+$

Spasojevic and Sandel (2010) used a different technique to infer the total ion escape via plasmaspheric plumes. They used the Extreme Ultraviolet (EUV) imager instrument onboard the IMAGE mission (Sandel et al., 2003), which is capable of imaging at 0.1 $R_E$ resolution the amount of $He^+$, by resolving its resonance line emission at 30.4 nm. They looked at five independent moderate disturbance events (Sym-H above −100 nT), and found that the average loss rate to the dayside magnetopause was of ∼0.38–2.1 × $10^{27}$ ions/s during the events, that is, somewhat higher than the results by Borovsky and Denton (2008). They assumed



19449208, 2021, 3, Downloaded from https://agupubs.onlinelibrary.wiley.com/doi/10.1029/2020RG000707 by Cochrane France, Wiley Online Library on [07/11/2022]. See the Terms and Conditions (https://onlinelibrary.wiley.com/terms-and-conditions) on Wiley Online Library for rules of use; OA articles are governed by the applicable Creative Commons License

a number density ratio $n_{He+}/n_{H+} \sim 0.05–0.15$ (Craven et al., 1997) at L-shell distances of 2–5, and that on average 65% of the depleted $He^+$ ions finally escape toward the dayside magnetopause. Assuming an effective area of the drainage plume region of $\sim 9 \times 12\ R_E$, and an average outflow velocity of ~15 km/s, the resulting ionospheric average density at the magnetopause in the drainage region corresponds to 6–32 $cm^{-3}$ during the plume events, that is, a factor of 2–10 larger than the estimation of Borovsky and Denton (2008). This discrepancy may be explained by the fact that the imaging method requires a minimum amount of $He^+$ density in the integrated line of sight of the instrument, which would result in only detecting high-density plumes.

#### 3.2.5. Comparison Between Studies

We summarize, in Table 1, the statistics provided by the works described above, at the subsolar-to-dusk magnetopause (drainage region) and the subsolar-to-dawn magnetopause. Comparing the statistical studies presented in this section is not an easy task, owing to their different solar cycle phase, orbits, methods and criteria for cold ion detection. Nonetheless, several conclusions are drawn from Table 1.

Near the dayside magnetopause there are cold to warm (electron volt to few hundred electron volt) ions of ionospheric origin most of the time, regardless of solar cycle phase. These ions have approximately the same density, that is, a few times 0.1 $cm^{-3}$, as keV magnetospheric ions (originally from the solar wind and the ionosphere). Cold ions in the dusk sector (drainage region) are found more frequently than in the dawn sector, and their density is higher. This is because the plasmaspheric material usually reaches the magnetopause in the dusk sector. By contrast, the WPC can be found in both sectors (Fuselier et al., 2017; Fuselier, Mukherjee, et al., 2019; Lee et al., 2016).

##### *3.2.5.1. Dusk Side*

The reported percent of time that plasmaspheric material is observed at the magnetopause has a large variability in the literature. Except for Fuselier et al. (2017), the studies suggest that this number is >20%–25% of the time, and some indicate that the percent is >70%–80%. This variation is mainly due to the following factors: the density threshold imposed for considering a detection, and the minimum energy that the method can detect. Different studies impose a more or less restrictive density threshold for considering detection of cold ions, which ranges from being above the noise of the method (typically less than 1 tenth $cm^{-3}$), for example, André and Cully (2012), Lee and Angelopoulos (2014), to more than ~5 $cm^{-3}$ for Walsh et al. (2013). The second important factor is that for most of the studies, the plasmaspheric material can go undetected for a significant fraction of the time, because their methods do not allow the detection of cold ions with total energy below the equivalent spacecraft potential energy. Only three studies tackle this shortcoming. André and Cully (2012) use various indirect techniques that can detect ions below the spacecraft potential energy. They find that cold ions are present >85% of the time, with $n_{H+}$ ~0.2–1 $cm^{-3}$, including a smaller fraction of time (~20%) when the cold ion number density is >3 $cm^{-3}$ (plumes). Lee and Angelopoulos (2014) only consider times when the convection speed is larger than the spacecraft potential, and therefore the cold ions will be detected if they are present. They find occurrence times (70%–95%) in accordance with to André and Cully (2012), with similar density estimates (>1 $cm^{-3}$). The other study that can detect ions below the spacecraft potential is Walsh et al. (2013), because it relies on estimating density from the spacecraft potential measurement rather than from particle measurements. However, these authors search only for high-density plumes, and impose density thresholds of ~5 $cm^{-3}$ (varying with radial distance to Earth). They find an occurrence probability of 26% and average densities of 5–10 $cm^{-3}$. Based on these results, we note that studies relying only on particle detector measurements cannot provide accurate occurrence probabilities, because the cold ions often do not reach the detectors due to the positive spacecraft potential, unless the dwell time is limited to periods with bulk drift energies larger than the equivalent spacecraft potential (Lee & Angelopoulos, 2014).

We conclude, based on André & Cully (2012) and Lee & Angelopoulos (2014) that cold ions are present at the dusk magnetopause >80% of the time, with average $H^+$ densities of at least a few times 0.1 $cm^{-3}$. This includes 20%–25% of the time when the density is >3 $cm^{-3}$. Periods of high density in the dusk region are often due to parts of the bulge region of the plasmasphere exiting and being sunward convected to the magnetopause, that is, the so-called plumes. Plumes occur predominantly during storm times and up to a few days later, while the lower density cold ions can come from various mechanisms, including the WPC,



19449208, 2021, 3, Downloaded from https://agupubs.onlinelibrary.wiley.com/doi/10.1029/2020RG000707 by Cochrane France, Wiley Online Library on [07/11/2022]. See the Terms and Conditions (https://onlinelibrary.wiley.com/terms-and-conditions) on Wiley Online Library for rules of use; OA articles are governed by the applicable Creative Commons License

Reviews of Geophysics

10.1029/2020RG000707

**Table 1**
*Studies of Ionospheric-Originating Ions Near the Earth's Magnetopause*

| | | Solar cycle phase | Density threshold for selection ($cm^{-3}$) | Relative occurrence (%) | Mean $n_{H+}$ Observed ($cm^{-3}$) | Energy range (eV) | Observed $n_{He+}/n_{H+}$ | Observed $n_{O+}/n_{H+}$ |
|---|---|---|---|---|---|---|---|---|
| Dusk-side magnetopause | Chappell (1974) | Maximum (1968–1970) | ~6 at $L = 9$ (decreasing with distance) | Convection dependent | 6–310 (peak values) | Few[a]–few tens | 0.1 | - |
| | Chen and Moore (2006) | Maximum (2000–2003) | - | >50 | - | Few[a]–400 | - | - |
| | Borovsky and Denton (2008) | Multiple phases (1993–1996) (2003–2004) | - | Whenever storm occurs | ~3 (extrapolated to 10 $R_E$) | - | - | - |
| | Lee et al. (2016) | Minimum (2007–2009) | Flux >$10^5$ keV/ $cm^2$s sr keV | 19 | 5.4 | 10[a]–1,000 | - | - |
| | Fuselier et al. (2017) | Declining (2015–2016) | 1.5 | 4 | 5 | Few[a]–several thousands | 0.015 (assumed at $L = \sim10$) | <0.015 |
| | Walsh et al. (2013) | Minimum (2008–2010) | ~5.7 at $L = 9$ (decreasing with distance) | 26 (high-density plumes) | >5–10 | - | - | - |
| | Lee and Angelopoulos (2014) | Minimum and ascending (2008–2013) | - | 70–95 | >1 | 5[a]–120 | <0.1 | <0.1 |
| | André and Cully (2012) | Minimum (2006–2009) | - | >85 including 20 | >0.2–1>3 | up to few tens | - | - |
| | Spasojevic and Sandel (2010) | Maximum (2001) | - | Disturbed times considered | 6–32 (extrapolated to 10 $R_E$) | - | 0.05–0.15 (assumed at $L = 2$–5) | - |
| Dawn-side magnetopause | Nagai et al. (1983) | Ascending (1978–1980) | - | >50 | - | 10[a]–100 | - | - |
| | Chappell et al. (2008) | Maximum (2001–2002) | - | >70 | 0.5–3 | 10[a]–400 | - | - |
| | Lee et al. (2016) | Minimum (2007–2009) | Flux > $10^5$ keV/ $cm^2$s sr keV | 8 | 5.2 | 10[a]–1,000 | - | - |
| | Fuselier et al. (2017) and Fuselier, Mukherjee, et al. (2019) | Declining (2015–2016) | 1.5 | 10 | 3 | Few[a]–several thousands | <0.02 | ~0.02/0.004 |
| | Lee and Angelopoulos (2014) | Minimum and ascending (2008–2013) | - | 30–70 | 0.15–0.7 | 5[a]–120 | ~0.5 | ~0.5 |
| | André and Cully (2012) | Minimum (2006–2009) | - | 50–70 | 0.1–1 | up to few tens | - | - |

*Note*. The dusk side corresponds roughly to 12–18 LT, and the dawn side roughly to 06–12 UT.
[a]The real lower energy threshold is defined by the spacecraft potential, which is variable depending on spacecraft and plasma conditions, in the range of few electron volt to tens of electron volt



19449208, 2021, 3, Downloaded from https://agupubs.onlinelibrary.wiley.com/doi/10.1029/2020RG000707 by Cochrane France, Wiley Online Library on [07/11/2022]. See the Terms and Conditions (https://onlinelibrary.wiley.com/terms-and-conditions) on Wiley Online Library for rules of use; OA articles are governed by the applicable Creative Commons License

high-latitude outflows, the plasmaspheric trough and plasmaspheric wind. The occurrences reported by these two studies were calculated during years near a solar cycle minimum, and one would expect that the occurrence rate and density are larger near solar cycle maximum. Finally, it is difficult to draw conclusions from the composition measurements of ionospheric-originating ions near the magnetopause. There are too few studies using composition to determine if, for example, there is a composition change in the plume with L-shell.

#### 3.2.5.2. Dawn Side

With respect to the dawn sector, which is mainly affected by the warm plasma cloak and high-latitude outflows, Table 1 reveals that the studies provide different results depending mainly on the density threshold they imposed for the definition of cold ions. Lee et al. (2016) and Fuselier et al. (2017) were more restrictive, and therefore their results reflect the statistics of the high-density events. The WPC can be identified by its field aligned, bi-directional ion flows. Furthermore, it is more easily detected by particle instruments than the plasmaspheric material, owing to its larger total energy, and hence the better agreement between studies than for the dusk side. Chappell et al. (2008) finds somewhat larger occurrences (>70%) and densities (0.5–3 $cm^{-3}$) than Nagai et al. (1983), Lee and Angelopoulos (2014), and André and Cully (2012). This is probably related to the higher upper energy limit they use (400 eV). The WPC can often be found at energies >100 eV, and these events would be missed by the other studies. In addition, the statistics reported by Chappell et al. (2008) were performed near the solar cycle maximum, as opposed to the other studies, which were performed during solar cycle minimum and ascending phases.

For the dawn side, we conclude that the probability of finding the WPC at the magnetopause in the dawn side is >50%–70%, with average $H^+$ densities of a few tenths of $cm^{-3}$ to a few $cm^{-3}$. For ~10% of the time, the average $H^+$ density is ≥3 $cm^{-3}$. Similar to the duskside studies, there are too few studies using composition to investigate composition differences with L-shell or local time.

### 3.2.6. Relative Importance of Ionospheric-Originating Ions at the Dayside Magnetopause

The other population that is always present on the magnetospheric side of the Earth's magnetopause is the plasma sheet ions, with energies in the keV to tens of keV range and densities of a few tenths of $cm^{-3}$. The origin of this population is both the solar wind and the ionosphere (e.g., Huddleston et al., 2005). For the dusk-side magnetopause, more than 80% of the time the density of cold ions is of the same order of magnitude as hot magnetospheric ions. The cold ion density is one order of magnitude larger than hot magnetospheric ions 20%–25% of the time. For the dawn-side magnetopause, the density of cold ions is of the same order of magnitude as hot magnetospheric ions >50%–70% of the time. For 10% of the time, the cold ion density is one order of magnitude larger than hot magnetospheric ions. Finally, on average, the plume (20%–25% of the time) and high-density WPC events (10% of the time) have proton number densities which are still ~one order of magnitude lower than the magnetosheath proton number density, which is found at the other side of the magnetopause. To these estimations, one needs to add the ionospheric $He^+$ and $O^+$ contributions to the total mass density near the magnetopause, which require further investigation to be properly characterized.

## 3.3. Quantification of Ionospheric-Originating Ions in the Earth's Magnetotail

The other main region where magnetic reconnection takes place is the Earth's magnetotail, which is divided into two main regions: the plasma sheet, a relatively thin layer (~6 $R_E$ thick on average, depending on the distance from Earth) which lies in the geomagnetic equatorial plane, and the lobes, that is, the regions that fill the space above and below the plasma sheet (see Figure 1). The particle populations in these regions of the magnetotail are quite different. As magnetotail reconnection onset occurs in the plasma sheet, its properties are important for controlling the initiation of reconnection. But as magnetic reconnection proceeds, the lobe field lines are also brought into the reconnection region and become the inflow material of the reconnection process. Therefore, plasma conditions on lobe field lines are also important. We now examine the ionospheric contributions to the plasma composition of the plasma sheet and the lobes.



19449208, 2021, 3, Downloaded from https://agupubs.onlinelibrary.wiley.com/doi/10.1029/2020RG000707 by Cochrane France, Wiley Online Library on [07/11/2022]. See the Terms and Conditions (https://onlinelibrary.wiley.com/terms-and-conditions) on Wiley Online Library for rules of use; OA articles are governed by the applicable Creative Commons License

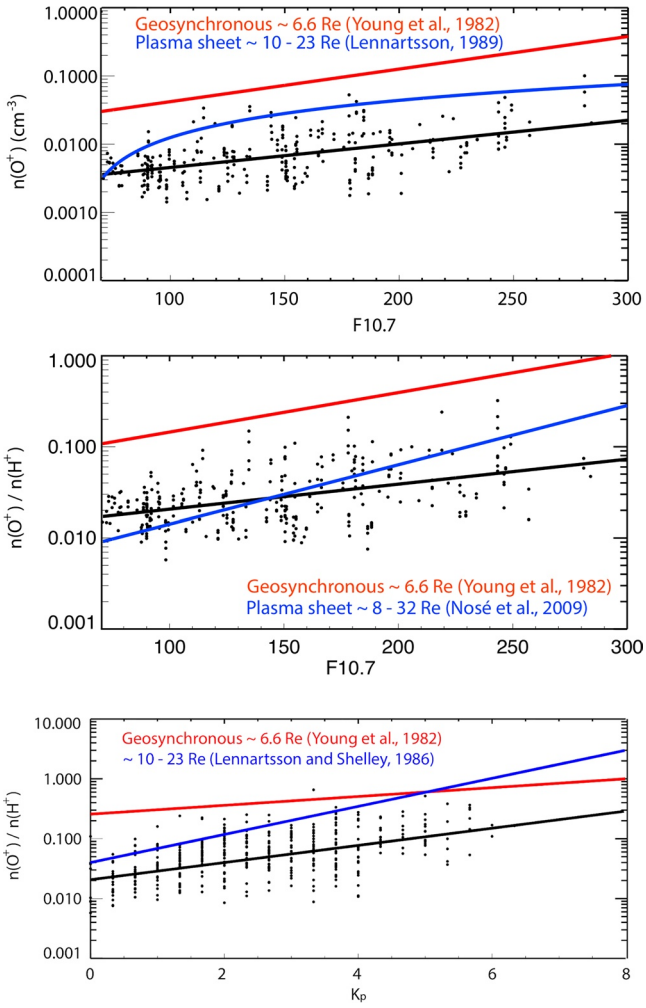



**Figure 10.** Variation in the $O^+$ number density and the density ratio with (a and b) F10.7, and (c) *Kp* for various L-shells. Adapted from Mouikis et al. (2010).

### 3.3.1. Plasma Sheet

The plasma sheet ion population is typically hot, and has temperatures in the range of few kilo electron volt to few tens of kilo electron volt. The ionospheric contribution to the plasma sheet is best determined by its composition, because ionospheric-originating ions have generally been energized and thermalized together with ions of solar wind origin through various processes in the magnetotail. Since both the ionospheric outflows and the solar wind contain significant $H^+$, they mix in the plasma sheet and their origin is thus difficult to discern once energized. However, $O^+$ can only come from the ionosphere, and so is often used as a tracer for the ionospheric source. $He^{++}$ in the plasma sheet is dominantly of solar wind origin, and high charge state CNO species, such as $O^{+6}$ are definitely of solar wind origin, and so these ions can be used to trace the solar wind component. Lennartsson and Sharp (1985) used the energy distributions of the $He^{++}$ and $O^+$, compared to the $H^+$ to estimate the fraction of $H^+$ from the ionosphere, and concluded that the ionosphere may contribute 30%, even during quiet times. Gloeckler and Hamilton (1987) used measurements from the AMPTE and IRM missions to estimate the ionospheric contribution through comparisons of the plasma sheet composition with average solar wind composition. They concluded that the $n_{H+}$ ionospheric contribution to the plasma sheet at 8–9 $R_E$ was 47% during quiet times, based on measurements in the 1.5–315 keV/e range. The $n_{H+}$ ionospheric contribution at 15 $R_E$ was 36% during quiet times and 65% during active times, based on measurements in the 26–228 keV/e range. However, these averages do not capture the variability of the ionospheric contribution with both solar EUV and geomagnetic activity.

Statistical studies of the mid-tail (distances of 10–30 $R_E$) plasma sheet meant to capture this variability have been performed using data from the ISEE satellites, Geotail, AMPTE, and Cluster. Lennartsson and Shelley (1986) and Lennartsson (1989) performed a statistical study of the plasma sheet ion composition using the Plasma Composition Experiment on ISEE 1, covering energies from 0.1 to 16 keV/e and radial distances from 10 to 23 $R_E$, during the rise of solar cycle 21, that is, 1978 and 1979. They compared their observations with geomagnetic activity using the Auroral Electrojet (AE) index, which measures the perturbations of the magnetic field in the auroral regions typically associated with substorm activity. They found a strong increase in the $n_{O+}/n_{H+}$ number density ratio with increasing AE, from 0.01 at low AE up to 0.6 at AE of 1,000 nT. This increase is due to an increase in the $O^+$ density by a factor of ~10, from 0.02 $cm^{-3}$ to 0.2 $cm^{-3}$, plus a reduction in $n_{H+}$ of a factor ~6. They also showed a distinct increase with solar EUV, with an increase of the $O^+$ density from 0.02 $cm^{-3}$ to 0.08 $cm^{-3}$ when the solar radio flux at 10.7 cm wavelength (F10.7 index, an excellent proxy for solar EUV activity), increase from 50 solar flux units (1 sfu = $10^{-22}$ $Wm^{-2}$ $Hz^{-1}$) to >200 sfu. Baumjohann et al. (1989) reported ion number densities for the plasma sheet at 9–14 $R_E$ using AMPTE and found values consistent with Lennartsson (1989). Nosé et al. (2009) used 16 years of data from the STICS instrument on Geotail (Energy range 9–212 keV) to examine the solar cycle variability. Their data set covered a wider range of distances, from 8 $R_E$ to 100 $R_E$. They showed the increase in the $n_{O+}/n_{H+}$ ratio from 0.01 to 0.06 as F10.7 increased from 70 to 200 sfu. Mouikis et al. (2010) performed a statistical analysis of the densities of $H^+$ and $O^+$ inside the plasma sheet using a more limited range of radial distances, 15–19 $R_E$, using 5 years of data (2001–2005) from the CIS/CODIF instrument in the Cluster mission. The instrument operates in the range of 40 eV–40 keV. Comparing the $O^+$ density as a function of F10.7 from Cluster with the results of Lennartsson (1989), Mouikis et al. (2010) find a similar increase with F10.7, although Lennartsson (1989) observed overall higher densities (Figure 10a). This is likely because the radial range extended to lower radial distances, where the density is higher (as will be discussed). Figure 10b compares the $O^+/H^+$ density ratio from the Cluster study as a function of F10.7 with



19449208, 2021, 3, Downloaded from https://agupubs.onlinelibrary.wiley.com/doi/10.1029/2020RG000707 by Cochrane France, Wiley Online Library on [07/11/2022]. See the Terms and Conditions (https://onlinelibrary.wiley.com/terms-and-conditions) on Wiley Online Library for rules of use; OA articles are governed by the applicable Creative Commons License

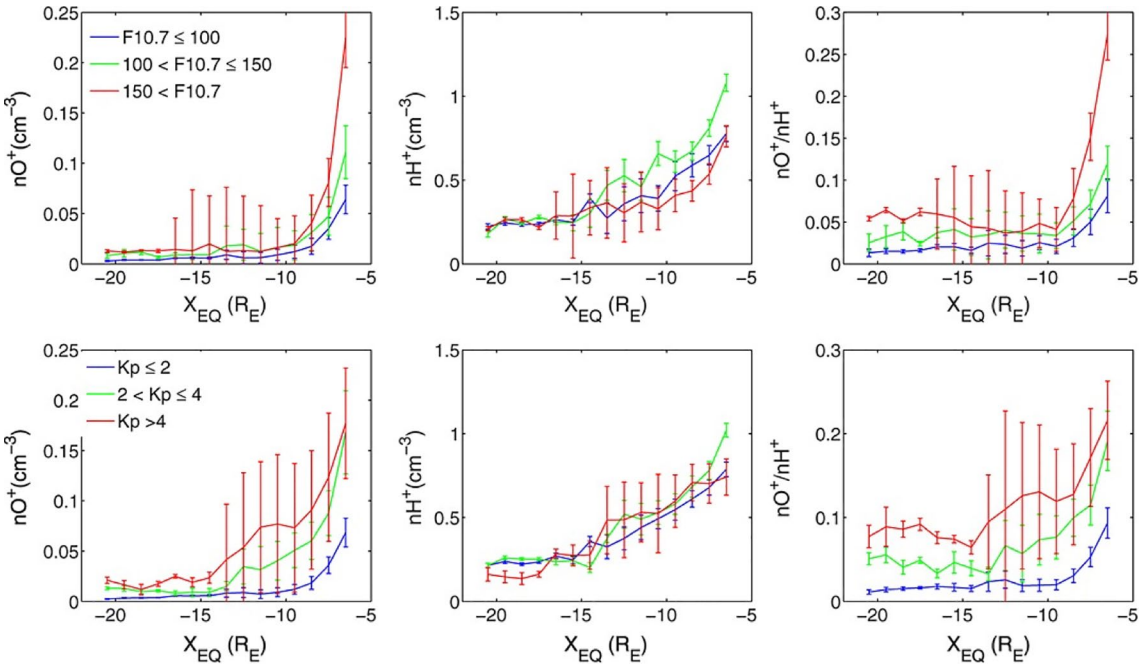



**Figure 11.** Radial dependence of the $O^+$ and $H^+$ densities in the plasma sheet, and their ratio. Adapted from Maggiolo and Kistler (2014).

the Nosé et al. (2009) results (blue). While the ratio level is about the same, Nosé et al. (2009) found a steeper slope with F10.7. This may be due to the higher energy range of the Nose study, or may be because the Geotail data accounted for all geomagnetic activity levels, while the Cluster data used are just for quiet times. Figure 10c compares the activity dependence found by the Cluster study with the results of Lennartsson and Shelley (1986) (blue). Again, the dependence is similar, but the ratio is higher in the ISEE study that covered closer radial distances. Clearly, all these studies agree that the density of $O^+$ and the $O^+/H^+$ density ratio increase both with solar EUV (as characterized by the F10.7 proxy), and with geomagnetic activity (characterized by the *Kp* or the AE indices). The solar EUV sets a baseline ratio for a given phase of the solar cycle, and geomagnetic activity further increases the $O^+$ content.

The plasma sheet densities closer to the Earth, at ~6–7 $R_E$, were characterized by Young et al. (1982) and Kistler and Mouikis (2016). Both studies cover the "hot" population, with Young et al. (1982) covering the 0.9–17 keV energy range using the GEOS data set (similar to the instrument on ISEE 1), and Kistler and Mouikis (2016) covering the 1–40 keV energy range using Cluster/CODIF. While the GEOS measurements were near-equatorial, the Cluster/CODIF measurements were taken at about ~30° latitude for this L-range, so the distribution was mapped along the field line to the equator to obtain comparable results. The $O^+$ density and the $O^+/H^+$ ratio in this region is about a factor of 10 higher than in the 15–19 $R_E$ region, as shown by the red lines in Figures 10a–10c, but show similar F10.7 and *Kp* dependencies. As was observed further out, EUV alone will increase the $O^+/H^+$ ratio by a factor of ~8, and then geomagnetic activity will increase it by another factor of 10.

Maggiolo and Kistler (2014) used a mapping technique to derive 2D maps of the $H^+$ and $O^+$ densities in the X-Y equatorial plane using the Cluster/CODIF data. Figure 11 shows the densities and density ratios as a function of the equatorial X position from this study. The $O^+$ density and the $O^+/H^+$ density ratios increase strongly inside $X = -10$, while the $H^+$ increases more gradually with decreasing distance. In the *Y*-direction, they did not observe a strong dawn-dusk asymmetry, but found the density and density ratios to be relatively flat from dawn to dusk across the magnetotail at distances of 15–20 $R_E$. Closer to the Earth, the densities peak close to midnight during quiet times, with the peak shifting dawnward for higher activity. However, the $O^+/H^+$ density ratio remains relatively uniform.

Figure 12, from Kistler and Mouikis (2016), summarizes the *Kp* dependence found in the near-earth plasma sheet from several studies. Data are shown for a medium range of F10.7, 100–150, but results for other F10.7



19449208, 2021, 3, Downloaded from https://agupubs.onlinelibrary.wiley.com/doi/10.1029/2020RG000707 by Cochrane France, Wiley Online Library on [07/11/2022]. See the Terms and Conditions (https://onlinelibrary.wiley.com/terms-and-conditions) on Wiley Online Library for rules of use; OA articles are governed by the applicable Creative Commons License

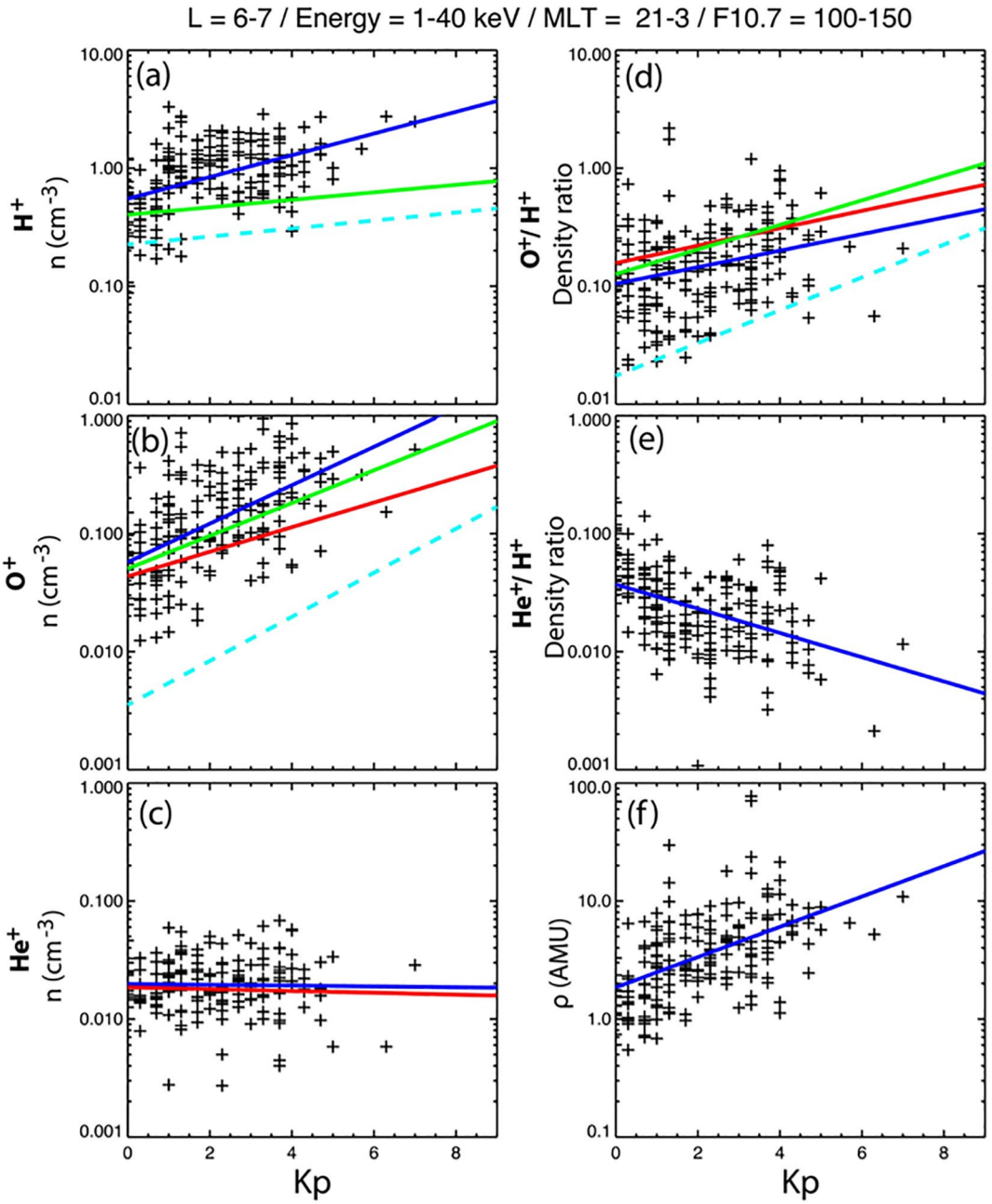



**Figure 12.** Ion composition as a function of geomagnetic activity (*Kp* index), comparing the studies of Kistler and Mouikis (2016) (black points and dark blue line fits, $L$ = 6–7), Maggiolo and Kistler (2014) (green lines, $L$ = 7–8), Young et al. (1982) (red lines, $L$ = 6.6), and Mouikis et al. (2010) (dashed light blue lines, $L$ = 15–19).

values are similar. The black points are the $L$ = 6–7 measurements from Kistler and Mouikis (2016), and the dark blue line is the fit to these points. The Maggiolo and Kistler (2014) fits for $L$ = 7–8 are shown in green, while the Young et al. (1982) fits are in red ($L$ = 6.6), and the Mouikis et al. (2010) results from $L$ = 15–19 are in light blue. The increase in $O^+$ and in the $O^+/H^+$ ratios with *Kp* agree very well between the three near-Earth studies, with the 15–19 $R_E$ study showing lower values, as expected because of the radial dependence. Surprisingly, $He^+$ shows almost no variation with *Kp*, which leads to a decreasing $He^+/H^+$ ratio with *Kp*. The final panel shows the increase in the overall mass density with *Kp*. This also increases by a factor of 10 with geomagnetic activity (Figure 12).



19449208, 2021, 3, Downloaded from https://agupubs.onlinelibrary.wiley.com/doi/10.1029/2020RG000707 by Cochrane France, Wiley Online Library on [07/11/2022]. See the Terms and Conditions (https://onlinelibrary.wiley.com/terms-and-conditions) on Wiley Online Library for rules of use; OA articles are governed by the applicable Creative Commons License

19449208, 2021, 3, Downloaded from https://agupubs.onlinelibrary.wiley.com/doi/10.1029/2020RG000707 by Cochrane France, Wiley Online Library on [07/11/2022]. See the Terms and Conditions (https://onlinelibrary.wiley.com/terms-and-conditions) on Wiley Online Library for rules of use; OA articles are governed by the applicable Creative Commons License

The studies described so far have analyzed the hot plasma sheet population, which is composed of a mixture of heated ions of both solar wind and ionospheric origin. There is also evidence of a cold, low-energy population of ionospheric origin in the plasma sheet, coexisting with the hot population. Seki et al. (2003) presented observations from time periods when the Geotail spacecraft is in eclipse and therefore photoelectron emission is suppressed, which causes the spacecraft to charge negatively due to electrons from the ambient plasma impacting the spacecraft. This negative potential attracts the positive cold ions, and brings them up to an energy where they can be observed. Observations during these eclipse time periods showed the existence of a cold population with density comparable to the hot population. This cold ion population becomes also detectable by particle detectors when the bulk drift energy is larger than the equivalent spacecraft potential energy but smaller than the thermal energy of the hot plasma sheet population (e.g., Alm et al., 2018, 2019; Xu et al., 2019). André et al. (2015), using the wake method (cf. Section 3.1), conducted a statistical survey in the magnetotail and found this cold population only ~10% of the time inside the plasma sheet. However, with their method it is difficult to detect cold ions in the plasma sheet because to detect an extended wake, indicating the presence of cold ions, requires the cold ion density to be at least about half of the total density, and the bulk drift energy to be less than the equivalent spacecraft charging, and one or both of these two conditions are often not satisfied in the plasma sheet. In addition, to estimate the cold ion flux, observations by the EDI instrument are also needed, which is designed to operate in a reasonably steady and strong magnetic field, and this is often not the case in the plasma sheet. Lee and Angelopoulos (2014) also examined the number density of cold ions (energy below 1 keV) in the near tail (distances of 6–12 $R_E$), using THEMIS observations over ~5 years (January 2008–May 2013). They found occurrence rates in the night sectors varying between 5% and 35% depending on the distance to Earth, with the largest occurrences at $L = 4$–6. They report average cold $H^+$ densities in the tail of ~0.05–0.1 $cm^{-3}$ (see Figure 8), with average temperatures of ~10 eV. They also calculated the average $He^+$ and $O^+$ densities and temperatures of the cold ions (below 1 keV). Interestingly, they find higher number densities (~0.1 $cm^{-3}$ for $He^+$ and ~0.2 $cm^{-3}$ for $O^+$) than for $H^+$, and also larger temperatures (~50 eV for $He^+$ and ~200 eV for $O^+$).

### 3.3.2. Lobes

Magnetic reconnection in the magnetotail occurs first in the plasma sheet, where the stretched magnetic field lines from the northern and southern hemispheres form a thin current sheet. Magnetic reconnection then proceeds with lobe field lines, above and below the plasma sheet, which are filled only by high-latitude ionospheric outflows. These outflows either end up in the plasma sheet or are lost in the distant tail. As discussed in Section 2.2.2, ion outflows from the cusp and polar cap are accelerated along the field line through centrifugal acceleration, and are dispersed by the velocity filter effect into the lobes. Thus, the populations normally observed in the lobes are cold, field-aligned streams of ions. Even if the source population has a broad energy range, the lobe population will have a narrow velocity distribution because only a particular velocity reaches a particular location. Ion species with the same velocity will have a different energy by their mass ratio. Thus, in the 15–20 $R_E$ region, where these cold ions have been well-characterized by data from the Cluster mission, the lobe population consists of protons with energies of tens of electron volt (André et al., 2015; Engwall et al., 2009) while the $O^+$ ions are in the 40 eV–1 keV range (Liao et al., 2015). Svenes et al. (2008) inferred the electron number density indirectly from the Cluster spacecraft potential using 7 years of data from the waning part of solar cycle 23, and found that more than two thirds of the time the electron density, $n_e$, was between 0.007 and 0.092 $cm^{-3}$, with a most probable value (mode) of 0.047 $cm^{-3}$. These averages were independent of solar wind and geomagnetic conditions, but for the high-density tail of the distribution ($n_e > 0.2$ $cm^{-3}$), a correlation with the 10.7 cm solar radio flux was present. André et al. (2015) performed an extensive study of the lobe ion population over a solar cycle. Again, the spacecraft potential was used to estimate the density and an extended spacecraft wake was used to detect streaming cold ions and to estimate the ion flux. They find that a cold population is present at least 64% of the time at distances of 5–20 $R_E$, with average densities of 0.2–0.4 $cm^{-3}$, and average field-aligned velocities of 25–30 km/s. The outflow flux increases by a factor of ~2 with geomagnetic activity and with solar EUV over the solar cycle. The increase is mainly due to the density increasing, while the velocity distribution remains about the same.

The $O^+$ in the lobes was characterized by Liao et al. (2010, 2012, and 2015). During solar maximum, 2001–2002, the occurrence frequency of $O^+$ beams in the lobes is almost 100% during storms, but even during nonstorm times, the occurrence frequency is ~50%. The location of the $O^+$ ions in the lobes shows a dawn-dusk

19449208, 2021, 3, Downloaded from https://agupubs.onlinelibrary.wiley.com/doi/10.1029/2020RG000707 by Cochrane France, Wiley Online Library on [07/11/2022]. See the Terms and Conditions (https://onlinelibrary.wiley.com/terms-and-conditions) on Wiley Online Library for rules of use; OA articles are governed by the applicable Creative Commons License

asymmetry that depends on IMF By. When IMF By is positive, the $O^+$ in the northern lobe tends to be on the dawn side, while the $O^+$ in the southern lobe tends to be on the dusk side. For negative By, the asymmetry reverses, but not as strongly. If there are different amounts of outflow in the northern and southern hemisphere, this could lead to dawn-dusk asymmetries in the plasma sheet as well. The occurrence of the $O^+$ beams decreased significantly with solar cycle, with the decreases stronger in the tail lobes than in the polar cap. This decrease could be because the flux decreased below the threshold level for the instrument, or because the transport paths were modified, due to changes during the minimum of the solar cycle, so the $O^+$ beams no longer reach the near-earth plasma sheet.

The $H^+$ and $O^+$ populations in the lobes are clearly related, but a focused study comparing the two has not been done. Backwards modeling indicates that the proton population comes from the full range of the polar cap (Li et al., 2013), while the more energetic $O^+$ is thought to come from the cusp. Liao et al. (2015) showed that during quiet times, the $O^+$ beam fluxes observed were consistent with the outflow fluxes from the cusp, while during more active times, some additional acceleration of the cusp outflow population was required. The densities and velocities of the two populations during the solar maximum time period are compared in Kronberg et al. (2014). The $H^+$ number density is significantly higher than the $O^+$ (average 0.14 $cm^{-3}$ for $H^+$, vs. 0.009–0.02 $cm^{-3}$ for $O^+$), but the velocity range is similar (~40 km/s), suggesting they come on average from the same source based on the velocity filter effect.

### 3.3.3. Comparison Between Studies

We summarize, in Table 2, the statistical observations of the $H^+$ number density ($n_{H+}$), $H^+$ percent of ionospheric origin when available, and $O^+/H^+$ number density ratio ($n_{O+}/n_{H+}$), for the various studies presented in the near-Earth plasma sheet (<10 $R_E$), distant plasma sheet (>10 $R_E$) and tail lobes. In the following subsections we discuss the implications of Table 2.

#### *3.3.3.1. Near-Earth Plasma Sheet (<10 $R_E$)*

The $H^+$ number density in the near-Earth plasma sheet (less than 10 $R_E$ from Earth) depends mainly on the distance to Earth and geomagnetic activity, and to a lesser degree on solar EUV. It is estimated that roughly half of $H^+$ ions are of ionospheric origin (Gloeckler & Hamilton, 1987). From Table 2, it is deduced that for ions with total energies above 1 keV, $n_{H+} \sim 0.3$–$0.8$ $cm^{-3}$ for quiet magnetospheric conditions ($Kp < 3$), and $n_{H+} \sim 0.4$–$1.3$ $cm^{-3}$ for disturbed conditions ($Kp > 3$). In addition, there is a cold ion component (total energy < 1 keV) with $n_{H+} < 0.1$ $cm^{-3}$ (Lee & Angelopoulos, 2014), likely of ionospheric origin. The ratio of $O^+/H^+$ number densities strongly depends on geomagnetic activity, with $n_{O+}/n_{H+} \sim 0.1$–$0.5$ for quiet conditions ($Kp < 3$) and $n_{O+}/n_{H+}$ 0.2–1.3 for disturbed conditions ($Kp > 3$). Both $H^+$ and $O^+$ number densities increase during disturbed conditions, but the increase in $O^+$ number density is larger. The number densities reported vary up to half an order of magnitude depending on the study, and this is attributable to multiple factors including solar cycle, distance to Earth, other orbital biases (magnetic local time, latitude), and ion energy range considered by each study.

#### *3.3.3.2. Distant Plasma Sheet (>10 $R_E$)*

In the distant tail, the total $H^+$ number density does not depend that much on geomagnetic activity (Maggiolo & Kistler, 2014; Mouikis et al., 2010) as in the near-Earth tail. Lennartsson and Shelley (1986) found an anti-correlation between geomagnetic activity and $H^+$ number density, as opposed to the near-Earth plasma sheet. However, the relative contributions of the ionosphere and the solar wind do depend on geomagnetic activity, with around one third of the $H^+$ ions coming from the ionosphere during quiet times, and around two thirds coming from the ionosphere during disturbed times. Overall, at distances of 15–20 $R_E$, $n_{H+} \sim 0.2$–$0.3$ $cm^{-3}$, and is somewhat larger ($n_{H+} \sim 0.5$ $cm^{-3}$) when distances at 10–15 $R_E$ are included in the study. The dependence of $n_{H+}$ with solar EUV is also small. On the other hand, the amount of ionospheric $O^+$ in the distant plasma sheet depends largely on geomagnetic activity, as for the near-Earth plasma sheet. Typical $O^+/H^+$ density ratios are $n_{O+}/n_{H+} < 0.1$ for quiet times and $n_{O+}/n_{H+} \sim 0.2$–$0.7$ for disturbed times. In addition, Seki et al. (2003) reported the existence of a cold, hidden plasma population of ionospheric origin (up to a few electron volt) that was only visible during spacecraft eclipses, with number densities of ~0.2 $cm^{-3}$ and present <50% of the time.

**Table 2**
*Statistical Studies of Number Density and Plasma Composition in the Earth's Magnetotail*

| | | Geocentric distance ($R_E$) | $n_{H+}$ of ionospheric origin (%) | Mean $n_{H+}$ Observed ($cm^{-3}$) | Energy range (keV/e) | Observed $n_{O+}/n_{H+}$ |
|---|---|---|---|---|---|---|
| Near-Earth Plasma sheet | Young et al. (1982) | 6–7 | - | 0.3–0.4[a] ($Kp < 3$) | 0.9–16 | 0.4–0.5[a] ($Kp < 3$) |
| | | | | | | 0.5–0.9[a] ($3 < Kp < 6$) |
| | | | | 0.4–0.5[a] ($3 < Kp < 6$) | | 0.9–1.4[a] ($Kp > 6$) |
| | | | | 0.5–0.6[a] ($Kp > 6$) | | |
| | Gloeckler and Hamilton (1987) | 8–9 | 47 | 0.35[b] (quiet) | 1.5–315 | 0.11[b] |
| | Lennartsson (1989) | <10 | - | 0.8[a] (F10.7 < 100) | 0.1–16 | 0.1[a] (F10.7 < 100) |
| | | | | 0.68[a] (100 < F10.7 < 150) | | - |
| | | | | 0.62[a] (150 < F10.7 < 200) | | - |
| | | | | 0.58[a] (F10.7 > 200) | | - |
| | Lee and Angelopoulos (2014) | 5–10 | - | <0.1[c] | <1 | >1[c] |
| | Maggiolo and Kistler (2014) [d] | 7–8 | - | 0.4–0.5[a] ($Kp < 3$) | 1–40 | 0.2–0.3[a] ($Kp < 3$) |
| | | | | | | 0.3–0.6[a] ($3 < Kp < 6$) |
| | | | | 0.5–0.7[a] ($3 < Kp < 6$) | | 0.6–1.3[a] ($Kp > 6$) |
| | | | | 0.7–0.8[a] ($Kp > 6$) | | |
| | Kistler and Mouikis (2016) [d] | 6–7 | - | 0.6–0.8[a] ($Kp < 2$) | | 0.1[a] ($Kp < 2$) |
| | | | | | | 0.1–0.2[a] ($2 < Kp < 4$) |
| | | | | 0.8–1.3[a] ($2 < Kp < 4$) | | 0.2–0.5[a] ($Kp > 4$) |
| | | | | >1.3[a] ($Kp > 4$) | | |
| Distant Plasma sheet | Lennartsson and Sharp (1985) | 10–23 | 20–30(AE <100) | - | 0.1–16 | <0.1 (AE < 100 nT) |
| | | | | | | 0.2–0.7 (AE > 300 nT) |
| | Lennartsson and Shelley (1986) | 10–23 | - | 0.5–1[a] (AE < 100) | | 0.01–0.08[a] (AE < 100 nT) |
| | | | | 0.2–0.3[a] (AE > 700) | | 0.6[a] (AE > 700 nT) |
| | Gloeckler and Hamilton (1987) | 15 | 37 (quiet) | 0.015[b] (quiet) | 28–226 | 0.09[b] (quiet) |
| | | | 65 (disturbed) | 0.03[b] (disturbed) | | 0.17[b] (disturbed) |
| | Baumjohann et al. (1989) | 9–14 | - | 0.5 (AE < 100) | 0.02–40 | - |
| | | | | 0.4 (AE > 100) | | |
| | Lennartsson (1989) | >10 | - | 0.65[a] (F10.7 < 100) | 0.1–16 | 0.03[a] (F10.7 < 100) |
| | | | | 0.55[a] (100 < F10.7 < 150) | | 0.05[a] (100 < F10.7 < 150) |
| | | | | 0.4[a] (150 < F10.7 < 200) | | 0.15[a] (150 < F10.7 < 200) |
| | | | | 0.48[a] (F10.7 > 200) | | 0.15[a] (F10.7 > 200) |
| | Seki et al. (2003) | 9–18 | ~50[c] | ~0.2[c] | <1 | < 0.5[c] |
| | Mouikis et al. (2010) | 15–19 | - | 0.2–0.3[a] | 1–40 | 0.01–0.07[a] |
| | Maggiolo and Kistler (2014) [d] | 15–20 | - | ~0.3[a] | | 0.01–0.05[a] ($Kp < 3$) |
| | | | | | | 0.05–0.2[a] ($3 < Kp < 6$) |
| | | | | | | 0.2–0.7[a] ($Kp > 6$) |



19449208, 2021, 3, Downloaded from https://agupubs.onlinelibrary.wiley.com/doi/10.1029/2020RG000707 by Cochrane France, Wiley Online Library on [07/11/2022]. See the Terms and Conditions (https://onlinelibrary.wiley.com/terms-and-conditions) on Wiley Online Library for rules of use; OA articles are governed by the applicable Creative Commons License

**Table 2**
*Continued*

| | | Geocentric distance ($R_E$) | $n_{H+}$ of ionospheric origin (%) | Mean $n_{H+}$ Observed ($cm^{-3}$) | Energy range (keV/e) | Observed $n_{O+}/n_{H+}$ |
|---|---|---|---|---|---|---|
| Tail lobes | Svenes et al. (2008) | 5–19 | >90%[e] | 0.047 | N/A[f] | - |
| | André et al. (2015) | 5–10 | | ~0.25 ($Kp < 3$) | Up to tens of electron volt | - |
| | | | | 0.3–0.7 ($Kp > 3$) | | |
| | | 10–15 | | 0.1–0.2 ($Kp < 3$) | | |
| | | | | 0.2–0.3 ($Kp > 3$) | | |
| | | 15–20 | | <0.1 ($Kp < 3$) | | |
| | | | | 0.1–0.2 ($Kp > 3$) | | |

[a]Considers $n_{H+}$ of ionospheric origin only. [b]Considers total $n_{H+}$, ionospheric plus solar wind origin. [c]The values reported in the table correspond to F10.7 = 100–150 sfu (1 sfu = $10^{-22}$ $Wm^{-2}H$ $z^{-1}$). [d]Accounts only for cold $n_{H+}$. [e]The ion number density is inferred indirectly from the spacecraft potential measurement. [f]Plasma in the lobes is almost entirely of ionospheric origin, although the studies presented do not attempt to quantify the origin.

#### *3.3.3.3. Lobes*

In the tail lobes, the main source of plasma is ionospheric outflows. The lobe populations are usually cold due to the cold nature of the classical polar wind and the velocity filter effect (cf. Section 2.2.2), and therefore they cannot be easily characterized using in situ ion detectors. We report the results of two studies that used an indirect technique to infer the ion number density in the lobes using the Cluster spacecraft. The average densities reported (cf. Table 2) are roughly consistent but the estimates are somewhat larger in André et al. (2015) than in Svenes et al. (2008). This difference can be explained by the different datasets employed. Svenes et al. (2008) inferred the ion number density from the spacecraft potential, and found the most probable number density to be $n = 0.047$ $cm^{-3}$. André et al. (2015) selected data when the spacecraft wake showed that a majority of the ions were cold, and also used the spacecraft potential to estimate the density. Only events with an observed wake (drifting cold ions) and reliable EDI observations were included in the density statistics. In addition, to avoid large errors, only events with $n > 0.01$ $cm^{-3}$ were included. These criteria result in the selection of observations with mainly cold ions and exclude observations with low density, especially at high altitudes. As a result, André et al. (2015) reported cold ion detections 64% of the time, and found $n > 0.1$ $cm^{-3}$ for most radial distances and geomagnetic conditions. The two methods showed correlation with geomagnetic activity ($Kp$ index) for the cases with large densities (above 0.2 $cm^{-3}$).

### 3.3.4. Relative Importance of Ionospheric-Originating Ions in the Earth's Magnetotail

It is well known that $O^+$, and cold $H^+$ in the lobes and in the plasma sheet are of ionospheric origin. However, hot $H^+$ in the plasma sheet are from both the solar wind and the ionosphere. From inspection of Table 2, the conclusions are that the ionospheric source is the dominant $H^+$ source during disturbed magnetospheric conditions. During quiet times, the dominant $H^+$ source is the solar wind, and on average, that is, quiet plus disturbed times, both $H^+$ sources are of the same order of magnitude. However, the number of statistical surveys that attempt to distinguish the two $H^+$ sources is small. In terms of mass density, the near-Earth plasma sheet is most of the time dominated by the ionospheric source, owing to the $O^+$ contributions. Various studies present the statistics as a function of geomagnetic activity or solar irradiance flux, but we also expect the correlation between plasma sheet parameters and IMF orientation to be large, because of increased convection of magnetic field lines from the lobes, favoring loading of the plasma sheet (e.g., Kistler, 2020).

## 4. Effects of Ionospheric-Originating Ions on Magnetic Reconnection

Magnetic reconnection is one of the most important transport and energy conversion process in collisionless plasmas. It causes the transport of mass, momentum and energy across topologically distinct plasma regions, initially separated by a thin current sheet. Reconnection regulates solar eruptions, plays a key role in determining the shape and dynamics of planetary magnetospheres, and is involved in major disruptions



19449208, 2021, 3, Downloaded from https://agupubs.onlinelibrary.wiley.com/doi/10.1029/2020RG000707 by Cochrane France, Wiley Online Library on [07/11/2022]. See the Terms and Conditions (https://onlinelibrary.wiley.com/terms-and-conditions) on Wiley Online Library for rules of use; OA articles are governed by the applicable Creative Commons License

19449208, 2021, 3, Downloaded from https://agupubs.onlinelibrary.wiley.com/doi/10.1029/2020RG000707 by Cochrane France, Wiley Online Library on [07/11/2022]. See the Terms and Conditions (https://onlinelibrary.wiley.com/terms-and-conditions) on Wiley Online Library for rules of use; OA articles are governed by the applicable Creative Commons License

in astrophysical systems, such as magnetar flares. Even on the ground, in the laboratory, reconnection is an important, albeit undesirable, process in fusion machines, as it can destroy magnetic field confinement. At the Earth's dayside magnetopause, it facilitates the entry of solar wind particles and magnetic energy into the magnetosphere. On the nightside, magnetic reconnection dissipates the accumulated magnetic energy, leading to substorms, storms and auroras, and powers the majority of the deleterious space environment effects collectively referred to as Space Weather.

Owing to its importance, magnetic reconnection has been studied for quite some time, see for instance the review by Yamada et al. (2010), and the review of observations of reconnection by Fuselier and Lewis (2011) and Cassak and Fuselier (2016). Decades of attempts to understand its inner machinery have recently culminated in breakthrough insights into how reconnection works, enabled by the combination of observations from the MMS spacecraft mission, theory and modeling. However, we still know very little about how it starts, and even less about how it stops.

Magnetic reconnection is enabled through a local decoupling between the particles and the magnetic field, which occurs at the smallest spatial scales of the plasma, that is, the electron inertial length and gyroradius, in the so-called Electron Diffusion Region (EDR). The coupling between the magnetic flux transport and the flow of ions and electrons is described by the equation of the electric field. A general way of looking for regions where this coupling is violated is by analyzing the generalized Ohm's law (Vasyliunas, 1975):

$$\mathbf{E}+\mathbf{v}\times\mathbf{B}=\eta\mathbf{J}+\frac{m_e}{e^2n}\left[\frac{\partial\mathbf{J}}{\partial t}+\nabla\cdot\left(\mathbf{J}\mathbf{v}+\mathbf{v}\mathbf{J}\right)\right]-\frac{\nabla\cdot\mathbf{P}_e}{en}+\frac{\mathbf{J}\times\mathbf{B}}{en}, \tag{1}$$

where $m_e$ is the electron mass, $e$ is the elementary charge, $\mathbf{v}$ is the plasma velocity, $\mathbf{J}$ is the current density, $n$ the plasma number density, $\eta$ the plasma resistivity and $\mathbf{P_e}$ the electron pressure tensor. The different terms on the right-hand side correspond to effects that violate the frozen-in condition ($\mathbf{E}+\mathbf{v}\times\mathbf{B}=0$), a condition where the magnetic field is carried together with the average plasma flow. For magnetic reconnection, such effects must be present to support the necessary electric field which allows the magnetic field to dissipate and merge, changing the topology of magnetic field lines.

The non-ideal terms (right-hand side terms of Equation 1) are characterized by characteristic time or spatial scales, related to the intrinsic properties of the plasma. Owing to the different mass of ions and electrons, they decouple at different scales. The largest of the characteristic scales in Equation 1 corresponds to the Hall term, $\mathbf{J}\times\mathbf{B}/\left(en\right)$, which describes when the ion motion differs from the electron motion and two-fluid effects are in play. This occurs in the Ion Diffusion Region (IDR), with a characteristic spatial scale corresponding to the ion inertial length.

The rest of the right-hand side terms of Equation 1 become non-negligible at electron scales, that is, in the Electron Diffusion Region (EDR). Space plasmas are very dilute and collisions between particles are often negligible. Therefore, dissipation of the magnetic field (positive $\mathbf{J}\cdot\mathbf{E}$) inside the EDR must occur in an unconventional way, since the collisional resistivity is too weak to explain the observations. One of the primary objectives of the MMS mission is to unravel which processes generate sufficient anomalous resistivity for the magnetic field to diffuse and reconfigure inside the EDR in collisionless plasmas. Wave-particle interactions are a strong candidate for the generation of anomalous resistivity (e.g., Burch et al., 2018; Graham et al., 2017b; Li et al., 2020).

The presence of additional plasma populations, for example, ions of ionospheric origin, with different temperature or mass, has an impact on the different characteristic time and spatial scales associated with the diffusion regions, and affects how the process converts magnetic energy into thermal and kinetic particle energy. Understanding how different plasma populations couple to the reconnection process is what renders the physical process elusive and challenging. The characteristics of the plasma particle gyro orbits around the magnetic field lines can be quantified by the Larmor radius or gyroradius ($R_{gs}$) and the cyclotron frequency ($\omega_{cs}$)

$$R_{gs}=\frac{m_s v_{Ts}}{q_s B},\quad \omega_{cs}=\frac{q_s B}{m_s}, \tag{2}$$

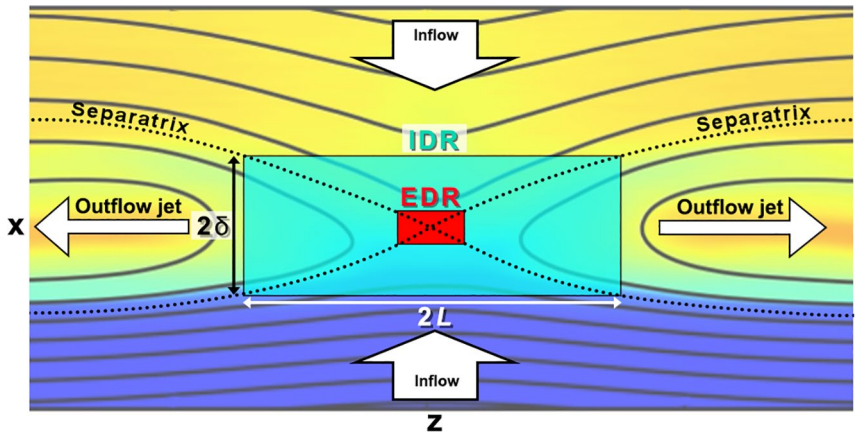



**Figure 13.** Particle-in-cell simulation of magnetic reconnection. The magnetic field lines (solid black lines) break and reconnect at the Electron Diffusion Region, generating reconnection outflow jets. In this 2D simulation, the two topological regions that reconnect, have different magnetic field strength and electron density (color-coded), imitating solar wind (top region) – magnetosphere (bottom region) magnetic reconnection. Credit: J. M. Domínguez, adapted from Dargent et al. (2017).

where subscript $s$ denotes the particle species, $v_T$ is the thermal speed, $q$ is the particle charge, $m$ is the particle mass and $B$ is the magnetic field magnitude. A colder plasma population will, for instance, have a smaller Larmor radius, while the cyclotron frequency remains unchanged, as it does not depend on the thermal speed. If the plasma contains a heavier plasma population (e.g., $He^+$, $O^+$), the cyclotron frequency will be smaller (assuming a comparable thermal speed), which has a profound influence on the time evolution of the reconnection process, as discussed in Section 4.2.

The ion inertial length is, by definition, equal to the Larmor radius when $v_{Ti} = v_A$, that is, the thermal velocity and Alfvén velocity ($v_A^2 = B^2 / \mu_0 \rho_i$) are equal. For a species $s$, the inertial length ($d_s$) and the plasma frequency ($\omega_{ps}$) are defined as

$$d_s = \frac{c}{\omega_{\mathrm{ps}}}, \quad \omega_{\mathrm{ps}} = \left( \frac{n_s q_s^2}{\varepsilon_0 m_s} \right)^{1/2}, \tag{3}$$

where $c$ is the speed of light, $\varepsilon_0$ is the vacuum dielectric permittivity, and $n_s$ is the species number density. The characteristic size of the IDR and EDR are more precisely described by the particles' bounce width, which involves the thermal velocity of the particles and therefore scales approximately as the Larmor radius.

Figure 13 shows a 2D particle-in-cell simulation model of asymmetric magnetic reconnection (Dargent et al., 2017) that mimics the conditions of coupling between the solar wind (top) and the magnetosphere (bottom). The main regions, namely the EDR, IDR, inflow regions, outflow regions, and separatrices, are sketched. Once the magnetic field reconnects at the EDR, its new topology consists of highly bent magnetic field lines, which accelerate the plasma to reduce their magnetic tension, generating the so-called reconnection jets, and can extend to spatial scales much larger than the EDR. The center of the EDR is known as the X-point in two dimensions, and extends out of the reconnection plane (XZ plane in Figure 13) forming an X-line in the $Y$ direction in the realistic three-dimensional case. Magnetic reconnection initiates and is maintained at the EDR, but its consequences extend to much larger spatial scales. For instance, in the Earth's magnetosphere, it mediates solar wind plasma entry and drives the global magnetospheric convection cycle.

As we have seen in Section 3.2 and 3.3, plasma of ionospheric origin can dominate the mass density on the magnetospheric side of the magnetopause and in the tail. The system is mass-loaded and the characteristic Alfvén speed is modified, resulting in modified reconnection efficiency. This effect is investigated further in Section 4.1. Additional plasma populations also modify the structure and dynamics of the reconnection region, owing to the introduction of multiple time and spatial scales. In Section 4.2, we discuss recent modeling and observational works focusing on these effects. The energy conversion due to magnetic



19449208, 2021, 3, Downloaded from https://agupubs.onlinelibrary.wiley.com/doi/10.1029/2020RG000707 by Cochrane France, Wiley Online Library on [07/11/2022]. See the Terms and Conditions (https://onlinelibrary.wiley.com/terms-and-conditions) on Wiley Online Library for rules of use; OA articles are governed by the applicable Creative Commons License

19449208, 2021, 3, Downloaded from https://agupubs.onlinelibrary.wiley.com/doi/10.1029/2020RG000707 by Cochrane France, Wiley Online Library on [07/11/2022]. See the Terms and Conditions (https://onlinelibrary.wiley.com/terms-and-conditions) on Wiley Online Library for rules of use; OA articles are governed by the applicable Creative Commons License

reconnection occurs on scales much larger than the tiny electron diffusion region, involving the ion diffusion region, the separatrices and the exhausts, where the bulk of magnetic energy is converted to particle energy, including the energy of incoming cold ions. We review recent works on the energy balance of magnetic reconnection involving ionospheric-originating ions in Section 4.3. In Section 4.4, we discuss how the presence of heavy ions (mainly $O^+$) in the magnetotail changes its effective thickness and stability, and how this affects reconnection onset. Section 4.5 discusses the capability of ionospheric populations to suppress magnetic reconnection at the dayside magnetopause.

### 4.1. Reconnection Rate and Mass-Loading (Macroscopic View)

To quantify the reconnection rate, that is, the amount of magnetic flux that is reconnected per unit time, we proceed with a scaling analysis of the quantities involved in the reconnection process. This scaling analysis will allow us to quantify the rate based on quantities measured in the inflow region alone. The aspect ratio ($\delta/L$) of the ion diffusion region (see Figure 13) follows from the mass continuity equation, and can be related to the rate at which magnetic reconnection proceeds, that is, the amount of magnetic flux that is reconnected per unit time. Assuming the system is in steady-state, the evolutionary equation for mass is

$$\oint_S d\mathbf{S}\cdot\left(\rho\mathbf{v}\right) = 0, \tag{4}$$

where $\mathbf{v}$ is the flow velocity, $\rho$ is the mass density and $d\mathbf{S}$ is the outward directed area element of the surface $\mathbf{S}$. By considering one quarter of the ion diffusion region in Figure 13, mass continuity relates the mass transport across the inflow surface and outflow surface:

$$\rho_{\text{in}} v_{in} L \sim \rho_{\text{out}} v_{\text{out}} \delta. \tag{5}$$

By evaluating the energy equation (assuming pressure does not contribute to the energy conversion), or by the momentum equation under the assumption that the outflow advection is driven by pressure (Sweet-Parker scheme), an expression for the outflow velocity is found:

$$v_{\text{out}}^2 = \frac{B_0^2}{\mu_0 \rho} = v_A^2, \tag{6}$$

where $\rho$ is the average mass density flowing into the diffusion region from both sides, and $B_0$ is the magnetic field magnitude adjacent to the diffusion region, which is assumed to be approximately equal to $B$ anywhere outside the field reversal region. Thus, the advection speed out of the diffusion region, and consequently the inflow speed, are approximately limited to the Alfvén speed just outside the diffusion region. For details, see Vasyliunas (1975).

The normalized reconnection rate is then readily defined as the ratio between the inflow and the outflow velocity, which can be related to the aspect ratio of the diffusion region

$$M_A = \frac{v_{\text{in}}}{v_A} \sim \frac{\delta}{L}, \tag{7}$$

where we have assumed an incompressible flow ($\nabla\cdot\mathbf{v} = 0$), and an outflow speed equal to the Alfvén speed. The reconnection rate is directly related to the out of plane electric field in the diffusion region for 2D geometries ($E_y$ in the coordinates of Figure 13, also known as reconnection electric field). We assume that $\mathbf{E} = -\mathbf{v}\times\mathbf{B}$ holds at the edges of the diffusion region, that is, the ions are frozen-in to the magnetic field outside the diffusion region, leading to $v_{\text{in}} B_x = v_{\text{out}} B_z$. Taking advantage of $\nabla\cdot\mathbf{B} = 0$, we find

$$E \sim v_A B_z = v_A B_x \frac{\delta}{L}. \tag{8}$$

In steady-state reconnection, the aspect ratio is typically $\delta/L \sim 0.1$, found consistently in numerical simulations, spacecraft observations and laboratory experiments (e.g., Cassak et al., 2017; Parker, 1973; Yamada et al., 2010). As part of the Geospace Environment Modeling (GEM) challenge (Birn et al., 2001), different

models of simulations were tested and all the models including the Hall term (multi-fluid, hybrid and full Particle-In-Cell) showed normalized reconnection rates comparable to the 0.1 value. Therefore, many concluded that the Hall term was the cause of the normalized reconnection rate having a rate of 0.1. However, subsequent works questioned this conclusion (Cassak et al., 2017, and references therein). Liu et al. (2017) recently proposed that this specific value of the reconnection rate likely arises from MHD scale physics. They showed that by maximizing the reconnection rate within MHD-scale constraints, one obtains a maximum reconnection rate around 0.1–0.2. Furthermore, they showed that the weakening of the upstream reconnecting field as it extends toward the X-line is more important to the reconnection rate than the weakening of the outflow speed. This is another clue that the MHD-scale play a more important role in this problem compared to the kinetic scales, that were of prior importance in the previous assumption of a Hall term dependence. Liu et al. (2018) generalized those results for asymmetric magnetic reconnection, obtaining similar results.

The reconnection electric field value depends, therefore, on the plasma conditions (magnetic field and mass density) upstream of the diffusion region. Varying plasma properties in the inflow region can directly be related to the reconnection electric field through the Alfvén velocity. As we have seen in Sections 2 and 3, ionospheric plasma contributions to the mass density in the reconnection regions are often significant. The additional mass lowers the Alfvén speed, resulting in a reduced reconnection electric field and reconnection rate. This effect is termed the "mass-loading effect". Intuitively, additional mass means that the flux tubes have more inertia, making it harder to push the reconnected flux tubes out of the way in the outflow region.

In a symmetric configuration, where the mass-density and the magnetic field of the two inflow regions is equal, the relation between the reconnection electric field, Alfvén velocity and aspect ratio is straightforward and given in Equation 8. For asymmetric reconnection, where both the density and magnetic field strength are different between the two inflow regions, the scaling must include the appropriate contributions from the two inflow regions (1 and 2) to find the effective Alfvén speed (Cassak & Shay, 2007):

$$E \sim \left( \frac{\rho_{\text{out}} B_1 B_2}{\rho_1 B_1 + \rho_2 B_2} \right) v_{\text{out}} \frac{2\delta}{L}, \tag{9}$$

which reduces to Equation 8 if the density at both inflow regions are the same and equal to the outflow density ($\rho_1 = \rho_2 = \rho_{\text{out}}$), and the magnetic field is symmetric ($B_1 = B_2$).

#### 4.1.1. Local, In Situ Observations of the Mass-Loading Effect of Ionospheric Plasma

Various works have attempted to measure the mass-loading effect on the reconnection rate at the dayside magnetopause, using in situ spacecraft observations. Su et al. (2000) provided the first observational evidence of the plasmaspheric plume participating in dayside magnetic reconnection. Their observations were made from satellites at geosynchronous orbit (6.6 $R_E$), and therefore their magnetopause observations correspond to times when the magnetosphere is highly compressed by the solar wind. They observed magnetosheath and plume plasma simultaneously in the same flux tube, concluding that the plume participated in reconnection instead of being convected toward the tail in closed field lines, indicating that the ionospheric-originating ions can potentially mass-load the reconnecting magnetopause. More recently, Walsh et al. (2013) performed a statistical study of reconnecting magnetopause observations with and without a plasmaspheric plume using the THEMIS mission (cf. Section 3.2.2). They found that the outflow velocity resulting from magnetic reconnection was on average smaller for the events with the plume, and attributed this behavior to mass-loading of the magnetopause by plasmaspheric ions, providing the first in situ evidence of the mass-loading effect of ionospheric ions. Walsh et al. (2014) also showed that when the reconnecting magnetopause is mass-loaded from the magnetosphere side, the jet is displaced toward the magnetosheath side. Wang et al. (2015) measured the reconnection electric fields in eight magnetopause crossings by the Cluster mission, and normalized them to the magnetosheath and magnetosphere upstream conditions, where some of them included cold protons and heavy ions ($O^+$) on the magnetospheric side. Comparing their measurements to the scaling law in Equation 9, they estimated an average aspect ratio of ~0.07. Slightly better correlation was obtained when only magnetosheath upstream parameters were used, providing an aspect ratio of 0.09. Overall, they found that the reconnection rate mainly depends on magnetosheath parameters, although significant changes (~20%) on the reconnection rate may be produced by



19449208, 2021, 3, Downloaded from https://agupubs.onlinelibrary.wiley.com/doi/10.1029/2020RG000707 by Cochrane France, Wiley Online Library on [07/11/2022]. See the Terms and Conditions (https://onlinelibrary.wiley.com/terms-and-conditions) on Wiley Online Library for rules of use; OA articles are governed by the applicable Creative Commons License

ionospheric ion mass loading. However, direct measures of the reconnection electric field based on local in situ measurements are challenging and require a number of assumptions and approximations. These include the dependence on distance to the X line, the ability to determine the reconnection plane, and the **E** field measurement itself, since the typical reconnection electric field values in the dayside magnetopause are a few mV/m (Genestreti et al., 2018).

Fuselier et al. (2017) and Fuselier, Mukherjee, et al. (2019) conducted a statistical survey using 5 months of MMS observations (phase 1a) and inferred the mass-loading capabilities of the ionospheric ions. More details on this study are found in Section 3.2. In contrast to Walsh et al. (2013) and Wang et al. (2015), the reconnection $E$ field is not directly measured, it is inferred from Equation 9. They concluded that, for nominal magnetospheric activity, the warm plasma cloak and the plasmaspheric plume can reduce the reconnection electric field by more than 20% only a few percent of the time. They also found that during geomagnetic storms the warm plasma cloak is rich in $O^+$ and dominates the magnetospheric mass density. During disturbed conditions, they found that the warm plasma cloak would reduce the reconnection electric field, due to mass-loading, by more than 20% about 25% of the time. By rewriting Equation 9 it is straightforward to show that the reduction of the reconnection electric field due to magnetospheric mass-loading (ML) can be rewritten as:

$$R = \frac{E_{\mathrm{ML}}}{E_s} = \frac{1}{\sqrt{1 + \frac{\rho_m B_s}{\rho_s B_m}}}, \tag{10}$$

where subscripts $m$ and $s$ correspond to magnetosphere and magnetosheath, respectively (Borovsky et al., 2013). If the magnetospheric mass density $\rho_m = 0$, then $R = 1$ and there is no reduction due to magnetospheric mass-loading. On the other hand, if $\rho_m >> \rho_s$, $R \sim 0$. Using typical values for magnetospheric and magnetosheath B field ($B_{\mathrm{m}} = 50$ nT, $B_{\mathrm{s}} = 20$ nT) and for magnetosheath mass density ($\rho_{\mathrm{s}} = 20$ amu·cm$^{-3}$, that is, atomic mass unit per cubic centimeter), one finds that the magnetosphere density has to be $\rho_m = 28$ amu·cm$^{-3}$ to produce a reduction of 20% in the reconnection rate due to magnetospheric mass-loading. Based on the results of Section 3.2, summarized in Table 1, this mass density at the magnetopause has been reported but it is rare. Very dense plasmaspheric material, rich $O^+$ warm plasma cloak or a highly compressed magnetosphere ($\rho_{\mathrm{m}} \sim 30$ amu·cm$^{-3}$ at L-shell = 5, Sheeley et al., 2001) can lead to densities of ~28 amu·cm$^{-3}$ at the magnetopause. Such high-density magnetospheric plasma near the magnetopause occurs mainly during geomagnetic storms. For instance, Fuselier, Haaland, et al. (2020) compiled a database of magnetopause crossings on the dayside with the highest $He^+$ densities. These events consisted of high-density plasmaspheric plume material. These extreme events showed that the magnetospheric mass density can reach values above 50 amu·cm$^{-3}$, which would cause a reduction of the reconnection rate of about 40%. In addition, during periods of northward IMF, $O^+$ escapes from high latitudes directly to the dayside magnetopause, where it can be accumulated until the IMF turns southward and reconnection initiates. Fuselier, Trattner, et al. (2019), studied a case in such a situation and predicted a transient reduction of the reconnection rate by ionospheric $O^+$ of 32%.

#### 4.1.2. Global Measurements of the Mass-Loading Effect of Ionospheric Plasma

The mass-loading effect of ionospheric plasma at the dayside magnetopause, and subsequent reduction of the reconnection rate, have also been studied by monitoring the magnetospheric activity using geomagnetic indices. The plasmaspheric drainage plume is a major source of cold plasma at the dayside magnetopause (cf. Section 3.2). Borovsky and Denton (2006) used four decades of data from various sources to study the effect of the plume on geomagnetic activity. They found a statistically significant reduction of the geomagnetic indices when plasmaspheric plumes were detected in the magnetosphere, for $Kp > 3$. They parametrized the solar wind as a function of $-vB_z$. The reduction is observed for $-vB_z > 3{,}000$ nT km/s, that is, strong flows and/or large southward IMF. Borovsky (2008, 2013) derived an empirical formula relating the main solar wind parameters (magnetic field, velocity and pressure) to the global reconnection rate, inferred from geomagnetic indices. They found that ionospheric plasma starts influencing the reconnection rate (they use the term *plasmasphere effect*) when $\rho_m > M_A^{0.87}\rho_{sw}$, where $\rho_m$ is the magnetospheric mass density, $M_A$ is the



19449208, 2021, 3, Downloaded from https://agupubs.onlinelibrary.wiley.com/doi/10.1029/2020RG000707 by Cochrane France, Wiley Online Library on [07/11/2022]. See the Terms and Conditions (https://onlinelibrary.wiley.com/terms-and-conditions) on Wiley Online Library for rules of use; OA articles are governed by the applicable Creative Commons License

19449208, 2021, 3, Downloaded from https://agupubs.onlinelibrary.wiley.com/doi/10.1029/2020RG000707 by Cochrane France, Wiley Online Library on [07/11/2022]. See the Terms and Conditions (https://onlinelibrary.wiley.com/terms-and-conditions) on Wiley Online Library for rules of use; OA articles are governed by the applicable Creative Commons License

solar wind Alfvén Mach number, and $\rho_{sw}$ is the solar wind mass density. Coronal Mass Ejections (CMEs) have low $M_A$, and therefore the plasmasphere effect is more likely to play a role in the impact of CMEs at the magnetopause (Lavraud & Borovsky, 2008).

#### 4.1.3. Local Versus Global Control of the Integrated Reconnection Rate

There has been some debate on whether the integrated dayside reconnection rate, that is, total amount of magnetic flux merged per unit time, between the solar wind and the Earth's magnetosphere is set by local parameters near the X line, for example, Borovsky and Birn (2014) (local control), or by the forcing exerted due to upstream conditions of the solar wind, for example, Lopez (2016) (global control). The local control hypothesis is implied in the works described in Section 4.1.2. The global control hypothesis argues that the merging magnetopause reconfigures itself to accommodate eventual magnetospheric mass-loading produced by ionospheric ions, and that there is no net effect over the integrated coupling across the magnetopause. This can be accomplished, for instance, by readjusting the length of the X line (Borovsky et al., 2013). Recent MHD multi-fluid modeling (Zhang et al., 2016, 2017) suggests that for a moderate amount of mass-loading (plasmaspheric plumes with $\rho_m < 8$ amu·cm$^{-3}$), the magnetosheath pressure remains unchanged and the integrated reconnection rate is not significantly affected (global control). On the other hand, for plumes impacting the magnetopause with $\rho_m \geq 16$ amu·cm$^{-3}$, the magnetosheath pressure in the inflow region increases owing to pile up of the plasma, leading to more solar wind flux diverted around the magnetosphere (local control). Based on these studies, the two hypotheses (local control vs. global control) seem to be complementary.

### 4.2. Kinetic Effects on Magnetic Reconnection (Microscopic View)

The most studied effect of ionospheric-originating ions on magnetic reconnection is the mass loading effect (cf. Section 4.1). It is considered as macroscopic effect, since it is based on fluid arguments. In this subsection, we focus on the kinetic consequences at the smallest scales of the plasma (microscopic view), and the modification of the plasma dynamics under the presence of cold or heavy ionospheric-originating ions. The behavior of the different plasma populations on kinetic scales depends on their characteristics, such as the Larmor radius and cyclotron frequencies (see Equations 2 and 3). The corresponding characteristic temporal and spatial scales determine which electromagnetic field fluctuations can be followed by the plasma population. Compared to warm protons, a cold proton population will have a smaller Larmor radius, and hence, will decouple from magnetic field at smaller spatial scales, leading to a new scale length in the system. Heavy ions (e.g., $He^+$, $O^+$) have a larger Larmor radii, and smaller gyrofrequency, compared to protons with the same thermal velocity. This would lead to an additional larger scale length of the system. In addition, these heavier species require that the timescales of the reconnection process to be large enough so that the heavy ions can keep up with the evolution. The inclusion of additional scales results in a multi-scale reconnection process, where the properties of the different plasma populations introduce various competing dynamics.

#### 4.2.1. Multiple Ion Scales

##### *4.2.1.1. Multi-Scale Separatrices*

Magnetic reconnection is initiated and maintained owing to magnetic field dissipation inside the EDR, with a characteristic spatial scale of a few electron inertial lengths. The EDR is surrounded by the IDR, where the ions become demagnetized. The IDR extends in the form of separatrices, that is, the boundary that separates the inflow from the outflow regions (see Figure 13). Most of the particles involved in reconnection do not cross the EDR or the IDR, and their energization occurs in the separatrices and in the outflow jet. The separatrices are characterized by a Hall **E** field region of widths comparable to the ion scales, sustained mainly by the $\mathbf{J} \times \mathbf{B}/en$ term of the Ohm's law (cf. Equation 1). The Hall **E** field accelerates the ions as they cross the separatrices. Wygant et al. (2005) investigated $H^+$ and $O^+$ ion energization across the normal electric field layer present in the separatrices of magnetotail reconnection. The observed normal electric field layer thickness was a few to several $H^+$ Larmor radii, allowing the $H^+$ and electron populations to $\mathbf{E} \times \mathbf{B}$ drift inside the layer and not being significantly energized, while the $O^+$ was ballistically accelerated by the electric field, resulting into an $O^+$ energization consistent with the equivalent potential drop observed across the layer. Lindstedt et al. (2010) observed a similar situation at the magnetopause near the cusps, where the normal

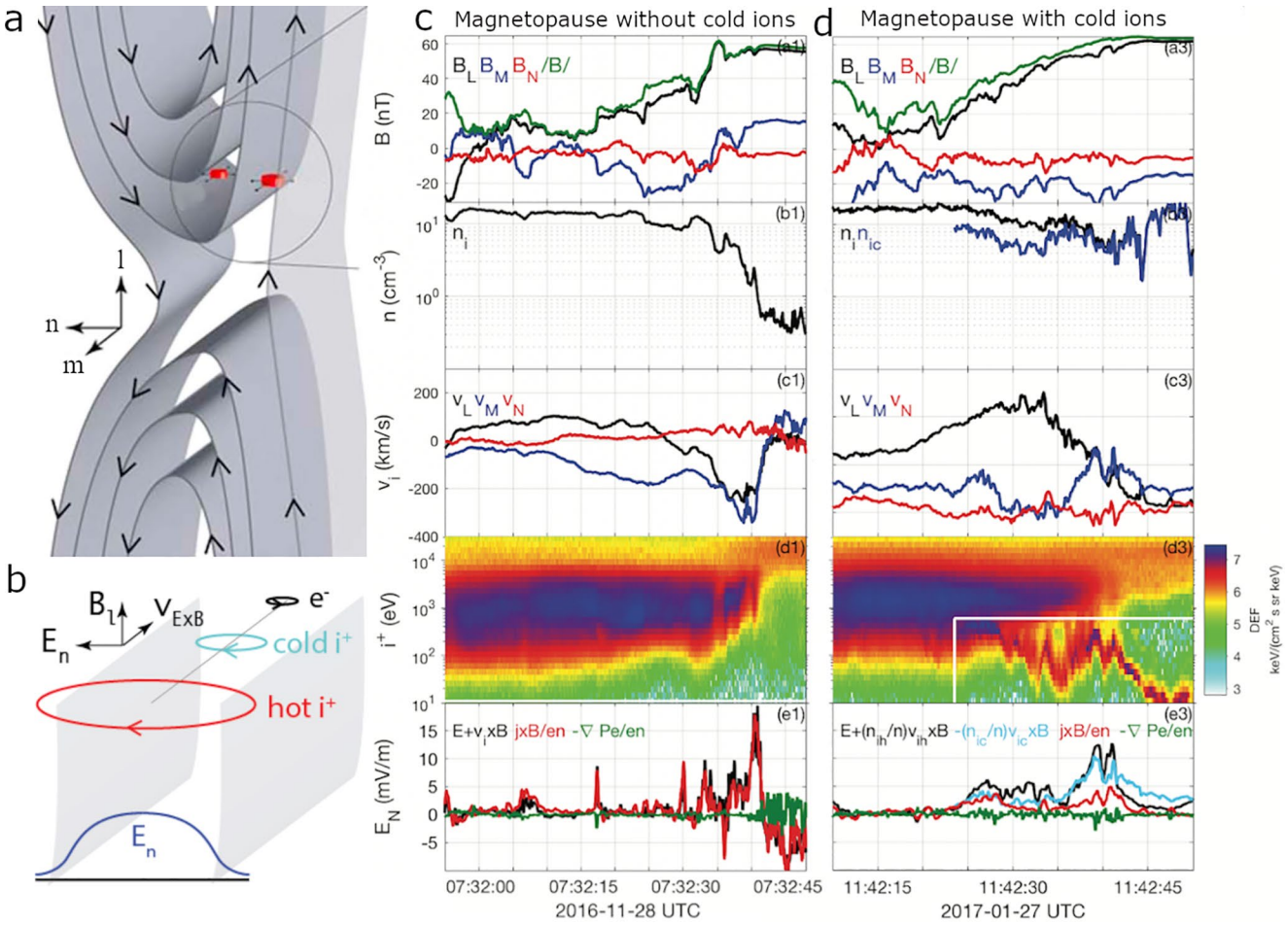



**Figure 14.** (a) Sketch of two spacecraft crossing the separatrix at the dayside magnetopause. Adapted from Toledo-Redondo et al. (2015). (b) Illustration comparing the width of the separatrix layer and its Hall electric field with the gyroradii of electrons, cold ions and hot ions. Adapted from Toledo-Redondo et al. (2015). (c) Magnetospheric Multiscale (MMS) observations of the separatrix region without cold ions. (d) MMS observations of the separatrix region with cold ions. Adapted from Toledo-Redondo et al. (2018).

**E** field near the separatrix of magnetic reconnection accelerated $H^+$ and $O^+$ to different energy levels, and they attributed it to the different degree of demagnetization of the $H^+$ and the $O^+$ inside the layer. André et al. (2010) and Toledo-Redondo et al. (2015) used Cluster spacecraft measurements to study the behavior of cold ions in the separatrix region of dayside magnetic reconnection. Figure 14a illustrates a 2-spacecraft crossing of the separatrix region, where a 2D, laminar model of magnetic reconnection is assumed. They found that cold ions, owing to their smaller Larmor radius, were able to remain magnetized inside the Hall **E** field region, $\mathbf{E}\times\mathbf{B}$ drifting together with electrons and therefore reducing the perpendicular currents associated with the Hall effect ($\mathbf{J}\times\mathbf{B}/en$ term). This situation is sketched in Figure 14b. They accounted for the reduction of the Hall effect by rewriting the steady state Ohm's law in a three-fluid form, including electrons (subscript e), cold ions (subscript c) and hot ions (subscript h):

$$\mathbf{E} = \frac{1}{en}\mathbf{J}\times\mathbf{B} - \frac{n_c}{n}\mathbf{v}_c\times\mathbf{B} - \frac{n_h}{n}\mathbf{v}_h\times\mathbf{B} - \frac{1}{en}\nabla\cdot\mathbf{P}_e \tag{11}$$

where the electron inertia is neglected and $\mathbf{J} = q(n_h\mathbf{v}_h + n_c\mathbf{v}_c - n_e\mathbf{v}_e)$ is the current density. More recently, using high-resolution MMS measurements, several works have confirmed quantitatively the differential ion behavior between cold and hot ions in the separatrices of magnetic reconnection, both at the dayside magnetopause (André et al., 2016; Toledo-Redondo et al., 2018) and in the magnetotail (Alm et al., 2018, 2019). Figures 14c and 14d show MMS crossings of the separatrix region, without and with cold ions, respectively. One can see that the Hall term of the Ohm's law, $\mathbf{J}\times\mathbf{B}/en$ (red curves in bottom panels of Figures 14c



19449208, 2021, 3, Downloaded from https://agupubs.onlinelibrary.wiley.com/doi/10.1029/2020RG000707 by Cochrane France, Wiley Online Library on [07/11/2022]. See the Terms and Conditions (https://onlinelibrary.wiley.com/terms-and-conditions) on Wiley Online Library for rules of use; OA articles are governed by the applicable Creative Commons License

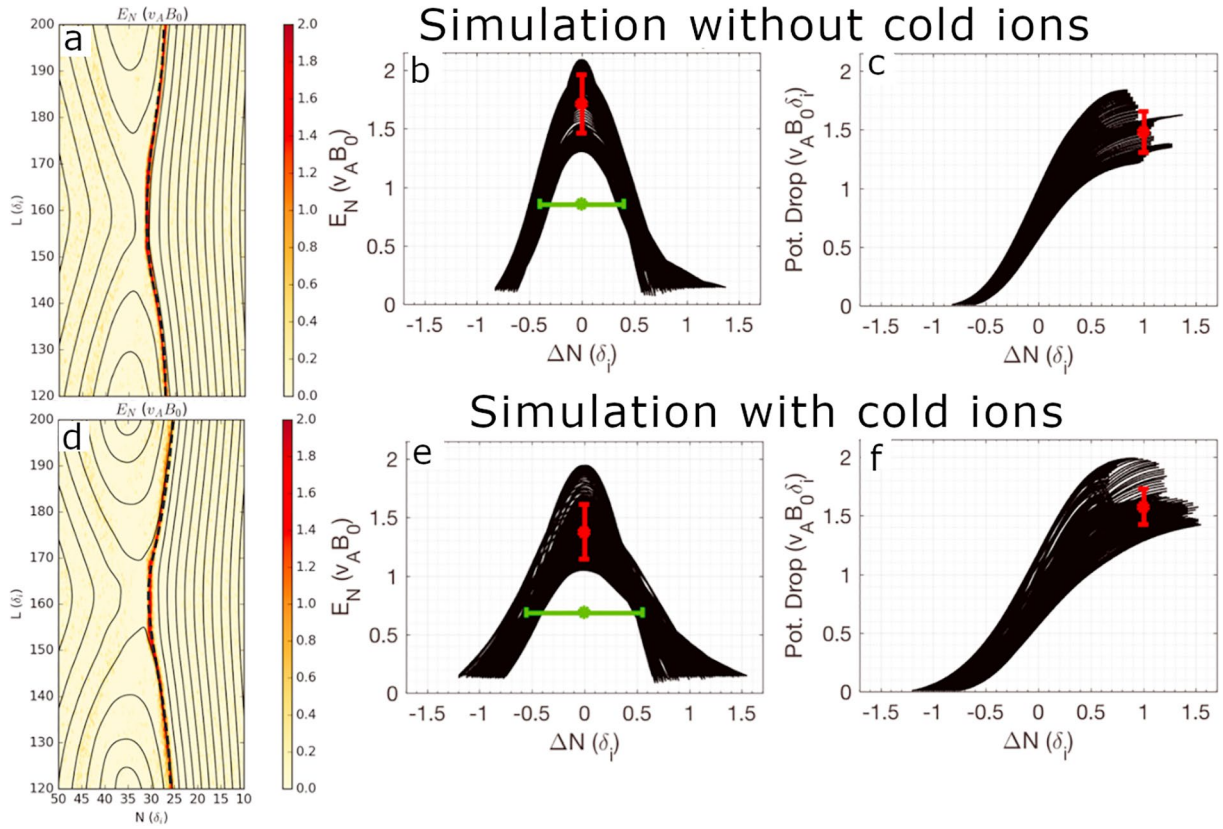



**Figure 15.** PIC simulations of dayside reconnection with and without cold ions. (a) Hall electric field for the run without cold ions. (b) Hall electric field statistics for the run without cold ions. (Black) horizontal cuts of panel a, centered at the maximum Hall electric field value (dashed line in panel a). (Red) Mean maximum value of the Hall electric field, error bars correspond to 1 standard deviation. (Green bars) Mean half-width of the Hall electric field. (c) Potential drop statistics for the run without cold ions. (Black) Potential drop for each horizontal cut of panel (a) (Red) Mean value and one standard deviation of the accumulated potential drop. (d–f) Same as (a–c) for the run with cold ions. Adapted from Toledo-Redondo et al. (2018).

and 14d), is smaller in the case with cold ions, because they remain magnetized and $\mathbf{E} \times \mathbf{B}$ drift together with electrons (cyan curve in bottom panel of Figure 14d).

The Hall **E** field in the separatrices energizes the demagnetized ions that cross it, and therefore one might expect that a reduction in the $\mathbf{J} \times \mathbf{B}/en$ term should result in a reduction of the ion energization across the separatrices. Toledo-Redondo et al. (2018) investigated that, using PIC simulations. They ran two simulations, one of which included both hot and cold ions in the magnetosphere side. The two simulations had identical asymptotic conditions, that is, magnetic field magnitude, and total particle density and temperature. They found that the maximum Hall **E** field (Figures 15a and 15d) was reduced in the separatrices in the simulations with cold ions, but that at the same time the Hall **E** field layer was wider (Figures 15b and 15e), resulting in very similar integrated potential drops across the separatrix (Figures 15c and 15f).

Finally, Dargent et al. (2017) ran two kinetic simulations of magnetic reconnection, with and without cold ions, and noticed the presence of a new electric field layer along the magnetospheric separatrices, adjacent to the Hall **E** field layer, but weaker and wider, and with an opposite sign. They argue that this new field results from cold ions being frozen-in at scales where hot ions begin to demagnetize within the proximity of the asymmetric layer. This field is also observable in other simulations (e.g., Dargent et al., 2020), although its relevance for energy conversion from the fields to the particles by reconnection remains unexplored.

#### *4.2.1.2. Multi-Scale Ion Diffusion Regions*

The presence of multiple ion populations in magnetic reconnection also affects the topology of the IDR. Each ion population has its own characteristic spatial scales, namely the ion inertial length and the Larmor radius, which depend on the atomic mass and temperature of the population. Therefore, each ion



19449208, 2021, 3, Downloaded from https://agupubs.onlinelibrary.wiley.com/doi/10.1029/2020RG000707 by Cochrane France, Wiley Online Library on [07/11/2022]. See the Terms and Conditions (https://onlinelibrary.wiley.com/terms-and-conditions) on Wiley Online Library for rules of use; OA articles are governed by the applicable Creative Commons License

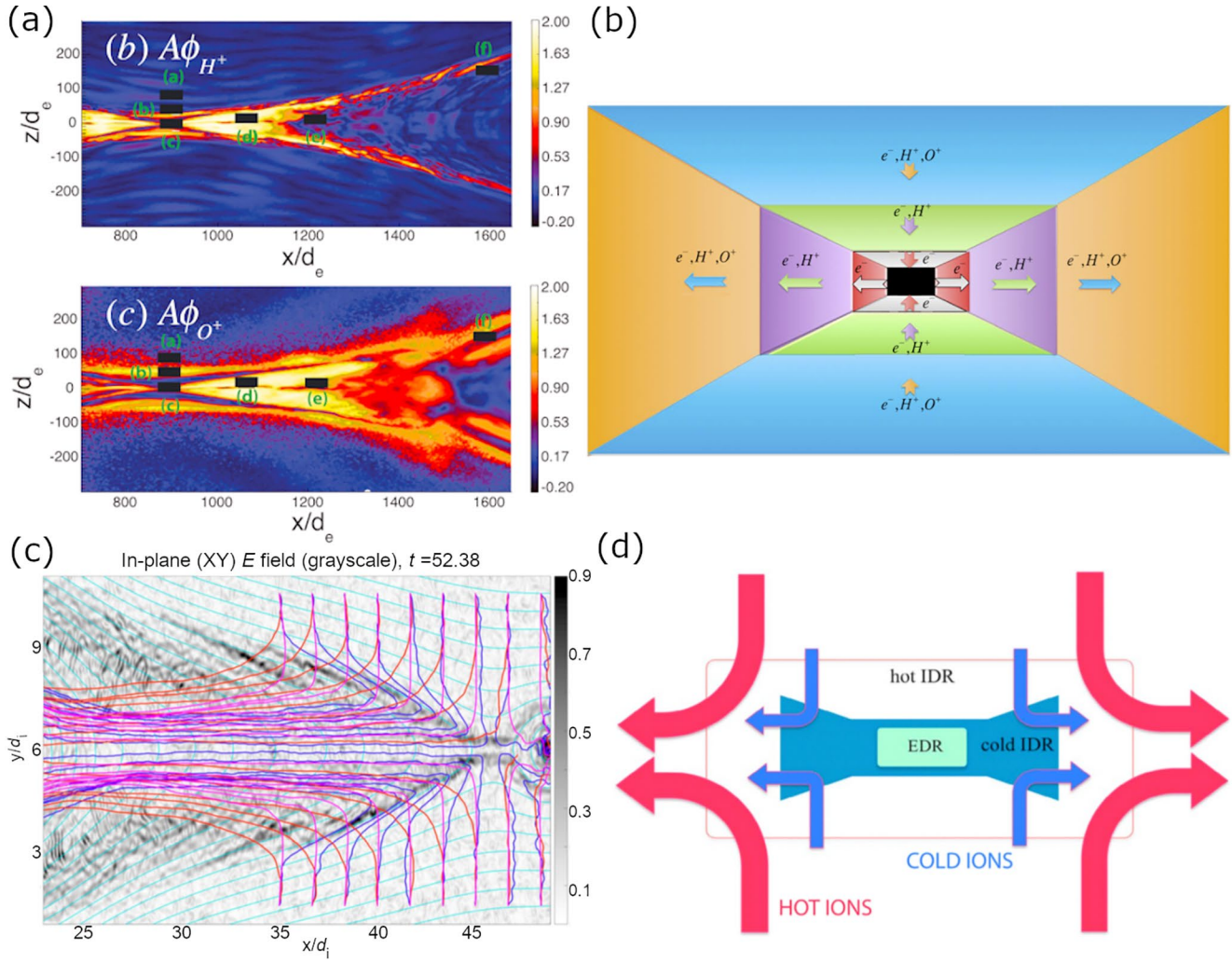



**Figure 16.** PIC simulations of symmetric magnetic reconnection including $O^+$ (top panels) and cold protons (bottom panels). (a) Agyrotropy of $H^+$ and $O^+$. Adapted from Liu et al. (2015). (b) Sketch of a multi-scale diffusion region including electrons, protons and oxygen. Adapted from Liu et al. (2015). (c) Trajectories of electrons (blue), cold ions (pink) and hot ions (orange) inside the diffusion region of symmetric magnetic reconnection. Adapted from Divin et al. (2016). (d) Sketch of a multi-scale diffusion region including electrons, cold protons and hot protons. Adapted from Divin et al. (2016).

population sets its own ion diffusion region, resulting in a multi-scale ion diffusion region (two or more layers). This behavior in magnetic reconnection has been observed using both PIC simulations and spacecraft observations at the Earth's magnetopause and in the magnetotail. Liu et al. (2015) ran 2.5D PIC simulations of symmetric magnetic reconnection, including electrons, $H^+$ and $O^+$. They found that, in the steady-state regime, the $O^+$ demagnetize at a larger scale than $H^+$, as measured by the agyrotropy of the populations (Figure 16a). This results in a three-scale diffusion region, one for each population, as sketched in Figure 16b. They compared the ion velocity distributions functions in their simulation to real observations made by Cluster in the Earth's magnetotail, and confirmed the multi-scale nature of the diffusion region when $O^+$ is present. Divin et al. (2016) also ran 2.5D PIC simulations of symmetric magnetic reconnection, and included cold $H^+$ in addition to hot $H^+$ and electrons. They also found a multi-scale diffusion region, where the cold ions remain magnetized down to smaller scales than the hot $H^+$, owing to their different Larmor radius. Figure 16c shows particle trajectories for hot $H^+$ (orange), cold $H^+$ (pink), and electrons (blue) in the vicinity of the X line. Electrons remain frozen into the inflowing magnetic field and reach the inner part of the current sheet, while hot ions are demagnetized upstream in the inflow region and follow distinct trajectories. Cold ions are demagnetized at intermediate distances between the center of the current



19449208, 2021, 3, Downloaded from https://agupubs.onlinelibrary.wiley.com/doi/10.1029/2020RG000707 by Cochrane France, Wiley Online Library on [07/11/2022]. See the Terms and Conditions (https://onlinelibrary.wiley.com/terms-and-conditions) on Wiley Online Library for rules of use; OA articles are governed by the applicable Creative Commons License

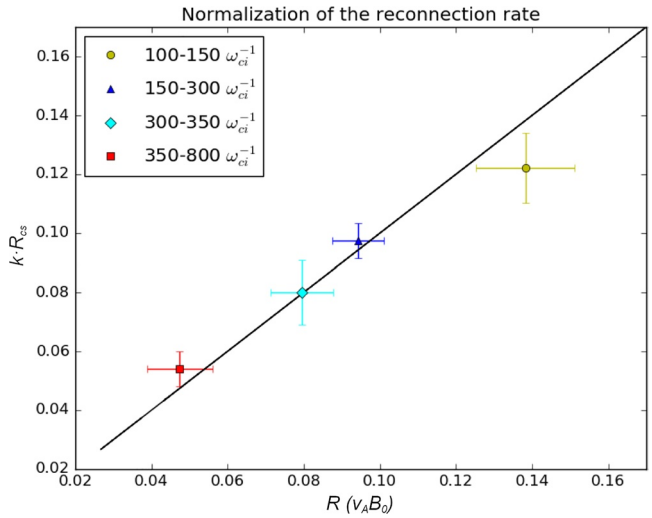



**Figure 17.** Scatter plot of the observed reconnection rate, R, versus the calculated rate, $R_{CS}$ (i.e., Equation 9 assuming $\delta/L = 0.1$), for the different phases of the simulation. The factor $\kappa = 0.127$ is calculated such as $\kappa R_{CS}/R$ scales along a slope of 1. Each point corresponds to the mean value of the reconnection rate on the time interval and the bars indicate one standard deviation. The given time intervals correspond to the different phases of the simulation: yellow, early unsteady magnetic reconnection; blue, steady magnetic reconnection without the plasmaspheric plume; light blue, transition phase with the impact of the plume; red, steady magnetic reconnection with the plasmaspheric plume. Adapted from Dargent et al. (2020).

sheet and the region where the hot ions are demagnetized. Figure 16d is a sketch of the multi-scale diffusion region due to electrons, cold $H^+$ and hot $H^+$.

The multi-scale nature of the ion diffusion region has been confirmed using spacecraft observations. A multi-scale ion diffusion region created by cold and hot $H^+$ was reported at the dayside magnetopause, using MMS observations (Toledo-Redondo, André, Khotyaintsev, et al., 2016). MMS traversed near the EDR of magnetic reconnection, with both northward and southward ion jets observed in the vicinity of the magnetopause crossing. The spacecraft separation was only ~15 km, that is, comparable to the cold $H^+$ gyroradius and much shorter than the hot $H^+$ gyroradius (~200 km). One of the spacecraft observed the cold $H^+$ being accelerated parallel to **E** in a thin region of ~15 km width, while the other spacecraft observed cold $H^+$ $\mathbf{E} \times \mathbf{B}$ drifting, in a region where the hot ions were already demagnetized. These regions were identified as the cold IDR and the hot IDR, respectively. At the Earth's magnetopause, the cold ions are of ionospheric origin and can be present only in the magnetospheric inflow region. Therefore, the topology of the multi-scale IDR must be asymmetric. A subjacent question that arises from the observation of multi-scale diffusion regions, both symmetric and asymmetric, is whether this results in an effective modification of the aspect ratio, that is, the normalized reconnection rate. This question is addressed in Section 4.2.2. Finally, it is known that cold plasma escaping from the ionosphere is composed of both cold electrons and cold ions. The effects of multiple electron populations (cold and hot) on magnetic reconnection have not been addressed in the literature, to our knowledge.

### 4.2.2. Kinetic Effects on Reconnection Rate

#### *4.2.2.1. Cold Ions and Reconnection Rate*

We have already seen in Section 4.1 that ions of ionospheric origin have a mass loading effect on the magnetic reconnection rate. However, based on the scaling analysis (see Equations 8 and 9) there is no direct dependence on temperature. For instance, a cold plasma population should not affect the reconnection rate as long as the total mass density remains constant. However, a cold population introduces a new length-scale and therefore should lead to a reconfiguration of the diffusion region. In particular, a cold ion population is expected to reduce the average height of the ion diffusion region ($\delta$). According to Equation 8 (Equation 9 for asymmetric magnetic reconnection), maintaining a constant reconnection rate would then imply that the diffusion region configures itself so that the length $L$ is reduced in order to keep constant the aspect ratio $\delta/L$.

Numerical simulations have shown that the inclusion of multiple ion populations with different temperatures has a negligible effect on the reconnection rate if the mass density is constant, both for symmetric reconnection (Divin et al., 2016; Tenfjord et al., 2020), and for asymmetric reconnection (Dargent et al., 2017, 2020). All these works observe a ratio $\delta/L \sim 0.1$, as expected by Liu et al. (2017, 2018). In particular, Dargent et al. (2020) studied how the reconnection rate evolves during the impact of a dense, cold, plasmaspheric plume at the reconnecting magnetopause. Figure 17 shows the observed reconnection rate $R$ versus the expected one, using Equation 9 for the calculation, assuming $\delta/L = 0.1$. The yellow dot represents the average value of the measured versus the expected reconnection rate during the early stage of the simulation. The observed reconnection rate is larger than the expected rate in this early stage of the simulation. This is a well-known feature of PIC simulations, often called the overshoot period, that occurs before the simulation reaches steady state (Shay et al., 2007). The blue, cyan, and red dots correspond to the simulation time prior to the arrival of the plasmaspheric plume to the reconnection region (blue), the transition time during the impact of the plume (cyan), and the new steady state reached by magnetic reconnection under the presence of the plume in the magnetospheric inflow region (red). The observed reconnection rate diminishes owing to the mass-loading effect of the plume (cyan and red dots). However, in each of the three



19449208, 2021, 3, Downloaded from https://agupubs.onlinelibrary.wiley.com/doi/10.1029/2020RG000707 by Cochrane France, Wiley Online Library on [07/11/2022]. See the Terms and Conditions (https://onlinelibrary.wiley.com/terms-and-conditions) on Wiley Online Library for rules of use; OA articles are governed by the applicable Creative Commons License

19449208, 2021, 3, Downloaded from https://agupubs.onlinelibrary.wiley.com/doi/10.1029/2020RG000707 by Cochrane France, Wiley Online Library on [07/11/2022]. See the Terms and Conditions (https://onlinelibrary.wiley.com/terms-and-conditions) on Wiley Online Library for rules of use; OA articles are governed by the applicable Creative Commons License

phases, the observed reconnection rate matches on average the calculated one using upstream conditions and assuming $\delta/L \sim 0.1$. Despite the dynamic evolution of magnetic reconnection when the plume impacts the layer, the results of Figure 17 indicate that the aspect ratio remains roughly constant on average, with a value of $\delta/L \sim 0.1$. A simulation study by Spinnangr et al. (2020) investigated how the reconnection process reorganizes itself on kinetic scales when cold protons are involved in the reconnection process. The authors found, as expected from arguments presented above, a significant reduction of $\delta$. From our scaling arguments we would then expect $L$ to be reduced by the same factor for the ratio to be kept at a constant $\delta/L \sim 0.1$. However, the length ($L$) was found to decrease less, which corresponded to a small discrepancy between the rescaled reconnection rate in a simulation with cold ions, and a run without. This suggests that, on ion-scales, some of the assumptions made in the scaling do not always hold. The reorganization of the aspect ratio was found to be enabled by temporal inertia of the cold population during a transition period. This result suggests that the process indeed reconfigures itself to account for the inclusion of an additional ion population with a lower temperature, resulting in a lower reconnection efficiency.

#### *4.2.2.2. Heavy Ions and Reconnection Rate*

The ion outflow from the high-latitude ionosphere is often composed of $He^+$ and $O^+$, in addition to $H^+$, and is believed to be a significant source of plasma for the terrestrial magnetosphere, and in particular for the tail, cf. Sections 2 and 3. This additional composition leads to an increased total mass density which affects fundamental plasma properties such as the Alfvén speed, plasma pressure and plasma $\beta$ (the ratio of thermal plasma pressure to magnetic pressure). During geomagnetically active times, $O^+$ can even dominate the mass density in the magnetotail (e.g., Kistler et al., 2005; Wygant et al., 2005). Similar to cold protons, the presence of heavier species also leads to multiple scales in the reconnection process. Heavier ion populations will have a larger diffusion region compared to that of protons with the same thermal velocity. Additionally, the presence of heavy ions can lead to different Hall dynamics (see Section 4.2.1.1) and also influence the dynamics of dipolarization fronts (Liang et al., 2017; Markidis et al., 2011). Heavier species such as $O^+$ can also, if magnetized for the spatiotemporal scales of interest, lead to a significant mass-loading of the reconnection process (Borovsky, 2013; Hesse & Birn, 2004; Shay & Swisdak, 2004). Additional effects of heavier ion species also include an impact on the tearing mode growth rate (Karimabadi et al., 2011), induced charge separation effects, that is, ambipolar electric fields (Liang et al., 2016) and may contribute to the generation of bifurcated current sheets (George & Jahn, 2020). Wang et al. (2014) investigated the role of $O^+$ and $H^+$ in a reconnection event using Cluster, and found that the $O^+$ energization depends on the location at which the $O^+$ enters the exhaust. If the $O^+$ ion enter close to the diffusion region they behave like pick-up ions (Drake, Swisdak, et al., 2009), whereas further downstream they retain their adiabatic motion and follow the rest of the plasma in the outlflow region (Drake, Cassak, et al., 2009).

Because of the large $O^+$ atomic mass, they introduce an additional time scale, due to the cyclotron frequency dependence on ion mass. The system must evolve slowly enough for the heavy ions to remain magnetized. Assuming a magnetic field of $B_0 = 20$ nT in the magnetotail lobes, the cyclotron period of $H^+$ is ~3 s, while for $O^+$ the cyclotron period is ~50 s (since the $O^+$ mass is 16 times that of $H^+$). Magnetic reconnection in the tail occurs in the plasma sheet, which is emptied by reconnection jets and refilled by plasma in the lobes. If we assume that a reconnection event in the tail (e.g., a Bursty Bulk Flow) lasts for about 200 proton cyclotron periods, that is, about 10 min, the heavy, sluggish $O^+$ has only had time to gyrate about the magnetic field 12 times. This affects the ability of the $O^+$ to stay magnetized, since in its frame of reference the evolutionary timescale of the reconnection process can be comparable or even faster than its own cyclotron period, preventing the actual system to reach steady state (Kolstø et al., 2020; Markidis et al., 2011; Tenfjord et al., 2018, 2019). The effect is that in the frame of the $O^+$, the frozen-in approximation no longer holds, and the ions lose the ability to add inertia to the flux tube. Consequently, the role of $O^+$ on the reconnection process can no longer adequately be described as a simple mass-loading process. Using PIC simulations, Tenfjord et al. (2018) investigated the behavior of $O^+$ as it was captured by reconnection in the tail. They found that $O^+$, as a consequence of being demagnetized, was ballistically accelerated, primarily by the Hall electric field. Simulations by Tenfjord et al. (2019) and Kolstø et al. (2020) show that for both symmetrically and asymmetrically distributed $O^+$, the reconnection rate is significantly reduced, but not as much as predicted by mass-loading. The authors describe a mechanism where the $O^+$ population (and the accompanying electrons) acts as an energy sink on the system, altering the energy partitioning. Even though $O^+$ ions do not directly influence the reconnection process through mass-loading, they do extract energy from the

fields that would otherwise be available for accelerating protons and electrons. Based on a scaling analysis the authors find a scaling based on the energy extracted by the unmagnetized species which describes the reduced reconnection rate.

While measurements of the variations in the local rate of reconnection in the tail with heavy ions are still elusive, the global effects of the reconnection rate can be determined by studying the substorm unloading. After substorm onset, reconnection occurs in the magnetotail, reducing the magnetic flux that has built up in the tail lobes during the growth phase. Therefore, the rate of unloading is related to the tail reconnection rate. Liu et al. (2013) studied the global effect of heavy ions on the substorm unloading rate using data from the Cluster mission, by correlating the rate of unloading with the mass density and $O^+/H^+$ ratio in the tail prior to substorm onset. They found that unloading rate is in fact faster when the $O^+$ density and $O^+/H^+$ ratios are higher. This faster rate is contrary to the expectation that increased $O^+$ should decrease the reconnection rate. Further, the faster rate indicates that other parameters, such as the generally higher activity that usually is associated with high $O^+$, or the width of the tail over which the reconnection is occurring may be playing a larger role in determining the unloading than the reconnection rate itself. On the other hand, magnetic reconnection at the dayside magnetopause is thought to occur more steadily, due to the dominant effect of the dense inflowing solar wind. In this scenario, the reconnection process can reach steady-state relative to the $O^+$ characteristic timescale. In this case, $O^+$ would have sufficient time to remain magnetized, and the reduction of the reconnection rate may be estimated based on mass-loading scaling (Fuselier, Mukherjee, et al., 2019; Karimabadi et al., 2011; Kistler et al., 2005; Liu et al., 2015).

#### *4.2.2.3. Effect of Streaming Ions (Suppression of Rate)*

An additional effect beyond the previously described slowdown scenarios is the involvement of a moving cold ion population in the inflow region. Ions originating from the ionosphere stream parallel to the magnetic field (e.g., Bouhram et al., 2004; Fuselier, Trattner, et al., 2019). The outward velocity is typically observed to be up to ~50 km/s (André et al., 2015; Haaland, Svenes, et al., 2012). Consequently, this additional plasma population adds net, tailward directed momentum to the reconnection process. At the dayside magnetopause, as we move away from the subsolar point, the differential motion between the draped solar wind and the magnetospheric convection also causes differential ion streams on both sides of the reconnection region. As soon as streaming ions become involved, they contribute to the overall momentum balance, altering the reconnection dynamics. Tenfjord et al. (2020) investigated the effect of a streaming cold proton population on the reconnection process using PIC-simulations. In the magnetotail, this results in a tailward propagation of the reconnection X line. The inclusion of streaming particles influenced the initially symmetric outflow regions, producing asymmetries in outflow velocities and temperatures. In a similar study, Kolstø et al. (2020) investigated the effect of a streaming oxygen population. As already discussed, $O^+$ remains demagnetized because the cyclotron period is much longer than the evolutionary timescale of the reconnection process. Even though $O^+$ did not exhibit a magnetized behavior they still impart the tailward directed momentum through electrostatic coupling. In addition, the authors observe the formation of an oxygen wave (Tenfjord et al., 2018) which becomes significantly altered by the added momentum. For cold protons, this additional momentum does not appear to cause any additional reduction of the reconnection rate, after correcting for the additional mass. For streaming $O^+$, the reduced rate corresponds to the scaling described in Tenfjord et al. (2019). However, both in the magnetotail and on the dayside, streaming ions can cause drift of the reconnection X line into regions where the plasma conditions are different, which could result in an effective change or even suppression of the reconnection process.

### 4.2.3. Additional Consequences of Multiple Ion Populations

#### *4.2.3.1. Cold Ion Crescents*

In weak guide field configurations, the dynamics of the ion populations inside the diffusion region are deeply affected. The magnetic field reversal in the center of the reconnecting current sheet implies a large B field gradient over less than an ion inertial length, and that the direction of a particle gyration is changing through the layer. Thus, the particles will be bouncing between the magnetic field lines on either side of the X-line instead of gyrating around one magnetic field line. The bounce-width of a population is therefore where the local thermal Larmor radius is equal to the distance to the center of the layer (Hesse et al., 2011). This bounce motion produces crescent-shaped distribution functions along the boundary of the bounce



19449208, 2021, 3, Downloaded from https://agupubs.onlinelibrary.wiley.com/doi/10.1029/2020RG000707 by Cochrane France, Wiley Online Library on [07/11/2022]. See the Terms and Conditions (https://onlinelibrary.wiley.com/terms-and-conditions) on Wiley Online Library for rules of use; OA articles are governed by the applicable Creative Commons License

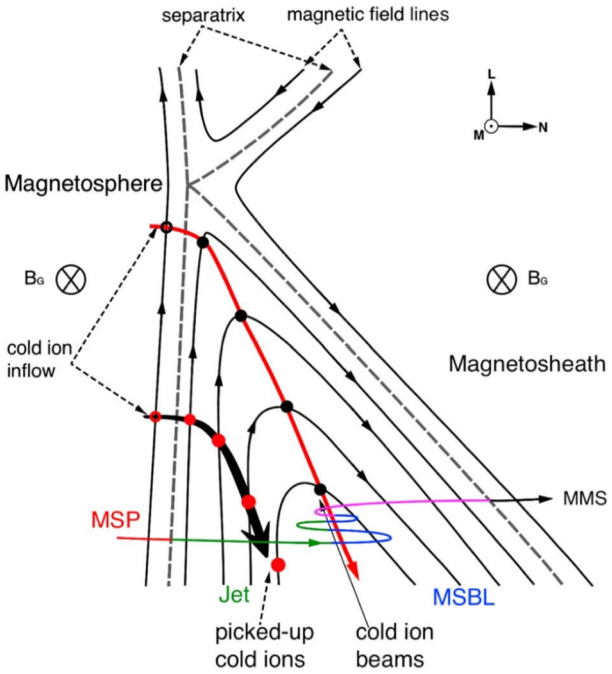



**Figure 18.** Diagram of the Magnetospheric Multiscale observations during a magnetopause crossing with ongoing magnetic reconnection. Near the magnetospheric edge of the ion outflow jet, heated cold ions are observed (black arrow). Near the magnetosheath edge of the ion outflow jet, cold ions with lower temperature are observed, indicating that the amount of cold ion heating imparted by reconnection depends on the distance to the X line where the cold ions cross the magnetopause boundary. Adapted from Li et al. (2017).

width. Such a signature in electron distribution functions has been proven to be a signature of magnetic reconnection (Bessho et al., 2016; Burch et al., 2016; Hesse et al., 2014), and is also expected for ions (Dargent et al., 2017; Shay et al., 2016). Dargent et al. (2019) showed another mechanism that can lead to the formation of such crescent-shaped distribution functions for cold ions. Cold ion distribution functions take a crescent shape along the magnetospheric separatrices, without magnetic field reversal. In this case, the driver of the signature is the Hall electric field, which accelerates and then decelerates the cold ions during one Larmor gyration.

#### *4.2.3.2. Cold Ion Beams and Lower Hybrid Instabilities*

In collisionless plasmas, waves play an important role in coupling the various particle populations. Graham, Khotyaintsev, et al. (2017) showed, using both spacecraft observations and linear theory modeling, that the presence of cold ion beams (ionospheric origin) near the ion diffusion region of magnetic reconnection at the Earth's magnetopause can be a free source of energy for the lower hybrid instability, when the cold ion beam interacts via an ion-ion instability with the solar wind population. The generated lower hybrid waves near the ion diffusion region heat the cold ions, acting as a preconditioner of the population in the magnetospheric inflow region.

### 4.3. Cold Ion Energization and Energy Budget of Magnetic Reconnection

One of the most important consequences of magnetic reconnection is the efficient conversion of magnetic energy into kinetic and thermal energies. Ionospheric ions, like any other particles, are energized by magnetic reconnection, in the form of bulk drift acceleration to form the outflow jets plus thermalization. Bulk acceleration is believed to occur in a similar way to pickup processes (e.g., Drake, Swisdak, et al., 2009) when the ionospheric ions enter the outflow jet. From the fluid description given in Section 4.1, one can see that the outflow velocity, that is, the Alfvén velocity, scales with the mass density in the inflow regions, and therefore magnetic energy conversion into bulk drift acceleration scales with the inverse of mass density. However, magnetic reconnection also produces heating of the particle populations. This heating is accomplished by means of various mechanisms, including the reconnection electric field, the Hall electric fields, and wave-particle interactions. These mechanisms occur at the kinetic scales of the particles, and other parameters, such as for instance the level of turbulence achieved in the outflow jet, may condition the amount of magnetic energy converted into heating.

#### 4.3.1. Cold Ion Energization at the Earth's Magnetopause

The typical temperature of the magnetosheath ions is approximately 100–200 eV, while the typical temperature of cold ionospheric ions reaching the magnetopause ranges from a few electron volt for plasmaspheric material to several hundred electron volt for the warm plasma cloak, in addition to the keV plasma sheet ions that can originate in the solar wind or in the ionosphere. Cold ions are accelerated and heated when entering the diffusion region, separatrices, and reconnection outflow region. In those regions, cold ions are mostly mixed together with the magnetosheath ions, and it becomes difficult to distinguish between the two populations. Li et al. (2017) presented an MMS study of a magnetopause crossing with high-density (10–60 $cm^{-3}$) cold ions and on-going reconnection, which is sketched in Figure 18. Near the magnetospheric edge of the ion jet, they observed a mixture of plasma sheet ions, magnetosheath ions and heated cold ions (Figure 18, black arrow). On the magnetosheath edge of the ion jet, two distinct ion populations were observed. One population with high parallel velocities (200–300 km/s) but rather low temperature (~90 eV) was identified to be a cold ion beam, while the other population was the magnetosheath ions. They



19449208, 2021, 3, Downloaded from https://agupubs.onlinelibrary.wiley.com/doi/10.1029/2020RG000707 by Cochrane France, Wiley Online Library on [07/11/2022]. See the Terms and Conditions (https://onlinelibrary.wiley.com/terms-and-conditions) on Wiley Online Library for rules of use; OA articles are governed by the applicable Creative Commons License

19449208, 2021, 3, Downloaded from https://agupubs.onlinelibrary.wiley.com/doi/10.1029/2020RG000707 by Cochrane France, Wiley Online Library on [07/11/2022]. See the Terms and Conditions (https://onlinelibrary.wiley.com/terms-and-conditions) on Wiley Online Library for rules of use; OA articles are governed by the applicable Creative Commons License

separated the distribution functions of the cold ion beams from the entire distribution functions, and computed the partial moments of the cold ion beams. The cold ion beams are hotter than the cold ions in the inflow region, but are still ~30% colder than the hot magnetosheath ions. In the DeHoffman-Teller frame (DeHoffmann & Teller, 1950), the field-aligned magnetosheath ions are nearly Alfvénic and move toward the jet region, while the field-aligned cold ions move toward the magnetosheath boundary layer, with much lower speeds. The results suggest that the cold ion beams are accelerated close to the X line (Figure 18, red arrow). The study illustrates that the cold ion heating by reconnection is not homogeneous along the separatrix and suggests it may be lower close to the X line. Toledo-Redondo, André, Vaivads, et al. (2016) and Toledo-Redondo et al. (2017) investigated which cold ion energization mechanisms take place in the reconnection separatrices. They used Cluster and MMS spacecraft observations of cold ion heating, and showed that both waves near the ion cyclotron frequency and gradients of the Hall electric field were consistent with the amount of heating observed. They estimated, for the four events investigated, that cold ion heating took 10%–25% of the energy that went into ion heating, while the other 75%–90% went into heating the more abundant magnetosheath ions. Graham, Khotyaintsev, Norgren, et al. (2017) showed MMS observations of lower hybrid drift waves inside the separatrix region, formed owing to the presence of a cold ion beam, cf. Section 4.2.3. All these findings indicate that the presence of cold ions modifies the energy partition that is converted from the fields into particle kinetic energy by magnetic reconnection, although quantification of the energy taken by cold ions in the form of bulk kinetic acceleration and heating from a statistical perspective remains unknown. Vines et al. (2017) also studied the energization mechanisms of ionospheric ions, including $H^+$, $He^+$, and $O^+$, at the separatrix of magnetopause reconnection, and concluded that the energization mechanisms at play act in a different way depending on the atomic mass unit of the population. They observed two different energization mechanisms. The first energization mechanism was observed inside the outflow jet, and corresponds to the pickup process by the jet, identified by the characteristic velocity-space ring distributions of the ions in the plasma frame. For cold $H^+$, the pickup process resulted mainly in bulk drift acceleration. However, they noted that for heavy ions ($He^+$ and $O^+$) the pickup process occurred non-adiabatically, due to their larger characteristic spatial and time scales (Larmor radius and gyrofrequency), leading to less well-organized ring distributions which included ion heating and velocity and temperature anisotropy. The second energization mechanism was observed near the magnetospheric separatrix region, where the cold $H^+$ was preferentially heated, and the heavy ions were not affected much. The $H^+$ heating in the separatrix region is associated with fluctuations generated by a two-stream instability and the lower-hybrid instability (cf. Section 4.2.3).

### 4.3.2. Cold Ion Energization in the Plasma Sheet

The plasma sheet boundary layer (PSBL) and the lobe region always contain certain amounts of cold ions of ionospheric origin. The amount of ionospheric plasma present in the magnetotail is variable, depends on magnetospheric activity (cf. Section 3.3), and can affect magnetic reconnection in the magnetotail. One prominent feature is that cold ions can create highly structured ion distribution functions including ion beams that deviate from a Maxwellian distribution. Among these distributions, counter-streaming cold-ion beams along the direction normal to the current sheet were frequently observed in the ion diffusion region (e.g., Divin et al., 2016; Nagai et al., 1998; Shay et al., 1998; Wygant et al., 2005). The counter-streaming cold ion beams are accelerated to several keV, but are still much colder than the plasma sheet hot ions. Using measurements from the Cluster spacecraft, Wygant et al. (2005) showed that the counter-streaming cold ions are accelerated by the large-amplitude Hall electric field in the ion diffusion region, and numerical simulations from Aunai et al. (2011) and Divin et al. (2016) showed a similar acceleration process of cold ions across the current sheet. Combining THEMIS observations and particle-in-cell simulations, Eastwood et al. (2015) illustrated that the ion beams originate from the thermal component of the preexisting plasma sheet hot ion, and are accelerated by the reconnection electric field and rotated from out-of-plane direction to the outflow direction by the Lorentz force. Some other studies argue that the Fermi effect is the main acceleration mechanism for the counter-streaming cold-ion beams (e.g., Birn et al., 2017; Runov et al., 2017; Xu et al., 2019). Quantitative and statistical analyses of the cold-ion beams are needed to assess the contribution from each acceleration mechanism.

19449208, 2021, 3, Downloaded from https://agupubs.onlinelibrary.wiley.com/doi/10.1029/2020RG000707 by Cochrane France, Wiley Online Library on [07/11/2022]. See the Terms and Conditions (https://onlinelibrary.wiley.com/terms-and-conditions) on Wiley Online Library for rules of use; OA articles are governed by the applicable Creative Commons License

### 4.4. Heavy Ion Effects on Reconnection Onset and Efficiency

Baker et al. (1982) proposed that $O^+$ would enhance the linear ion tearing instability in the plasma sheet, and so decrease the stability of the tail to reconnection. Multiple studies since then have attempted to test this. One way to test it is to determine if $O^+$ is generally enhanced prior to substorm onset. Daglis et al. (1990) found that $O^+$ was enhanced in the near-earth plasma sheet, but studies further down the tail closer to the reconnection region did not find that $O^+$ is enhanced prior to onset except during storm-time sawtooth events (Kistler et al., 2016; Lennartsson et al., 1993; Liao et al., 2014). Another method to test this is to determine whether there are more substorm onsets when there is more $O^+$. Lennartsson et al. (1993) and Nosé et al. (2009) performed long-term studies, and they both showed the well-known correlation between $O^+/H^+$ and F10.7, but found no correlation between $O^+/H^+$ ratio and the frequency of substorms over a solar cycle. A final method is to examine the effect of $O^+$ on loading during substorms. The amount of loading that occurs before substorm onset gives an indication of how unstable the tail is to reconnection onset. If the plasma sheet is more unstable, we would expect there to be less loading before reconnection is triggered. Liu et al. (2013) used Cluster data to determine the correlation between the amount of loading and the $O^+$ in the tail. The amount of loading was positively correlated with the amount of $O^+$ in the tail, which would indicate that the $O^+$ in fact makes it harder to trigger substorm onset. They also found that, once reconnection was triggered, the magnetic flux was dissipated faster when $O^+$ was present, suggesting either an increased reconnection rate or an increased length of the X line in the dawn-dusk direction. Using observations and multi-fluid simulation, Winglee and Harnett (2011) found that $O^+$ can play a role in the development of substorms, as $O^+$-enriched reconnected flux tubes can influence the energy dissipation and modify the plasma distribution in the plasma sheet. Various numerical studies indicate that the ionospheric outflow favors the creation and enhancement of substorms, moves the X line earthward and may be responsible for sawtooth events (e.g., Brambles et al., 2010, 2013; Wiltberger et al., 2010; Zhang et al., 2020). On the contrary, the results by Lund et al. (2018), using Cluster observations, seem to indicate that sawtooth events are not produced by the ionospheric outflow.

### 4.5. Change of Plasma $\beta$ and Reconnection Suppression

For asymmetric reconnection, where the plasma density and temperature vary greatly across the reconnection region, the net diamagnetic drift of the plasma in the reconnection exhaust can influence, and even suppress, the progression and efficiency of reconnection (Cassak & Fuselier, 2016; Phan et al., 2013; Swisdak et al., 2003, 2010). Diamagnetic drift arises from a thermal plasma pressure gradient as the result of ions and electrons effectively gyrating in opposite directions about the magnetic field. An apparent flow is created if there is a gradient in temperature (gradient in average particle thermal speeds), density (gradient in the number of gyrocenters) or both. During magnetic reconnection this leads to the reconnection X-line moving along the direction of the electron diamagnetic drift due to the ability of electrons to remain magnetized down to smaller scales. When the diamagnetic drift velocity exceeds the Alfvén speed, reconnection can no longer continue, as the force due to the outflowing reconnected magnetic field is unable to overcome the force arising from the effective net plasma drift induced by the pressure gradient (Swisdak et al., 2003). The suppression mechanism may be altered when there is a gradient in temperature but no substantial density gradients present, as demonstrated by Liu and Hesse (2016) using PIC simulations.

The conditions that may suppress reconnection via diamagnetic drift can be expressed in terms of the difference in plasma $\beta$ on either side of the current sheet ($\Delta\beta$) and the magnetic shear angle ($\theta$), that is, the change in magnetic field orientation across the reconnection site:

$$\Delta\beta > 2\left(L/d_i\right)\tan\left(\theta/2\right), \tag{12}$$

where $L$ is the current sheet width and $d_i$ is the ion inertial length (Swisdak et al., 2010). For small values of $\Delta\beta$, where the plasma populations and magnetic field strength are similar on both sides of the reconnection site, the effect of diamagnetic drift is not substantial, and so reconnection can proceed for a wide range of magnetic field orientations. It is important to note, however, that Equation 12 is a necessary, but not sufficient condition for reconnection to proceed (e.g., Vernisse et al., 2020). As the difference in plasma β

**Table 3**
*Representative Plasma Conditions for Different Populations and Effect on Δβ at the Earth's Magnetopause*

| Plasma population | Proton density ($cm^{-3}$) | Proton temperature (keV) | B[a] (nT) | β | $\Delta\beta = \lvert\beta_{sh}-\beta_{sp}\rvert$ | Presence at Earth's magnetopause |
|---|---|---|---|---|---|---|
| Magnetosheath | 15–20 | 0.05–0.10 | ~20 | 0.80[b] | - | Always |
| Plasma sheet (PS) | ~0.1 | ~10 | 50 | 0.16 | 0.64 | Always |
| Plasma sheet (PS) plus warm plasma cloak (WPC) | PS: ~0.1<br>WPC: 0.5–2[c] | PS: ~10<br>WPC: 0.1–1.0[c] | 50 | 0.17–0.48 | 0.32–0.63 | 50%–70% of the time in the dawn sector[c] |
| Plasma sheet (PS) plus plasmaspheric plume | PS: ~0.1<br>Plume: 5–10[c] | PS: ~10<br>Plume: 0.001–0.01[c] | 50 | 0.16–0.18 | 0.62–0.64 | 20%–25% of the time in the dusk sector[c] |
| Plasma sheet (PS) plus heated plasmaspheric plume | PS: ~0.1<br>Plume: 10–60[d] | PS: ~10<br>Plume: 0.1–0.125[d] | 50 | 0.32–1.37 | 0–0.57 | ? |
| Plasma sheet plus detached plasmaspheric material (PM) | PS: ~0.1<br>PM: ~1[c] | PS: ~10<br>PM: 0.001–0.01[c] | 50 | 0.16 | 0.64 | >80% of the time in the dusk sector[c] |
| Plasma sheet plus heated plasmaspheric material (PM) | PS: ~0.1<br>PM: 1–2[e] | PS: ~10<br>PM: 0.2–0.4[e] | 50 | 0.19–0.29 | 0.51–0.61 | ? |

[a]Nominal magnetic field strength observed in the subsolar magnetosheath and in the Earth's outer magnetosphere near the subsolar magnetopause. [b]Most probable magnetosheath β given typical magnetosheath conditions (Cassak & Fuselier, 2016). [c]Values obtained in Section 3.2.5, see Table 1. [d]Event reported by Li et al. (2017), cf. Section 4.3.1. [e]Event reported by Toledo-Redondo et al. (2017), cf. Section 4.3.1.

increases, the locations of reconnection sites become increasingly confined to regions of anti-parallel magnetic fields (i.e., regions where magnetic shear angles are closer to 180°) (Cassak & Fuselier, 2016; Swisdak et al., 2003, 2010).

When ionospheric plasma is present on one side of the reconnection site, as is often the case for the Earth's magnetopause (see Table 1), the diamagnetic drift relationship can be altered locally. Through changes in $\Delta\beta$ due to the plasma temperature and density on one side of the reconnection region, the ionospheric-originating plasma reaching the magnetopause may affect reconnection beyond mass-loading the reconnection site, as discussed in Sections 4.1–4.3. Taking, for instance, typical plasma conditions in the Earth's magnetosheath and normal magnetic field strengths in the magnetosheath and outer magnetosphere, listed in Table 3 and in Cassak and Fuselier (2016), the largest values of $\Delta\beta$ (and so the most restrictive conditions for reconnection to proceed with regards to the diamagnetic drift effect) occur when the magnetospheric population consists of the plasma sheet population alone, which is always present.

We computed the resulting $\Delta\beta$ for various magnetospheric plasma conditions inferred from Sections 3 and 4, which are summarized in Table 3. In these calculations we only consider protons, which have been extensively described in Section 3. The changes in $\Delta\beta$ will be larger if heavy ions are accounted for. When the warm plasma cloak population reaches the magnetopause, it contributes to the magnetospheric plasma β (i.e., increasing the temperature and density), resulting in smaller $\Delta\beta$ across the magnetopause. For dense and cold plasma reaching the magnetopause, as when the plume extends to the outer magnetosphere during geomagnetic storms, the resulting $\Delta\beta$ using typical magnetosheath conditions is very similar to the $\Delta\beta$ observed for nominal magnetospheric plasma conditions when no dense, cold populations are present, because the plume population does not contribute significantly to the plasma pressure. The situation is different if we consider that cold plasma can be heated near the magnetopause boundary, as commented in Section 4.3.1. Using the cold ion densities and temperatures reported in the case studies by Li et al. (2017) and Toledo-Redondo et al. (2017), one finds that $\Delta\beta$ can be significantly reduced under the presence of ionospheric ions. However, to our knowledge, there are no statistical studies about cold ion heating at the magnetopause, so we do not know if the $\Delta\beta$ reduction due to heated plasmaspheric ions is a common situation. Therefore, the presence of the warm plasma cloak or, similarly, heated plasmaspheric material can increase the range of magnetic field orientations across the magnetopause at which magnetic reconnection can proceed, relaxing the condition for the diamagnetic drift suppression mechanism.



19449208, 2021, 3, Downloaded from https://agupubs.onlinelibrary.wiley.com/doi/10.1029/2020RG000707 by Cochrane France, Wiley Online Library on [07/11/2022]. See the Terms and Conditions (https://onlinelibrary.wiley.com/terms-and-conditions) on Wiley Online Library for rules of use; OA articles are governed by the applicable Creative Commons License

19449208, 2021, 3, Downloaded from https://agupubs.onlinelibrary.wiley.com/doi/10.1029/2020RG000707 by Cochrane France, Wiley Online Library on [07/11/2022]. See the Terms and Conditions (https://onlinelibrary.wiley.com/terms-and-conditions) on Wiley Online Library for rules of use; OA articles are governed by the applicable Creative Commons License

The varying plasma conditions under which reconnection suppression due to diamagnetic drift occurs have implications for where reconnection regions at the magnetopause are expected to be located, both for Earth and for other planets like Jupiter and Saturn. The moons of Jupiter and Saturn produce very large amounts of cold, dense plasma, and the very fast rotation of those planets confines the plasma to low-latitudes (Bagenal & Delamere, 2011; Louarn et al., 2015; Vasyliunas, 1983 and references therein). Coupled with a much weaker IMF in the outer solar system and a much stronger planetary magnetic field of these planets, reconnection is thought to be generally suppressed across most of the magnetopause at Jupiter and Saturn via this mechanism of diamagnetic drift (e.g., Desroche et al., 2013). While the diamagnetic drift-induced suppression is just one possible mechanism that may control the continuation after onset and efficiency of reconnection, the simple example above of how an inner plasma source may alter the plasma β at Earth's magnetopause, as well as observations of Saturn's magnetopause (Fuselier et al., 2014; Masters et al., 2012), shows the complex effect that cold plasma populations can have on reconnection dynamics.

Unlike the magnetopause, in the Earth's magnetotail, the diamagnetic drift suppression mechanism is not expected to be important because the magnitude of β in the plasma sheet is typically smaller than in the magnetosheath. In addition, reconnection in the magnetotail is typically symmetric and involves the plasma sheet populations in both sides, and therefore no substantial $\Delta\beta$ is expected across the current sheet.

### 4.6. Summary of the Effects of Cold and Heavy Ionospheric Ions on Magnetic Reconnection

Plasma sheet ions (mainly $H^+$, with number densities <1 $cm^{-3}$ and temperatures of a few to tens of kilo electron volt) are present both at the dayside magnetopause and in the magnetotail, and their origin is both the solar wind and the ionosphere, with variable contributions depending on solar and geomagnetic activity. The contribution of each source to the plasma sheet is still subject of debate and we discuss it in Section 5. In addition to plasma sheet ions, cold and heavy ionospheric outflows, detached plasmaspheric material and the WPC populations can also be present at the reconnection regions (cf. Sections 2.1 and 2.2). Section 4 has focused on reviewing the effects of these cold and heavy ionospheric-originating populations in magnetic reconnection. Cold and heavy ionospheric ions are often present and have non-negligible contributions to the mass density in the two key reconnecting regions: the dayside magnetopause and the magnetotail. These ionospheric ions mass-load the reconnecting flux tubes, and locally reduce the reconnection efficiency. This reduction is estimated to be significant (>20%) when the magnetospheric mass density is >28 amu·$cm^{-3}$. However, as it is deduced from analyzing various statistical studies in Section 3.2, such mass densities are possible but uncommon at the magnetopause. Significant reductions of the reconnection efficiency due to magnetospheric mass-loading occur mainly during storm times, when the production of detached plasmasphere material and WPC, which can include large amounts of $O^+$, is larger (Fuselier et al., 2017; Fuselier, Mukherjee, et al., 2019; Fuselier, Haaland, et al., 2020). There is also indirect evidence, using geomagnetic indices, of global reduction of the coupling to the solar wind when large amounts of ionospheric ions are present at the magnetopause, that is, during storm times (Borovsky et al., 2013).

In addition, cold and heavy ionospheric ions introduce multiple spatial and time scales into the reconnection process, owing to the dependence of gyroradius and gyrofrequency on temperature and particle mass. As concluded in Section 3.2, reconnection at the dayside magnetopause usually involves cold ions: more than 70% of the time at the dawn side and more than 80% of the time at the dusk side. In Section 3.3, we concluded that $O^+$ density was a significant contributor of the mass density most of the time. In the near-Earth plasma sheet (<10 $R_E$), the $n_{O+}/n_{H+}$ ratio varies between 0.1 and 1.3, depending on geomagnetic activity, and in the distant plasma sheet (<10 $R_E$) $n_{O+}/n_{H+} < 0.1$ for quiet times and $n_{O+}/n_{H+} \sim 0.2$–0.7 for disturbed times. A large set of microphysical effects, including multiple-scale IDRs, wave-particle interactions, and so on are enabled by these multiple ion populations. One then may think that the effective aspect ratio of the diffusion region and the energy conversion mechanisms are changed, resulting in modified reconnection efficiencies. However, according to recent PIC simulations, cold ions do not significantly modify the normalized reconnection rate once a steady state has been reached (Dargent et al., 2017, 2020; Divin et al., 2016). The reconnection rate, on average, may be set by MHD constraints, as suggested by Liu et al. (2017), when no other large-scale forcing acts over the process. A key question is when and for how long magnetic reconnection reaches steady state at the magnetopause. On the other hand, $O^+$ may not have time to reach steady state in magnetotail reconnection, resulting in a modified reconnection efficiency (Tenfjord et al., 2019).

19449208, 2021, 3, Downloaded from https://agupubs.onlinelibrary.wiley.com/doi/10.1029/2020RG000707 by Cochrane France, Wiley Online Library on [07/11/2022]. See the Terms and Conditions (https://onlinelibrary.wiley.com/terms-and-conditions) on Wiley Online Library for rules of use; OA articles are governed by the applicable Creative Commons License

**Table 4**
*Summary of Open Questions in the Role of Ionospheric Ions and Magnetic Reconnection in the Magnetosphere*

| | |
|---|---|
| Global magnetospheric dynamics | What is the relative contribution of solar wind versus ionospheric-originating $H^+$ to the magnetosphere? |
| | How is the plasma sheet formed? |
| | Does the variable magnetospheric density affect the global coupling with the solar wind efficiency? |
| Kinetic physics of magnetic reconnection | How do the microphysics introduced by multiple ion populations change reconnection at MHD scales? |
| | Does the WPC alter the suppression of magnetic reconnection? |
| | Which portion of the reconnection energy is taken by cold and heavy ions? |
| | What are the effects of cold electrons in magnetic reconnection? |
| | How ionospheric ions in the plasma sheet condition the onset of magnetic reconnection? |

Abbreviation: WPC, warm plasma cloak.

Another key question is to what extent the local properties (MHD and microphysics) of the reconnecting boundary can control the global efficiency of solar wind—magnetosphere coupling versus the global forcing driven by the solar wind (cf. Section 4.1.3).

There is direct evidence that cold and heavy ions are heated and accelerated by reconnection in the tail and the dayside magnetopause, and therefore they take a portion of the energy budget of reconnection. Toledo-Redondo et al. (2017), based on four case studies, found that cold ions take 10%–25% of the energy that goes into ion heating. However, statistical studies of the energy budget at the magnetopause and magnetotail accounting for ionospheric ions have not been conducted.

Along with effects on the local microphysics of magnetic reconnection, the presence of cold and heavy ionospheric-originating ions can affect dynamics on a more global scale in the magnetosphere. In Section 3.3 we discussed how common is $O^+$ in the magnetotail plasma sheet, cf. Table 2. Baker et al. (1982) predicted that the tearing instability threshold should be reduced by the presence of $O^+$, favoring the onset of magnetic reconnection. However, spacecraft observations have found that fewer substorms are observed when the magnetotail is loaded with $O^+$ (Liu et al., 2013).

For the dayside, ionospheric-originating ions can alter local, and possibly global, conditions required for reconnection to occur. The dayside magnetopause is typically asymmetric, with shocked solar wind on one side and magnetospheric plasma on the other. If $\Delta\beta$ is large across the reconnecting boundary, then magnetic reconnection can be suppressed by the diamagnetic drift. Based on theoretical computations using average magnetosheath conditions and reproducing the ionospheric contributions deduced from Section 3.2, it is expected that ionospheric ions will facilitate magnetic reconnection to proceed at the dayside magnetopause at smaller IMF clock angles by reducing $\Delta\beta$. More work and observations are needed to further our understanding of the complex cross-scale dynamics resulting from the presence of ionospheric-originating ion populations at reconnection sites.

## 5. Remaining Issues and Open Questions

We list below what we consider the most outstanding open questions inferred from this review work, related to ionospheric-originating ions in the magnetosphere and their effects on magnetic reconnection. Table 4 summarizes these open questions, grouped in two categories.

### 5.1. What is the Relative Contribution of Solar Wind Versus Ionospheric-Originating $H^+$ to the Magnetosphere?

The sources of magnetospheric plasma at all energies are the ionosphere and the solar wind. Because the dominant ion population in the magnetosphere is $H^+$, and $H^+$ comes from both the ionosphere and the solar wind, we cannot directly determine the origin of the $H^+$ in the magnetosphere: it all looks the same. Separating the sources can be done using the minor ion composition (e.g., Kistler, 2020), or using modeling (e.g., Glocer et al., 2020). It is well documented that the ionospheric source becomes dominant during southward

IMF periods associated with increased geomagnetic activity. Overall, the relative contributions of the ionosphere and the solar wind are estimated to be of the same order of magnitude, but precise quantitative knowledge of the relative contributions is missing. Global modeling is the most straightforward method to discriminate the origin of $H^+$, but these models are challenging because they need to account for many processes occurring at very different scales.

### 5.2. How is the Plasma Sheet Formed?

The plasma sheet boundary layer is a key transition region in which the inflowing lobe ions from the ionosphere enter the plasma sheet region and are energized to become part of it. The lobe ions (electron volt to hundreds of electron volt) are energized to the 1–10 keV energies typically observed in the plasma sheet, which contains remnants of solar wind and energized polar wind ions from earlier time periods, as well as from more distant places down the magnetotail. It is this changing mix that sets the stage for the reconnection that is observed. MMS measurements across the plasma sheet boundary layer between the lobes and the neutral sheet can show us how this takes place. Model trajectories combined with differential measurement capabilities can show how the plasma sheet is created.

### 5.3. Does the Variable Magnetospheric Density Affect the Global Coupling With the Solar Wind Efficiency?

Solar wind - magnetosphere coupling via magnetic reconnection depends mostly on solar wind parameters, in particular the orientation of the IMF, but mass density and magnetic field magnitude also affect the efficiency of the coupling. The magnetospheric mass density at the magnetopause depends on the time history of the magnetosphere. It is not clear to what extent the magnetospheric forcing in general, and the ionospheric source in particular, can exert control of the efficiency of the coupling. Recent modeling (cf. Section 4.1.3) suggests that for a moderate variation of magnetospheric conditions at the magnetopause the system can respond and the efficiency is defined by solar wind parameters. On the other hand, for large mass density changes on the magnetospheric side of the magnetopause, the coupled system efficiency can be modified. Further modeling in this direction, in connection with large statistical surveys of available space and ground datasets may help improving our understanding of what controls the reconnection efficiency between the solar wind and the magnetosphere.

### 5.4. How do the Microphysics Introduced by Multiple Ion Populations Change Magnetic Reconnection at MHD Scales?

Recent spacecraft observations have shown that several changes are produced at kinetic scales of magnetic reconnection when multiple ion populations are present. These changes include for instance the generation of ion-ion instabilities or modification of the ion diffusion region. However, recent simulations indicate that these changes by themselves seem not to affect the reconnection efficiency, once a steady state is reached. How magnetic reconnection self-arranges at fluid scales and how the information of the processes at kinetic scales is transferred to these fluid scales remains a mystery. PIC models of magnetic reconnection are a very powerful tool to improve our understanding on how the system self-arranges at large scales under the presence of multiple ion populations.

### 5.5. Does the WPC Alter the Suppression of Magnetic Reconnection?

As discussed in Section 4.5, the warm plasma cloak can reduce the difference in plasma $\beta$between the two sides of the dayside magnetopause, and this may facilitate magnetic reconnection to proceed under smaller **B** field clock angles. This reasoning comes from the current understanding of analytical theory of magnetic reconnection, but this hypothetical effect of the WPC has not been shown. Global modeling of the magnetosphere including the WPC population can be used to test this effect. In addition, performing statistics of local observations of the flank magnetopause, where this effect should be more pronounced, in the SW parameter space can also help understanding the relative importance of the WPC in altering the suppression of reconnection.



19449208, 2021, 3, Downloaded from https://agupubs.onlinelibrary.wiley.com/doi/10.1029/2020RG000707 by Cochrane France, Wiley Online Library on [07/11/2022]. See the Terms and Conditions (https://onlinelibrary.wiley.com/terms-and-conditions) on Wiley Online Library for rules of use; OA articles are governed by the applicable Creative Commons License

19449208, 2021, 3, Downloaded from https://agupubs.onlinelibrary.wiley.com/doi/10.1029/2020RG000707 by Cochrane France, Wiley Online Library on [07/11/2022]. See the Terms and Conditions (https://onlinelibrary.wiley.com/terms-and-conditions) on Wiley Online Library for rules of use; OA articles are governed by the applicable Creative Commons License

### 5.6. Which Portion of the Reconnection Energy is Taken by Cold and Heavy Ions?

When cold and heavy ions of ionospheric origin are present in the reconnection region, they are both accelerated and heated. Therefore, they take a portion of the converted magnetic energy by reconnection, although there exists no quantification on how the available magnetic energy is partitioned among the various ion and electron populations. The heating mechanisms and their relative importance are not well understood, and hence is difficult to include them in modeling. On the other hand, performing statistics on spacecraft observations of heated cold ions at the magnetopause is achievable with current datasets.

### 5.7. What are the Effects of Cold Electrons in Magnetic Reconnection?

There is observational evidence that the cold ion populations in the magnetosphere are accompanied by cold electrons. The possible effects of this cold electron population to magnetic reconnection or the magnetospheric dynamics has not been widely addressed. However, these electrons are challenging to measure, because they are often intermixed with spacecraft-originating photoelectrons, and new instrumentation capable of adequately resolving the velocity distribution function of cold electrons may be required.

### 5.8. How Ionospheric Ions in the Plasma Sheet Condition the Onset of Magnetic Reconnection?

During disturbed times, the mass density of the magnetotail is usually dominated by $O^+$. The presence of such heavy ions should reduce the tearing instability threshold and therefore facilitate the onset of magnetic reconnection. However, various observational studies seem to indicate the contrary, that is, that reconnection becomes more difficult to trigger reconnection when $O^+$ is present (cf. Section 4.4). How ionospheric ions modify the onset of reconnection and therefore affect the driving storms and substorms remains not well understood. More reconnection modeling including multiple ion populations can help understanding the role of the ionospheric source.

## 6. Summary and Concluding Remarks

The ionosphere is a prime source of particles for the magnetosphere. The polar wind is constantly outflowing at mid and high latitudes, creating low-energy (electron volt to tens of electron volt), light ion populations ($H^+$ and $He^+$). At high latitudes, additional energy sources such as waves in the cusp and auroral oval create more energetic (hundreds of electron volt) outflows, that include $O^+$ in addition to light ions. These outflowing ions travel along the magnetic field lines and are convected together with them. Depending on the orientation of the solar wind IMF, which drives the convection, the initial parallel velocity of the outflowing ions, and their starting latitude and longitude location in the ionosphere, they will end up in the magnetotail, in the outer dayside magnetosphere, or will be trapped in the inner plasmasphere. Each of these paths may result in various energization levels, and the outflows will become part of the plasma sheet, the ring current, the plasmasphere, or the warm plasma cloak. Most of these ions do not return to the ionosphere, and escape the magnetosphere at an average rate of $\sim 10^{26}$ ions/s.

Magnetic reconnection takes place at the dayside magnetopause and in the magnetotail, is responsible for the coupling of the magnetosphere to the solar wind, drives storms and substorms, as well as magnetospheric convection, and supplies magnetic energy that is converted to kinetic and thermal energies of the particle populations. Near the magnetopause, the magnetospheric mass density is composed of plasma sheet ions (kilo electron volt to tens of kilo electron volt) of both solar wind and ionospheric origin, plus various colder populations (electron volt to hundreds of electron volt) of ionospheric origin. The magnetospheric mass density near the magnetopause is variable and dominated by the ionospheric source, although this density is usually smaller than the solar wind density on the other side of the magnetopause. In the tail, the near-Earth plasma sheet mass density is dominated by the ionospheric source all the time. In the distant tail, the ionospheric source becomes dominant during active magnetospheric times. During periods of southward IMF, which are associated with increased geomagnetic activity, more ionospheric-originating ions are found at the magnetopause and in the plasma sheet. These variable contributions to the plasma in the reconnecting regions modulate how reconnection proceeds. Additional mass reduces the rate of magnetic energy conversion at the dayside. In addition, a number of kinetic effects are introduced by the different

masses and temperatures of the ionospheric-originating ion populations. For instance, waves are generated by ion-ion instabilities in the reconnection regions, which heat the ions. Cold ions have smaller intrinsic spatial scales (gyroradius), and therefore create different ion diffusion regions. In addition, they can remain magnetized inside the separatrices of reconnection, modifying the perpendicular currents associated with this region. Heavy ions have larger intrinsic time scales (smaller gyrofrequency), and may not be able to follow the intermittent and bursty evolution of magnetic reconnection in the tail.

The complexity of the magnetospheric system and its dynamics is enormous. Our knowledge has been growing significantly since satellite missions enabled in situ and remote measurements of it, and with the aid of computer simulations. We now understand that the ionospheric source is a major supplier of plasma and that the variability of this source affects magnetic reconnection in various ways. However, there still remain open questions, in particular about how the system responds to this variability in a global sense.

## Data Availability Statement

No new data analysis was done for this research.

**Acknowledgments**
The discoverer of energetic $O^+$ and $He^+$ of ionospheric origin in the magnetosphere, Dr. Edward G. Shelley, passed away in 2020. This review paper is dedicated to his enduring legacy. We are grateful to the International Space Science Institute (ISSI), who made possible this review by funding the international team *Cold plasma of ionospheric origin in the Earth's magnetosphere*.

## References

Akasofu, S. I. (2015). Paradigm transitions in solar–terrestrial physics from 1900: My personal view. *History of Geo-and Space Sciences*, *6*(1), 23–43. https://doi.org/10.5194/hgss-6-23-2015

Alm, L., André, M., Graham, D. B., Khotyaintsev, Y. V., Vaivads, A., Chappell, C. R., et al. (2019). MMS observations of multiscale hall physics in the magnetotail. *Geophysical Research Letters*, *46*, 10230–10239. https://doi.org/10.1029/2019gl084137

Alm, L., André, M., Vaivads, A., Khotyaintsev, Y. V., Torbert, R. B., Burch, J. L., et al. (2018). Magnetotail hall physics in the presence of cold ions. *Geophysical Research Letters*, *45*(20), 10941–10950. https://doi.org/10.1029/2018GL079857

André, M., & Cully, C. M. (2012). Low-energy ions: A previously hidden solar system particle population. *Geophysical Research Letters*, *39*(3). https://doi.org/10.1029/2011GL050242

André, M., Li, K., & Eriksson, A. I. (2015). Outflow of low-energy ions and the solar cycle. *Journal of Geophysical Research: Space Physics*, *120*(2), 1072–1085. https://doi.org/10.1002/2014JA020714

André, M., Li, W., Toledo-Redondo, S., Khotyaintsev, Y. V., Vaivads, A., Graham, D. B., et al. (2016). Magnetic reconnection and modification of the Hall physics due to cold ions at the magnetopause. *Geophysical Research Letters*, *43*(13), 6705–6712. https://doi.org/10.1002/2016GL069665

André, M., Toledo-Redondo, S., & Yau, A. W. (2020). Cold ionospheric ions in the magnetosphere, space physics and aeronomy collection volume 2: Magnetospheres in the Solar System. In *Geophysical monograph 259* (1st ed.). John Wiley & Sons. https://doi.org/10.1002/9781119507512

André, M., Vaivads, A., Khotyaintsev, Y. V., Laitinen, T., Nilsson, H., Stenberg, G., et al. (2010). Magnetic reconnection and cold plasma at the magnetopause. *Geophysical Research Letters*, *37*(22). https://doi.org/10.1029/2010gl044611

André, M., & Yau, A. (1997). Theories and observations of ion energization and outflow in the high latitude magnetosphere. *Space Science Reviews*, *80*, 27–48. https://doi.org/10.1023/A:1004921619885

Aunai, N., Belmont, G., & Smets, R. (2011). Proton acceleration in antiparallel collisionless magnetic reconnection: Kinetic mechanisms behind the fluid dynamics. *Journal of Geophysical Research*, *116*(A9). https://doi.org/10.1029/2011ja016688

Axford, W. I. (1968). The polar wind and the terrestrial helium budget. *Journal of Geophysical Research*, *73*(21), 6855–6859. https://doi.org/10.1029/ja073i021p06855

Bagenal, F. P., & Delamere, P. A. (2011). Flow of mass and energy in the magnetospheres of Jupiter and Saturn. *Journal of Geophysical Research*, *116*, A05209. https://doi.org/10.1029/2010JA016294

Baker, D. N., Hones, E. W., Jr, Young, D. T., & Birn, J. (1982). The possible role of ionospheric oxygen in the initiation and development of plasma sheet instabilities. *Geophysical Research Letters*, *9*(12), 1337–1340. https://doi.org/10.1029/gl009i012p01337

Banks, P. M., & Holzer, T. E. (1968). The polar wind. *Journal of Geophysical Research*, *73*(21), 6846–6854. https://doi.org/10.1029/ja073i021p06846

Banks, P. M., Nagy, A. F., & Axford, W. I. (1971). Dynamical behavior of thermal protons in the mid-latitude ionosphere and magnetosphere. *Planetary and Space Science*, *19*(9), 1053–1067. https://doi.org/10.1016/0032-0633(71)90104-8

Barakat, A. R., & Schunk, R. W. (2006). A three-dimensional model of the generalized polar wind. *Journal of Geophysical Research*, *111*(A11). https://doi.org/10.1029/2006ja011662

Baumjohann, W., Paschmann, G., & Cattell, C. A. (1989). Average plasma properties in the central plasma sheet. *Journal of Geophysical Research*, *94*(A6), 6597–6606. https://doi.org/10.1029/ja094ia06p06597

Benson, R. F. (2010). Four decades of space-born radio sounding. *Radio Science Bulletin*, *333*(13), 6705–6712. https://doi.org/10.1002/2016GL069665

Berube, D., Moldwin, M. B., Fung, S. F., & Green, J. L. (2005). A plasmaspheric mass density model and constraints on its heavy ion concentration. *Journal of Geophysical Research*, *110*, A04212. https://doi.org/10.1029/2004JA010684

Bessho, N., Chen, L.-J., & Hesse, M. (2016). Electron distribution functions in the diffusion region of asymmetric magnetic reconnection. *Geophysical Research Letters*, *43*(5), 1828–1836. https://doi.org/10.1002/2016GL067886

Birn, J., Drake, J. F., Shay, M. A., Rogers, B. N., Denton, R. E., Hesse, M., et al. (2001). Geospace Environmental Modeling (GEM) magnetic reconnection challenge. *Journal of Geophysical Research*, *106*(A3), 3715–3719. https://doi.org/10.1029/1999ja900449

Birn, J., Runov, A., & Zhou, X.-Z. (2017). Ion velocity distributions in dipolarization events: Distributions in the central plasma sheet. *Journal of Geophysical Research: Space Physics*, *122*(8), 8014–8025. https://doi.org/10.1002/2017ja024230



19449208, 2021, 3, Downloaded from https://agupubs.onlinelibrary.wiley.com/doi/10.1029/2020RG000707 by Cochrane France, Wiley Online Library on [07/11/2022]. See the Terms and Conditions (https://onlinelibrary.wiley.com/terms-and-conditions) on Wiley Online Library for rules of use; OA articles are governed by the applicable Creative Commons License

Birn, J., Yur, G., Rahman, H. U., & Minami, S. (1992). On the termination of the closed field line region of the magnetotail. *Journal of Geophysical Research*, *97*, 14833–14840. https://doi.org/10.1029/92JA01145
Borovsky, J. E. (2008). The rudiments of a theory of solar wind/magnetosphere coupling derived from first principles. *Journal of Geophysical Research*, *113*(A8). https://doi.org/10.1029/2007ja012646
Borovsky, J. E. (2013). Physical improvements to the solar wind reconnection control function for the Earth's magnetosphere. *Journal of Geophysical Research: Space Physics*, *118*(5), 2113–2121. https://doi.org/10.1002/jgra.50110
Borovsky, J. E., & Birn, J. (2014). The solar wind electric field does not control the dayside reconnection rate. *Journal of Geophysical Research: Space Physics*, *119*(2), 751–760. https://doi.org/10.1002/2013ja019193
Borovsky, J. E., & Denton, M. H. (2006). Differences between CME-driven storms and CIR-driven storms. *Journal of Geophysical Research*, *111*(A7), A07S08. https://doi.org/10.1029/2005JA011447.7
Borovsky, J. E., & Denton, M. H. (2008). A statistical look at plasmaspheric drainage plumes. *Journal of Geophysical Research*, *113*, A09221. https://doi.org/10.1029/2007JA012994
Borovsky, J. E., Denton, M. H., Denton, R. E., Jordanova, V. K., & Krall, J. (2013). Estimating the effects of ionospheric plasma on solar wind/magnetosphere coupling via mass loading of dayside reconnection: Ion-plasma-sheet oxygen, plasmaspheric drainage plumes, and the plasma cloak. *Journal of Geophysical Research: Space Physics*, *118*, 5695–5719. https://doi.org/10.1002/jgra.50527
Borovsky, J. E., Thomsen, M. F., McComas, D. J., Cayton, T. E., & Knipp, D. J. (1998). Magnetospheric dynamics and mass flow during the November 1993 storm. *Journal of Geophysical Research*, *103*(A11), 26373–26394. https://doi.org/10.1029/97ja03051
Bouhram, M., Klecker, B., Miyake, W., Reme, H., Sauvaud, J. A., Malingre, M., et al. (2004). On the altitude dependence of transversely heated O+ distributions in the cusp/cleft. *Annales Geophysicae*, *22*(5), 1787–1798. https://doi.org/10.5194/angeo-22-1787-2004
Brace, L. H. (2013). *Langmuir probe measurements in the ionosphere* (pp. 23–35). American Geophysical Union (AGU). https://doi.org/10.1029/GM102p0023
Brambles, O. J., Lotko, W., Damiano, P. A., Zhang, 1., Wiltberger, M., & Lyon, J. (2010). Effects of causally driven cusp O+ outflow on the storm time magnetosphere-ionosphere system using a multifluid global simulation. *Journal of Geophysical Research*, *115*(A9). https://doi.org/10.1029/2010ja015469
Brambles, O. J., Lotko, W., Zhang, B., Ouellette, J., Lyon, J., & Wiltberger, M. (2013). The effects of ionospheric outflow on ICME and SIR driven sawtooth events. *Journal of Geophysical Research: Space Physics*, *118*, 6026–6041. https://doi.org/10.1002/jgra.50522
Burch, J. L., Ergun, R. E., Cassak, P. A., Webster, J. M., Torbert, R. B., Giles, B. L., et al. (2018). Localized oscillatory energy conversion in magnetopause reconnection. *Geophysical Research Letters*, *45*, 1237–1245. https://doi.org/10.1002/2017gl076809
Burch, J. L., Torbert, R. B., Phan, T. D., Chen, L.-J., Moore, T. E., Ergun, R. E., et al. (2016). Electron-scale measurements of magnetic reconnection in space. *Science*. https://doi.org/10.1126/science.aaf2939
Carpenter, D. L., Giles, B. L., Chappell, C. R., Decreau, P. M. E., Anderson, R. R., Persoon, A. M., et al. (1993). Plasmasphere dynamics in the duskside bulge region: A new look at an old topic. *Journal of Geophysical Research*, *98*, 19253–19271. https://doi.org/10.1029/93ja00922
Cassak, P. A., & Fuselier, S. A. (2016). Reconnection at Earth's dayside magnetopause. In W. Gonzalez, & E. Parker (Eds.), *Magnetic reconnection, astrophysics and space science library, 427*. Springer. https://doi.org/10.1007/978-3-319-26432-5_6
Cassak, P. A., Liu, Y. H., & Shay, M. A. (2017). A review of the 0.1 reconnection rate problem. *Journal of Plasma Physics*, *83*(5). https://doi.org/10.1017/s0022377817000666
Cassak, P. A., & Shay, M. A. (2007). Scaling of asymmetric magnetic reconnection: General theory and collisional simulations. *Physics of Plasmas*, *14*(10), 102114. https://doi.org/10.1063/1.2795630
Chappell, C. R. (1972). Recent satellite measurements of the morphology and dynamics of the plasmasphere. *Reviews of Geophysics*, *10*(4), 951–979. https://doi.org/10.1029/rg010i004p00951
Chappell, C. R. (1974). Detached plasma regions in the magnetosphere. *Journal of Geophysical Research*, *79*(13), 1861–1870. https://doi.org/10.1029/ja079i013p01861
Chappell, C. R. (1988). The terrestrial plasma source: A new perspective in solar-terrestrial processes from Dynamics Explorer. *Reviews of Geophysics*, *26*(2), 229–248. https://doi.org/10.1029/rg026i002p00229
Chappell, C. R. (2015). The role of the ionosphere in providing plasma to the terrestrial magnetosphere—An historical overview. *Space Science Reviews*, *192*, 5–25. https://doi.org/10.1007/s11214-015-0168-5
Chappell, C. R., Baugher, C. R., & Horwitz, J. L. (1980). New advances in thermal plasma research. *Reviews of Geophysics*, *18*(4), 853–861. https://doi.org/10.1029/RG018i004p00853
Chappell, C. R., Harris, K. K., & Sharp, G. W. (1971). The dayside of the plasmasphere. *Journal of Geophysical Research*, *76*(31), 7632–7647. https://doi.org/10.1029/ja076i031p07632
Chappell, C. R., Huddleston, M. M., Moore, T. E., Giles, B. L., & Delcourt, D. C. (2008). Observations of the warm plasma cloak and an explanation of its formation in the magnetosphere. *Journal of Geophysical Research*, *113*(A9). https://doi.org/10.1029/2007ja012945
Chappell, C. R., Moore, T. E., & Waite Jr, J. H. (1987). The ionosphere as a fully adequate source of plasma for the Earth's magnetosphere. *Journal of Geophysical Research*, *92*(A6), 5896–5910. https://doi.org/10.1029/ja092ia06p05896
Chen, S. H., & Moore, T. E. (2006). Magnetospheric convection and thermal ions in the dayside outer magnetosphere. *Journal of Geophysical Research*, *111*(A3). https://doi.org/10.1029/2005ja011084
Cladis, J. B., Collin, H. L., Lennartsson, O. W., Moore, T. E., Peterson, W. K., & Russel, C. T. (2000). Observations of centrifugal acceleration during compression of magnetosphere. *Geophysical Research Letters*, *27*, 915. https://doi.org/10.1029/1999GL010737
Cladis, J. B., & Francis, W. E. (1992). Distribution in magnetotail of O+ ions from cusp/cleft ionosphere: A possible substorm trigger. *Journal of Geophysical Research*, *97*(A1), 123–130. https://doi.org/10.1029/91ja02376
Collin, H. L., Peterson, W. K., Lennartsson, O. W., & Drake, J. F. (1998). The seasonal variation of auroral ion beams. *Geophysical Research Letters*, *25*(21), 4071–4074. https://doi.org/10.1029/1998gl900090
Comfort, R. H. (1998). The magnetic mirror force in plasma fluid models. In T. E. Moore, In J. H. Waite Jr., T. W. Moorehead, & W. B. Hanson (Eds.). *Modeling magnetospheric plasma, Volume 44, AGU Geophysical Monograph Series*. https://doi.org/10.1029/GM044p0051
Craven, P. D., Gallagher, D. L., & Comfort, R. H. (1997). Relative concentration of He+ in the inner magnetosphere as observed by the DE 1 retarding ion mass spectrometer. *Journal of Geophysical Research*, *102*(A2), 2279–2289. https://doi.org/10.1029/96ja02176
Craven, P. D., Olsen, R. C., Chappell, C. R., & Kakani, L. (1985). Observations of molecular ions in the Earth's magnetosphere. *Journal of Geophysical Research*, *90*(A8), 7599–7605. https://doi.org/10.1029/ja090ia08p07599
Cully, C. M., Donovan, E. F., Yau, A. W., & Arkos, G. G. (2003). Akebono/Suprathermal Mass Spectrometer observations of low-energy ion outflow: Dependence on magnetic activity and solar wind conditions. *Journal of Geophysical Research*, *108*, 1093. https://doi.org/10.1029/2001JA009200



19449208, 2021, 3, Downloaded from https://agupubs.onlinelibrary.wiley.com/doi/10.1029/2020RG000707 by Cochrane France, Wiley Online Library on [07/11/2022]. See the Terms and Conditions (https://onlinelibrary.wiley.com/terms-and-conditions) on Wiley Online Library for rules of use; OA articles are governed by the applicable Creative Commons License

Daglis, I. A., Sarris, E. T., & Kremser, G. (1990). Indications for ionospheric participation in the substorm process from AMPTE/CCE observations. *Geophysical Research Letters*, *17*(1), 57–60. https://doi.org/10.1029/gl017i001p00057

Daly, P. W. (1986). Structure of the distant terrestrial magnetotail. *Advances in Space Research*, *6*, 245. https://doi.org/10.1016/0273-1177(86)90041-4

Dandouras, I. (2013). Detection of a plasmaspheric wind in the Earth's magnetosphere by the Cluster spacecraft. *Annales Geophysicae*, *31*(7), 0992768. https://doi.org/10.5194/angeo-31-1143-2013

Dargent, J., Aunai, N., Lavraud, B., Toledo-Redondo, S., & Califano, F. (2019). Signatures of cold ions in a kinetic simulation of the reconnecting magnetopause. *Journal of Geophysical Research: Space Physics*, *124*(4), 2497–2514. https://doi.org/10.1029/2018JA026343

Dargent, J., Aunai, N., Lavraud, B., Toledo-Redondo, S., & Califano, F. (2020). Simulation of plasmaspheric plume impact on dayside magnetic reconnection. *Geophysical Research Letters*. https://doi.org/10.1029/2019GL086546.8

Dargent, J., Aunai, N., Lavraud, B., Toledo-Redondo, S., Shay, M. A., Cassak, P. A., & Malakit, K. (2017). Kinetic simulation of asymmetric magnetic reconnection with cold ions. *Journal of Geophysical Research: Space Physics*, *122*(5), 5290–5306. https://doi.org/10.1002/2016JA023831

DeHoffmann, F., & Teller, E. (1950). Magnetohydrodynamic shocks. *Physical Review*, *80*, p692. https://doi.org/10.1103/physrev.80.692

Delcourt, D. C., Chappell, C. R., Moore, T. E., & Waite, J. H., Jr (1989). A three-dimensional numerical model of ionospheric plasma in the magnetosphere. *Journal of Geophysical Research*, *94*(A9), 11893–11920. https://doi.org/10.1029/ja094ia09p11893

Delcourt, D. C., Sauvaud, J. A., & Moore, T. E. (1993). Polar wind ion dynamics in the magnetotail. *Journal of Geophysical Research*, *98*(A6), 9155–9169. https://doi.org/10.1029/93ja00301

Denton, M. H., Henderson, M. G., Maruyama, N., & Fuselier, S. A. (2019). The cold ion population at geosynchronous orbit and transport to the dayside magnetopause: September 2015 to February 2016. *Journal of Geophysical Research*, *124*, 8685–8694. https://doi.org/10.1029/2019JA026973

Denton, R. E., Goldstein, J., & Menietti, J. D. (2002). Field line dependence of magnetospheric electron density. *Geophysical Research Letters*, *29*(24), 581–584. https://doi.org/10.1029/2002gl015963

Desroche, M., Bagenal, F., Delamere, P. A., & Erkaev, N. (2013). Conditions at the magnetopause of Saturn and implications for the solar wind interaction. *Journal of Geophysical Research: Space Physics*, *118*, 3087–3095. https://doi.org/10.1002/jgra.50294

Divin, A., Khotyaintsev, Y. V., Vaivads, A., André, M., Toledo-Redondo, S., Markidis, S., & Lapenta, G. (2016). Three-scale structure of diffusion region in the presence of cold ions. *Journal of Geophysical Research: Space Physics*, *121*(12), 12001–12013. https://doi.org/10.1002/2016JA023606

Drake, J. F., Cassak, P. A., Shay, M. A., Swisdak, M., & Quataert, E. (2009). A magnetic reconnection mechanism for ion acceleration and abundance enhancements in impulsive flares. *The Astrophysical Journal Letters*, *700*(1), L16. https://doi.org/10.1088/0004-637x/700/1/l16

Drake, J. F., Swisdak, M., Phan, T. D., Cassak, P. A., Shay, M. A., Lepri, S. T., et al. (2009). Ion heating resulting from pickup in magnetic reconnection exhausts. *Journal of Geophysical Research*, *114*(A5). https://doi.org/10.1029/2008ja013701

Dungey, J. W. (1963). Interactions of solar plasma with the geomagnetic field. *Planetary and Space Science*, *10*, 233–237. https://doi.org/10.1016/0032-0633(63)90020-5

Eastwood, J. P., Goldman, M. V., Hietala, H., Newman, D. L., Mistry, R., & Lapenta, G. (2015). Ion reflection and acceleration near magnetotail dipolarization fronts associated with magnetic reconnection. *Journal of Geophysical Research: Space Physics*, *120*(1), 511–525. https://doi.org/10.1002/2014ja020516

Engwall, E., Eriksson, A. I., Cully, C. M., André, M., Torbert, R., & Vaith, H. (2009). Earth's ionospheric outflow dominated by hidden cold plasma. *Nature Geoscience*, *2*, 24–27. https://doi.org/10.1038/ngeo387

Foster, J. C., Erickson, P. J., Coster, A. J., Goldstein, J., & Rich, F. J. (2002). Ionospheric signatures of plasmaspheric tails. *Geophysical Research Letters*, *29*(13), 1. https://doi.org/10.1029/2002gl015067

Fuselier, S. A. (2020). Ionospheric oxygen ions in the dayside magnetosphere. *Journal of Atmospheric and Solar-Terrestrial Physics*, *210*, 105448. https://doi.org/10.1016/j.jastp.2020.105448

Fuselier, S. A., Burch, J. L., Mukherjee, J., Genestreti, K. J., Vines, S. K., Gomez, R., et al. (2017). Magnetospheric ion influence at the dayside magnetopause. *Journal of Geophysical Research: Space Physics*, *122*, 8617–8631. https://doi.org/10.1002/2017JA024515

Fuselier, S. A., Dayeh, M. A., Galli, A., Funsten, H. O., Schwadron, N. A., Petrinec, S. M., et al. (2020). Neutral atom imaging of the solar wind-magnetosphere-exosphere interaction near the subsolar magnetopause. *Geophysical Research Letters*, *47*(19), e2020GL089362. https://doi.org/10.1029/2020gl089362

Fuselier, S. A., Frahm, R., Lewis, R. W. S., Masters, A., Mukherjee, J., Petrinec, S. M., & Sillanpaa, I. J. (2014). The location of magnetic reconnection at Saturn's magnetopause: A comparison with Earth. *Journal of Geophysical Research: Space Physics*, *119*, 2563–2578. https://doi.org/10.1002/2013JA019684

Fuselier, S. A., Haaland, S., Tenfjord, P., Paschmann, G., Toledo-Redondo, S., Malaspina, D., et al. (2020). High-density magnetospheric He+ at the dayside magnetopause and its effect on magnetic reconnection. *Journal of Geophysical Research: Space Physics*, *126*. https://doi.org/10.1029/2020ja028722

Fuselier, S. A., Klumpar, D. M., Peterson, W. K., & Shelley, E. G. (1989). Direct injection of ionospheric O+ into the dayside low latitude boundary layer. *Geophysical Research Letters*, *16*(10), 1121–1124. https://doi.org/10.1029/gl016i010p01121

Fuselier, S. A., & Lewis, W. S. (2011). Properties of near-Earth magnetic reconnection from in-situ observations. *Space Science Reviews*, *160*(1–4), 95. https://doi.org/10.1007/978-1-4614-3046-9_6

Fuselier, S. A., Mukherjee, J., Denton, M. H., Petrinec, S. M., Trattner, K. J., Toledo-Redondo, S., et al. (2019). High-density $O^+$ in Earth's outer magnetosphere and its effect on dayside magnetopause magnetic reconnection. *Journal of Geophysical Research: Space Physics*, *124*. https://doi.org/10.1029/10.1029/2019ja027396

Fuselier, S. A., Trattner, K., Petrinec, S., Denton, M., Toledo-Redondo, S., André, M., et al. (2019). Mass-loading the Earth's dayside magnetopause boundary layer and its effect on magnetic reconnection. *Geophysical Research Letters*, *3*, 6204–6213. https://doi.org/10.1029/2019gl082384

Garcia, K. S., Merkin, V. G., & Hughes, W. J. (2010). Effects of nightside O+ outflow on magnetospheric dynamics: Results of multifluid MHD modeling. *Journal of Geophysical Research*, *115*(A12). https://doi.org/10.1029/2010ja015730

Garcia-Sage, K., Moore, T. E., Pembroke, A., Merkin, V. G., & Hughes, W. J. (2015). Modeling the effects of ionospheric oxygen outflow on bursty magnetotail flows. *Journal of Geophysical Research: Space Physics*, *120*(10), 8723–8737.

Garrett, H. B. (1981). The charging of spacecraft surfaces. *Reviews of Geophysics*, *19*(4), 577–616. https://doi.org/10.1029/RG019i004p00577

Genestreti, K. J., Goldstein, J., Corley, G. D., Farner, W., Kistler, L. M., Larsen, B. A., et al. (2017). Temperature of the plasmasphere from Van Allen Probes HOPE. *Journal of Geophysical Research: Space Physics*, *122*(1), 310–323. https://doi.org/10.1002/2016ja023047



19449208, 2021, 3, Downloaded from https://agupubs.onlinelibrary.wiley.com/doi/10.1029/2020RG000707 by Cochrane France, Wiley Online Library on [07/11/2022]. See the Terms and Conditions (https://onlinelibrary.wiley.com/terms-and-conditions) on Wiley Online Library for rules of use; OA articles are governed by the applicable Creative Commons License

Genestreti, K. J., Nakamura, T. K. M., Nakamura, R., Denton, R. E., Torbert, R. B., Burch, J. L., et al. (2018). How accurately can we measure the reconnection rate EM for the MMS diffusion region event of 11 July 2017? *Journal of Geophysical Research: Space Physics*, *123*(11), 9130–9149. https://doi.org/10.1029/2018ja025711

George, D. E., & Jahn, J. M. (2020). Energized oxygen in the magnetotail: Current sheet bifurcation from Speiser motion. *Journal of Geophysical Research: Space Physics*, *125*(2), e2019JA027339. https://doi.org/10.1029/2019ja027339

Glocer, A., Toth, G., & Fok, M. C. (2018). Including kinetic ion effects in the coupled global ionospheric outflow solution. *Journal of Geophysical Research: Space Physics*, *123*(4), 2851–2871. https://doi.org/10.1002/2018ja025241

Glocer, A., Tóth, G., Ma, Y., Gombosi, T., Zhang, J. C., & Kistler, L. M. (2009). Multifluid block-adaptive-tree solar wind roe-type upwind scheme: Magnetospheric composition and dynamics during geomagnetic storms—Initial results. *Journal of Geophysical Research: Space Physics*, *114*(A12). https://doi.org/10.1029/2009ja014418

Glocer, A., Welling, D., Chappell, C. R., Toth, G., Fok, M. C., Komar, C., et al. (2020). A case study on the origin of near-Earth plasma. *Journal of Geophysical Research: Space Physics*, *125*, e2020JA028205. https://doi.org/10.1029/2020JA028205

Gloeckler, G., & Hamilton, D. C. (1987). AMPTE ion composition results. *Physica Scripta*, *1987*(T18), 73. https://doi.org/10.1088/0031-8949/1987/t18/009

Goldstein, J., Denton, R. E., Hudson, M. K., Miftakhova, E. G., Young, S. L., Menietti, J. D., & Gallagher, D. L. (2001). Latitudinal density dependence of magnetic field lines inferred from Polar plasma wave data. *Journal of Geophysical Research*, *106*(A4), 6195–6201. https://doi.org/10.1029/2000ja000068

Goldstein, J., Sandel, B. R., Thomsen, M. F., Spasojević, M., & Reiff, P. H. (2004). Simultaneous remote sensing and in situ observations of plasmaspheric drainage plumes. *Journal of Geophysical Research: Space Physics*, *109*(A3). https://doi.org/10.1029/2003ja010281

Graham, D. B., Khotyaintsev, Y. V., Norgren, C., Vaivads, A., André, M., Toledo-Redondo, S., et al. (2017). Lower hybrid waves in the ion diffusion and magnetospheric inflow regions. *Journal of Geophysical Research: Space Physics*, *122*(1), 517–533. https://doi.org/10.1002/2016ja023572

Graham, D. B., Khotyaintsev, Y V., Vaivads, A., Norgren, C., André, M., Webster, J. M., et al. (2017). Instability of agyrotropic electron beams near the electron diffusion region. *Physical Review Letters*, *119*(2), 025101. https://doi.org/10.1103/physrevlett.119.025101

Grande, M., Perry, C. H., Hall, A., Fennell, J., Nakamura, R., & Kamide, Y. (2003). What is the effect of substorms on the ring current ion population during a geomagnetic storm? *GMS*, *142*, 75. https://doi.org/10.1029/142gm08

Grard, R. J. L. (1973). Properties of the satellite photoelectron sheath derived from photoemission laboratory measurements. *Journal of Geophysical Research*, *78*(16), 2885–2906. https://doi.org/10.1029/JA078i016p02885

Haaland, S. E., Eriksson, A., Engwall, E., Lybekk, B., Nilsson, H., Pedersen, A., et al. (2012). Estimating the capture and loss of cold plasma from ionospheric outflow. *Journal of Geophysical Research*, *117*. https://doi.org/10.1029/2012JA017679

Haaland, S. E., Li, K., Eriksson, A., André, M., Engwall, E., Forster, M., et al. (2012). Cold ion outflow as a source of plasma for the magnetosphere. *Geophysical Monograph Series*, *199*, 341–353. https://doi.org/10.1029/2012GM001317

Haaland, S. E., Svenes, K., Lybekk, B., & Pedersen, A. (2012). A survey of the polar cap density based on Cluster EFW probe measurements: Solar wind and solar irradiation dependence. *Journal of Geophysical Research*, *117*. https://doi.org/10.1029/2011JA017250

Hamilton, D. C., Gloeckler, G., Ipavich, F. M., Wilken, B., & Stuedemann, W. (1988). Ring current development during the great geomagnetic storm of February 1986. *Journal of Geophysical Research*, *93*, 14343–14355. https://doi.org/10.1029/JA093iA12p14343

Hesse, M., Aunai, N., Sibeck, D., & Birn, J. (2014). On the electron diffusion region in planar, asymmetric, systems. *Geophysical Research Letters*, *41*, 8673–8680. https://doi.org/10.1002/2014GL061586

Hesse, M., & Birn, J. (2004). On the cessation of magnetic reconnection. *Annales Geophysicae*, *22*(2), 603–612.

Hesse, M., Neukirch, T., Schindler, K., Kuznetsova, M., & Zenitani, S. (2011). The diffusion region in collisionless magnetic reconnection. *Space Science Reviews*, *160*(1–4), 3–23. https://doi.org/10.1007/s11214-010-9740-1

Hoffman, J. H., Dodson, W. H., Lippincott, C. R., & Hammack, H. D. (1974). Initial ion composition results from the Isis 2 satellite. *Journal of Geophysical Research*, *79*(28), 4246–4251. https://doi.org/10.1029/ja079i028p04246

Howarth, A., & Yau, A. W. (2008). The effects of IMF and convection on thermal ion outflow in magnetosphere-ionosphere coupling. *Journal of Atmospheric and Solar-Terrestrial Physics*, *70*(17), 2132–2143. https://doi.org/10.1016/j.jastp.2008.08.008

Huddleston, M. M., Chappell, C. R., Delcourt, D. C., Moore, T. E., Giles, B. L., & Chandler, M. O. (2005). An examination of the process and magnitude of ionospheric plasma supply to the magnetosphere. *Journal of Geophysical Research*, *110*(A12). https://doi.org/10.1029/2004ja010401

Ilie, R., & Liemohn, M. W. (2016). The outflow of ionospheric nitrogen ions: A possible tracer for the altitude-dependent transport and energization processes of ionospheric plasma. *Journal of Geophysical Research: Space Physics*, *121*(9), 9250–9255. https://doi.org/10.1002/2015ja022162

Jahn, J. M., Goldstein, J., Kurth, W. S., Thaller, S., De Pascuale, S., Wygant, J., et al. (2020). Determining plasmaspheric density from the upper hybrid resonance and from the spacecraft potential: How do they compare? *Journal of Geophysical Research: Space Physics*, *125*(3), e2019JA026860. https://doi.org/10.1029/2019ja026860

Jahn, J. M., Goldstein, J., Reeves, G. D., Fernandes, P. A., Skoug, R. M., Larsen, B. A., & Spence, H. E. (2017). The warm plasma composition in the inner magnetosphere during 2012–2015. *Journal of Geophysical Research: Space Physics*, *122*(11), 11–018. https://doi.org/10.1002/2017ja024183

Karimabadi, H., Roytershteyn, V., Mouikis, C. G., Kistler, L. M., & Daughton, W. (2011). Flushing effect in reconnection: Effects of minor-ity species of oxygen ions. *Planetary and Space Science*, *59*(7), 526–536. https://doi.org/10.1016/j.pss.2010.07.014

Kasahara, S., Hasegawa, H., Keika, K., Miyashita, Y., Nishino, M. N., Sotirelis, T., et al. (2008). Escape of high-energy oxygen ions through magnetopause reconnection under northward IMF. *Annales Geophysicae*, *26*, 3955–3966. https://doi.org/10.5194/angeo-26-3955-2008

Kelley, M. C. (2009). *The Earth's ionosphere: Plasma physics and electrodynamics*. Academic Press.

Kistler, L. M. (2016). The impact of O+ on magnetotail dynamics. In *Magnetosphere-ionosphere coupling in the solar system*. https://doi.org/10.1002/9781119066880.ch6

Kistler, L. M. (2020). Ionospheric and solar wind contributions to the storm-time near-earth plasma sheet. *Geophysical Research Letters*, *47*. https://doi.org/10.1029/2020GL090235

Kistler, L. M., Mouikis, C., Moebius, E., Klecker, B., Sauvaud, J. A., Reme, H., et al. (2005). Contribution of nonadiabatic ions to the cross-tail current in an $O^+$ dominated thin current sheet. *Journal of Geophysical Research*, *110*(A6). https://doi.org/10.1029/2004JA010653

Kistler, L. M., & Mouikis, C. G. (2016). The inner magnetosphere ion composition and local time distribution over a solar cycle. *Journal of Geophysical Research: Space Physics*, *121*(3), 2009–2032. https://doi.org/10.1002/2015JA021883

Kistler, L. M., Mouikis, C. G., Spence, H. E., Menz, A. M., Skoug, R. M., Funsten, H. O., et al. (2016). The source of O+ in the storm time ring current. *Journal of Geophysical Research: Space Physics*, *121*(6), 5333–5349. https://doi.org/10.1002/2015ja022204



19449208, 2021, 3, Downloaded from https://agupubs.onlinelibrary.wiley.com/doi/10.1029/2020RG000707 by Cochrane France, Wiley Online Library on [07/11/2022]. See the Terms and Conditions (https://onlinelibrary.wiley.com/terms-and-conditions) on Wiley Online Library for rules of use; OA articles are governed by the applicable Creative Commons License

Knudsen, D. J., Burchill, J. K., Buchert, S. C., Eriksson, A. I., Gill, R., Wahlund, J.-E., et al. (2017). Thermal ion imagers and Langmuir probes in the Swarm electric field instruments. *Journal of Geophysical Research: Space Physics*, *122*(2), 2655–2673. https://doi.org/10.1002/2016JA022571

Kolstø, H. M., Hesse, M., Norgren, C., Tenfjord, P., Spinnangr, S. F., & Kwagala, N. (2020). Collisionless magnetic reconnection in an asymmetric oxygen density configuration. *Geophysical Research Letters*, *47*(1). https://doi.org/10.1029/2019gl085359

Krcelic, P., Haaland, S., Maes, L., Slapak, R., & Schillings, A. (2019). Estimating the fate of oxygen ion outflow from the high altitude cusp. *Annales Geophysicae*. https://doi.org/10.5194/angeo-37-125-2019

Kronberg, E. A., Ashour-Abdalla, M., Dandouras, I., Delcourt, D. C., Grigorenko, E. E., Kistler, L. M., et al. (2014). Circulation of heavy ions and their dynamical effects in the magnetosphere: Recent observations and models. *Space Science Reviews*, *184*(1–4), 173–235. https://doi.org/10.1007/s11214-014-0104-0

Laakso, H., & Pedersen, A. (1998). Ambient electron density derived from differential potential measurements. *Geophysical Monograph-American Geophysical Union*, *102*, 49–54.

Lavraud, B., & Borovsky, J. E. (2008). Altered solar wind-magnetosphere interaction at low Mach numbers: Coronal mass ejections. *Journal of Geophysical Research*, *113*(A9). https://doi.org/10.1029/2008ja013192

Lavraud, B., Dunlop, M. W., Phan, T. D., Reme, H., Bosqued, J. M., Dandouras, et al. (2002). Cluster observations of the exterior cusp and its surrounding boundaries under northward IMF. *Geophysical Research Letters*, *29*(20), 561–564. https://doi.org/10.1029/2002gl015464

Lavraud, B., & Larson, D. E. (2016). Correcting moments of in situ particle distribution functions for spacecraft electrostatic charging. *Journal of Geophysical Research: Space Physics*, *121*(9), 8462–8474. https://doi.org/10.1002/2016ja022591

Lavraud, B., Rème, H., Dunlop, M. W., Bosqued, J. M., Dandouras, I., Sauvaud, J.-A., et al. (2005). Cluster observes the high-altitude cusp region. *Surveys in Geophysics*, *26*(No. 1–3), 135–175. https://doi.org/10.1007/s10712-005-1875-3

Lee, J. H., & Angelopoulos, V. (2014). On the presence and properties of cold ions near Earth's equatorial magnetosphere. *Journal of Geophysical Research: Space Physics*, *119*(3), 1749–1770. https://doi.org/10.1002/2013ja019305

Lee, J. H., Chen, L., Angelopoulos, V., & Thorne, R. M. (2012). THEMIS observations and modeling of multiple ion species and EMIC waves: Implications for a vanishing He+ stop band. *Journal of Geophysical Research: Space Physics*, *117*(A6). https://doi.org/10.1029/2012ja017539

Lee, S. H., Zhang, H., Zong, Q. G., Otto, A., Rème, H., & Liebert, E. (2016). A statistical study of plasmaspheric plumes and ionospheric outflows observed at the dayside magnetopause. *Journal of Geophysical Research: Space Physics*, *121*(1), 492–506. https://doi.org/10.1002/2015ja021540

Lemaire, J., & Schunk, R. W. (1992). Plasmaspheric wind. *Journal of Atmospheric and Terrestrial Physics*, *54*(3–4), 467–477. https://doi.org/10.1016/0021-9169(92)90026-h

Lennartsson, O. W., Klumpar, D. M., Shelley, E. G., & Quinn, J. M. (1993). Experimental investigation of possible geomagnetic feedback from energetic (0.1 to 16 keV) terrestrial O+ ions in the magnetotail current sheet. *Journal of Geophysical Research*, *98*(A11), 19443–19454. https://doi.org/10.1029/93ja01991

Lennartsson, W. (1989). Energetic (0.1-to 16-keV/e) magnetospheric ion composition at different levels of solar F10. 7. *Journal of Geophysical Research*, *94*(A4), 3600–3610. https://doi.org/10.1029/ja094ia04p03600

Lennartsson, W., & Sharp, R. D. (1985). Relative contributions of terrestrial and solar wind ions in the plasma sheet. *Advances in Space Research*, *5*(4), 411–414. https://doi.org/10.1016/0273-1177(85)90167-x

Lennartsson, W., & Shelley, E. G. (1986). Survey of 0.1- to 16-keV/e plasmasheet ion composition. *Journal of Geophysical Research*, *91*, 3061–3076. https://doi.org/10.1029/ja091ia03p03061

Li, K., Haaland, S., Eriksson, A., André, M., Engwall, E., Wei, Y., et al. (2013). Transport of cold ions from the polar ionosphere to the plasma sheet. *Journal of Geophysical Research: Space Physics*, *118*(9), 5467–5477. https://doi.org/10.1002/jgra.50518

Li, Q., Winglee, R. M., Wilber, M., Chen, L., & Parks, G. (2000). The geopause in relation to the plasma sheet and the low-latitude boundary layer: Comparison between Wind observations and multifluid simulations. *Journal of Geophysical Research*, *105*(A2), 2563–2587. https://doi.org/10.1029/1999JA900369

Li, W. Y., Andre, M., Khotyaintsev, Y. V., Vaivads, A., Fuselier, S. A., Graham, D. B., et al. (2017). Cold ionospheric ions in the magnetic reconnection outflow region. *Journal of Geophysical Research: Space Physics*, *122*(10), 10194–10202. https://doi.org/10.1002/2017ja024287

Li, W. Y., Graham, D. B., Khotyaintsev, Y. V., Vaivads, A., André, M., Min, K., et al. (2020). Electron Bernstein waves driven by electron crescents near the electron diffusion region. *Nature Communications*, *11*(1), 141. https://doi.org/10.1038/s41467-019-13920-w

Liang, H., Ashour-Abdalla, M., Lapenta, G., & Walker, R. J. (2016). Oxygen impacts on dipolarization fronts and reconnection rate. *Journal of Geophysical Research: Space Physics*, *121*(2), 1148–1166. https://doi.org/10.1002/2015ja021747

Liang, H., Lapenta, G., Walker, R. J., Schriver, D., El-Alaoui, M., & Berchem, J. (2017). Oxygen acceleration in magnetotail reconnection. *Journal of Geophysical Research: Space Physics*, *122*(1), 618–639. https://doi.org/10.1002/2016ja023060

Liao, J., Cai, X., Kistler, L. M., Clauer, C. R., Mouikis, C. G., Klecker, B., & Dandouras, I. (2014). The relationship between sawtooth events and O+ in the plasma sheet. *Journal of Geophysical Research: Space Physics*, *119*(3), 1572–1586. https://doi.org/10.1002/2013JA019084

Liao, J., Kistler, L. M., Mouikis, C. G., Klecker, B., & Dandouras, I. (2012). Solar cycle dependence of the cusp O+ access to the near-Earth magnetotail. *Journal of Geophysical Research*, *117*. https://doi.org/10.1029/2012ja017819

Liao, J., Kistler, L. M., Mouikis, C. G., Klecker, B., & Dandouras, I. (2015). Acceleration of O+ from the cusp to the plasma sheet. *Journal of Geophysical Research: Space Physics*, *120*(2), 1022–1034. https://doi.org/10.1002/2014ja020341

Liao, J., Kistler, L. M., Mouikis, C. G., Klecker, B., Dandouras, I., & Zhang, J. C. (2010). Statistical study of O+ transport from the cusp to the lobes with Cluster CODIF data. *Journal of Geophysical Research*, *115*. https://doi.org/10.1029/2010ja015613

Liemohn, M. W., Moore, T. E., & Craven, P. D. (2007). Geospace activity dependence of cold, streaming ions in the near-Earth magnetotail. *Journal of Atmospheric and Solar-Terrestrial Physics*, *69*(1–2), 135–141. https://doi.org/10.1016/j.jastp.2006.07.018

Lindstedt, T., Khotyaintsev, Y. V., Vaivads, A., André, M., Nilsson, H., & Waara, M. (2010). Oxygen energization by localized perpendicular electric fields at the cusp boundary. *Geophysical Research Letters*, *37*, L09103. https://doi.org/10.1029/2010GL043117

Liu, Y., Kistler, L. M., Mouikis, C. G., Klecker, B., & Dandouras, I. (2013). Heavy ion effects on substorm loading and unloading in the Earth's magnetotail. *Journal of Geophysical Research: Space Physics*, *118*(5), 2101–2112. https://doi.org/10.1002/jgra.50240

Liu, Y. H., & Hesse, M. (2016). Suppression of collisionless magnetic reconnection in asymmetric current sheets. *Physics of Plasmas*, *23*(6), 060704. https://doi.org/10.1063/1.4954818

Liu, Y.-H., Hesse, M., Cassak, P. A., Shay, M. A., Wang, S., & Chen, L.-J. (2018). On the collisionless asymmetric magnetic reconnection rate. *Geophysical Research Letters*, *45*(8), 3311–3318. https://doi.org/10.1002/2017GL076460

Liu, Y. H., Hesse, M., Guo, F., Daughton, W., Li, H., Cassak, P. A., & Shay, M. A. (2017). Why does steady-state magnetic reconnection have a maximum local rate of order 0.1? *Physical Review Letters*, *118*(8), 1–6. https://doi.org/10.1103/PhysRevLett.118.085101



19449208, 2021, 3, Downloaded from https://agupubs.onlinelibrary.wiley.com/doi/10.1029/2020RG000707 by Cochrane France, Wiley Online Library on [07/11/2022]. See the Terms and Conditions (https://onlinelibrary.wiley.com/terms-and-conditions) on Wiley Online Library for rules of use; OA articles are governed by the applicable Creative Commons License

Liu, Y. H., Mouikis, C. G., Kistler, L. M., Wang, S., Roytershteyn, V., & Karimabadi, H. (2015). The heavy ion diffusion region in magnetic reconnection in the Earth's magnetotail. *Journal of Geophysical Research*, *120*(5), 3535–3551. https://doi.org/10.1002/2015JA020982

Lopez, R. E. (2016). The integrated dayside merging rate is controlled primarily by the solar wind. *Journal of Geophysical Research: Space Physics*, *121*(5), 4435–4445. https://doi.org/10.1002/2016ja022556

Louarn, P., Andre, N., Jackman, C. M., Kasahara, S., Kronberg, E. A., & Vogt, M. F. (2015). Magnetic reconnection and associated transient phenomena within the magnetospheres of Jupiter and Saturn. *Space Science Reviews*, *187*, 181–227. https://doi.org/10.1007/s11214-014-0047-5

Lund, E. J., Nowrouzi, N., Kistler, L. M., Cai, X., & Frey, H. U. (2018). On the role of ionospheric ions in sawtooth events. *Journal of Geophysical Research: Space Physics*, *123*(1), 665–684. https://doi.org/10.1002/2017JA024378

Lybekk, B., Pedersen, A., Haaland, S., Svenes, K., Fazakerley, A. N., Masson, A., et al. (2012). Solar cycle variations of the Cluster spacecraft potential and its use for electron density estimations. *Journal of Geophysical Research*, *117*, A01217. https://doi.org/10.1029/2011JA016969

Maggiolo, R., & Kistler, L. M. (2014). Spatial variation in the plasma sheet composition: Dependence on geomagnetic and solar activity. *Journal of Geophysical Research: Space Physics*, *119*(4), 2836–2857. https://doi.org/10.1002/2013ja019517

Markidis, S., Lapenta, G., Bettarini, L., Goldman, M., Newman, D., & Andersson, L. (2011). Kinetic simulations of magnetic reconnection in presence of a background O+ population. *Journal of Geophysical Research*, *116*(A1). https://doi.org/10.1029/2011ja016429

Masters, A., Eastwood, J. P., Swisdak, M., Thomsen, M. F., Russell, C. T., Sergis, N., et al. (2012). The importance of plasma β conditions for magnetic reconnection at Saturn's magnetopause. *Geophysical Research Letters*, *39*, L08103. https://doi.org/10.1029/2012GL051372

McComas, D. J., Bame, S. J., Barraclough, B. L., Donart, J. R., Elphic, R. C., Gosling, J. T., et al. (1993). Magnetospheric plasma analyzer: Initial three-spacecraft observations from geosynchronous orbit. *Journal of Geophysical Research*, *98*(A8), 13453–13465. https://doi.org/10.1029/93ja00726

Moldwin, M. B., Zou, S., & Heine, T. (2016). The story of plumes: The development of a new conceptual framework for understanding magnetosphere and ionosphere coupling. *Annales Geophysicae*, *34*(12), 1243–1253. https://doi.org/10.5194/angeo-34-1243-2016

Moore, T. E., Chandler, M. O., Fok, M. C., Giles, B. L., Delcourt, D. C., Horwitz, J. L., & Pollock, C. J. (2001). Ring currents and internal plasma sources. *Space Science Reviews*, *95*(1–2), 555–568. https://doi.org/10.1023/a:1005264907107

Moore, T. E., Chappell, C. R., Chandler, M. O., Craven, P. D., Giles, B. L., Pollock, C. J., et al. (1997). High-altitude observations of the polar wind. *Science*, *277*, 349–351. https://doi.org/10.1126/science.277.5324.349

Moore, T. E. & Delcourt, D. C. (1995). The geopause. *Reviews of Geophysics*, *33*(2), 175–209. https://doi.org/10.1029/95rg00872

Moore, T. E., Fok, M. C., Chandler, M. O., Chappell, C. R., Christon, S. P., Delcourt, D. C., et al. (2005). Plasma sheet and (nonstorm) ring current formation from solar and polar wind sources. *Journal of Geophysical Research*, *110*(A2). https://doi.org/10.1029/2004ja010563

Moore, T. E., & Horwitz, J. L. (2007). Stellar ablation of planetary atmospheres. *Reviews of Geophysics*, *45*, RG3002. https://doi.org/10.1029/2005RG000194

Mouikis, C. G., Kistler, L. M., Liu, Y. H., Klecker, B., Korth, A., & Dandouras, I. (2010). H+ and O+ content of the plasma sheet at 15–19 Re as a function of geomagnetic and solar activity. *Journal of Geophysical Research*, *115*(A12). https://doi.org/10.1029/2010ja015978

Nagai, T., Fujimoto, M., Saito, Y., Machida, S., Terasawa, T., Nakamura, R., et al. (1998). Structure and dynamics of magnetic reconnection for substorm onsets with geotail observations. *Journal of Geophysical Research*, *103*(A3), 4419–4440. https://doi.org/10.1029/97ja02190

Nagai, T., Johnson, J. F. E., & Chappell, C. R. (1983). Low-energy (<100 eV) ion pitch angle distributions in the magnetosphere by ISEE 1. *Journal of Geophysical Research*, *88*(A9), 6944–6960. https://doi.org/10.1029/ja088ia09p06944

Nilsson, H., Engwall, E., Eriksson, A., Puhl-Quinn, P. A., & Arvelius, S. (2010). Centrifugal acceleration in the magnetotail lobes. *Annales Geophysicae*, *28*, 569. https://doi.org/10.5194/angeo-28-569-2010

Nilsson, H., Waara, M., Marghitu, O., Yamauchi, M., Lundin, R., Reme, H., et al. (2008). An assessment of the role of the centrifugal acceleration mechanism in high altitude polar cap oxygen ion outflow. *Annales Geophysicae*, *26*, 145. https://doi.org/10.5194/angeo-26-145-2008

Nishida, A., Mukai, T., Yamamoto, T., Saito, Y., & Kokubun, M. (1996). Magnetotail convection in geomagnetically active times, 1. Distance to the neutral lines. *Journal of Geomagnetism and Geoelectricity*, *48*, 489. https://doi.org/10.5636/jgg.48.489

Nosé, M., Ieda, A., & Christon, S. P. (2009). Geotail observations of plasma sheet ion composition over 16 years: On variations of average plasma ion mass and O+ triggering substorm model. *Journal of Geophysical Research*, *114*. https://doi.org/10.1029/2009ja014203

Ober, D. M., Horwitz, J. L., & Gallagher, D. L. (1997). Formation of density troughs embedded in the outer plasmasphere by subauroral ion drift events. *Journal of Geophysical Research*, *102*(A7), 14595–14602. https://doi.org/10.1029/97ja01046

Ogawa, Y., Häggström, I., Buchert, S. C., Oksavik, K., Nozawa, S., Hirahara, M., et al. (2009). On the source of the polar wind in the polar top- side ionosphere: First results from the EISCAT Svalbard radar, *Geophysical Research Letters*, *36*, L24103. https://doi.org/10.1029/2009GL041501

Parker, E. N. (1973). The reconnection rate of magnetic fields. *The Astrophysical Journal*, *180*, 247. https://doi.org/10.1086/151959

Peroomian, V., & Ashour-Abdalla, M. (1995). Relative contribution of the solar wind and the auroral zone to near-Earth plasmas. *Geophysical Monograph-American Geophysical Union*, *93*, 213–218. https://doi.org/10.1029/gm093p0213

Peroomian, V., El-Alaoui, M., Abdalla, M. A., & Zelenyi, L. M. (2007). A comparison of solar wind and ionospheric plasma contributions to the September 24–25, 1998 magnetic storm. *Journal of Atmospheric and Solar-Terrestrial Physics*, *69*(3), 212–222. https://doi.org/10.1016/j.jastp.2006.07.025

Peterson, W. K., Andersson, L., Callahan, B. C., Collin, H. L., Scudder, J. D., & Yau, A. W. (2008). Solar-minimum quiet time ion energization and outflow in dynamic boundary related coordinates. *Journal of Geophysical Research*, *113*, A07222. https://doi.org/10.1029/2008JA013059

Peterson, W. K., Collin, H. L., Lennartsson, O. W., & Yau, A. W. (2006). Quiet time solar illumination effects on the fluxes and characteristic energies of ionospheric outflow. *Journal of Geophysical Research*, *111*, A11S05. https://doi.org/10.1029/2005JA011596

Phan, T. D., Paschmann, G., Gosling, J. T., Oieroset, M., Fujimoto, M., Drake, J. F., & Angelopoulos, V. (2013). The dependence of magnetic reconnection on plasma β and magnetic shear: Evidence from magnetopause observations. *Geophysical Research Letters*, *40*(1), 11–16. https://doi.org/10.1029/2012gl054528

Pollock, C. J., Burch, J. L., Henderson, M. G., Jahn, J. M., Mccomas, D. J., Mende, S. B., et al. (2003). The role and contributions of energetic neutral atom (ENA) imaging in magnetospheric substorm research. In *Magnetospheric imaging—The image prime mission* (pp. 155–182). Springer. https://doi.org/10.1007/978-94-010-0027-7_8

Runov, A., Angelopoulos, V., Artemyev, A., Birn, J., Pritchett, P. L., & Zhou, X.-Z. (2017). Characteristics of ion distribution functions in dipolarizing flux bundle: Event studies. *Journal of Geophysical Research: Space Physics*, *122*(6), 5965–5978. https://doi.org/10.1002/2017ja024010

Sandel, B. R., Goldstein, J., Gallagher, D. L., & Spasojevic, M. (2003). Extreme ultraviolet imager observations of the structure and dynamics of the plasmasphere. *Space Science Reviews*, *109*, 25–46. https://doi.org/10.1023/B10.1023/b:spac.0000007511.47727.5b



19449208, 2021, 3, Downloaded from https://agupubs.onlinelibrary.wiley.com/doi/10.1029/2020RG000707 by Cochrane France, Wiley Online Library on [07/11/2022]. See the Terms and Conditions (https://onlinelibrary.wiley.com/terms-and-conditions) on Wiley Online Library for rules of use; OA articles are governed by the applicable Creative Commons License

Sauvaud, J.-A., Lundin, R., Rème, H., McFadden, J. P., Carlson, C., Parks, G. K., et al. (2001). Intermittent thermal plasma acceleration linked to sporadic motions of the magnetopause, first Cluster results. *Annales Geophysicae*. https://doi.org/10.5194/angeo-19-1523-2001

Schillings, A., Slapak, R., Nilsson, H., Yamauchi, M., Dandouras, I., & Westerberg, L. G. (2019). Earth atmospheric loss through the plasma mantle and its dependence on solar wind parameters. *Earth Planets and Space*, *71*(1), 1–13. https://doi.org/10.1186/s40623-019-1048-0

Schunk, R. W. (2007). Time-dependent simulations of the global polar wind. *Journal of Atmospheric and Solar-Terrestrial Physics*, *69*(16), 2028–2047. https://doi.org/10.1016/j.jastp.2007.08.009

Schunk, R. W., Raitt, W. J., & Banks, P. M. (1975). Effect of electric fields on the daytime high-latitude E and F regions. *Journal of Geophysical Research*, *80*(22), 3121–3130. https://doi.org/10.1029/ja080i022p03121

Seki, K., Hirahara, M., Hoshino, M., Terasawa, T., Elphic, R. C., Saito, Y., et al. (2003). Cold ions in the hot plasma sheet of Earth's magnetotail. *Nature*, *422*(6932), 589–592. https://doi.org/10.1038/nature01502

Shay, M. A., Drake, J. F., Denton, R. E., & Biskamp, D. (1998). Structure of the dissipation region during collisionless magnetic reconnection. *Journal of Geophysical Research*, *103*(A5), 9165–9176. https://doi.org/10.1029/97ja03528

Shay, M. A., Drake, J. F., & Swisdak, M. (2007). Two-scale structure of the electron dissipation region during collisionless magnetic reconnection. *Physical Review Letters*, *99*(15), 155002. https://doi.org/10.1103/physrevlett.99.155002

Shay, M. A., Phan, T. D., Haggerty, C. C., Fujimoto, M., Drake, J. F., Malakit, K., et al. (2016). Kinetic signatures of the region surrounding the X line in asymmetric (magnetopause) reconnection. *Geophysical Research Letters*, *43*, 4145–4154. https://doi.org/10.1002/2016GL069034

Shay, M. A., & Swisdak, M. (2004). Three-species collisionless reconnection: Effect of O+ on magnetotail reconnection. *Physical Review Letters*, *93*(17), 175001.

Sheeley, B. W., Moldwin, M. B., Rassoul, H. K., & Anderson, R. R. (2001). An empirical plasmasphere and trough density model: CRRES observations. *Journal of Geophysical Research: Space Physics*, *106*(A11), 25631–25641. https://doi.org/10.1029/2000ja000286

Shelley, E. G., Johnson, R. G., & Sharp, R. D. (1972). Satellite observations of energetic heavy ions during a geomagnetic storm. *Journal of Geophysical Research*, *77*(31), 6104–6110. https://doi.org/10.1029/ja077i031p06104

Shen, Y., Knudsen, D. J., Burchill, J. K., Howarth, A. D., Yau, A. W., Miles, D. M., et al. (2018). Low-altitude ion heating, downflowing ions, and elf waves in the return current region. *Journal of Geophysical Research: Space Physics*, *123*(4), 3087–3110. https://doi.org/10.1002/2017JA024955

Slapak, R., Hamrin, M., Pitkänen, T., Yamauchi, M., Nilsson, H., Karlsson, T., & Schillings, A. (2017). Quantification of the total ion transport in the near-Earth plasma sheet. *Annales Geophysicae*, *35*, 869–877. https://doi.org/10.5194/angeo-35-869-2017

Slapak, R., Nilsson, H., & Westerberg, L. G. (2015). O+ transport in the dayside magnetosheath and its dependence on the IMF direction. *Annales Geophysicae*, *33*(3), 301–307. https://doi.org/10.5194/angeo-33-301-2015

Slapak, R., Schillings, A., Nilsson, H., Yamauchi, M., Westerberg, L.-G., & Dandouras, I. (2017). Atmospheric loss from the dayside open polar region and its dependence on geomagnetic activity: Implications for atmospheric escape on evolutionary timescales. *Annales Geophysicae*, *35*(3), 721–731. https://doi.org/10.5194/angeo-35-721-2017

Sorathia, K. A., Merkin, V. G., Ukhorskiy, A. Y., Allen, R. C., Nykyri, K., & Wing, S. (2019). Solar wind ion entry into the magnetosphere during northward IMF. *Journal of Geophysical Research: Space Physics*, *124*(7), 5461–5481. https://doi.org/10.1029/2019ja026728

Spasojevic, M., & Sandel, B. R. (2010). Global estimates of plasmaspheric losses during moderate disturbance intervals. *Annales Geophysicae*, *28*(1), 27–36. https://doi.org/10.5194/angeo-28-27-2010

Spinnangr, S. F., Hesse, M., Tenfjord, P., Norgren, C., Kolsto, H. M., Kwagala, N. K., & Jorgensen, T. M. (2020). The micro-macro coupling of mass-loading symmetric magnetic reconnection with cold ions. *Geophysical Research Letters*.

Stern, D. P. (1977). Large-scale electric fields in the earth's magnetosphere. *Reviews of Geophysics*, *15*(2), 156–194. https://doi.org/10.1029/rg015i002p00156

Strangeway, R. J., Ergun, R. E., Su, Y. J., Carlson, C. W., & Elphic, R. C. (2005). Factors controlling ionospheric outflows as observed at intermediate altitudes. *Journal of Geophysical Research*, *110*, A03221. https://doi.org/10.1029/2004JA010829

Su, Y. J., Borovsky, J. E., Thomsen, M. F., Elphic, R. C., & McComas, D. J. (2000). Plasmaspheric material at the reconnecting magnetopause. *Journal of Geophysical Research*, *105*(A4), 7591–7600. https://doi.org/10.1029/1999ja000266

Su, Y.-J., Horwitz, J. L., Moore, T. E., Giles, B. L., Chandler, M. O., Craven, P. D., et al. (1998). Polar wind survey with the Thermal Ion Dynamics Experiment/Plasma Source Instrument suite aboard POLAR. *Journal of Geophysical Research*, *103*, 29305–29338. https://doi.org/10.1029/98JA02662

Svenes, K. R., Lybekk, B., Pedersen, A., & Haaland, S. (2008). Cluster observations of near-Earth magnetospheric lobe plasma densities—A statistical study. *Annales Geophysicae*, *26*, 2845–2852. https://doi.org/10.5194/angeo-26-2845-2008

Swisdak, M., Opher, M., Drake, J. F., & Alouani Bibi, F. (2010). The vector direction of the interstellar magnetic field outside the heliosphere. *The Astrophysical Journal*, *710*(2), 1769–1775. https://doi.org/10.1088/0004-637X/710/2/1769

Swisdak, M., Rogers, B. N., Drake, J. F., & Shay, M. A. (2003). Diamagnetic suppression of component magnetic reconnection at the magnetopause. *Journal of Geophysical Research*, *108*(A5), 1218. https://doi.org/10.1029/2002JA009726

Takahashi, K., Denton, R. E., Anderson, R. R., & Hughes, W. J. (2004). Frequencies of standing Alfvén wave harmonics and their implication for plasma mass distribution along geomagnetic field lines: Statistical analysis of CRRES data. *Journal of Geophysical Research*, *109*(A8). https://doi.org/10.1029/2003ja010345

Tenfjord, P., Hesse, M., Norgren, C., Spinnangr, S. F., & Kolstø, H. (2019). The impact of oxygen on the reconnection rate. *Geophysical Research Letters*, *46*(12), 6195–6203. https://doi.org/10.1029/2019GL082175.10

Tenfjord, P., Hesse, M., Norgren, C., Spinnangr, S. F., Kolstø, H., & Kwagala, N. (2020). Interaction of cold streaming protons with the reconnection process. *Journal of Geophysical Research: Space Physics*, *125*(6), e2019JA027619. https://doi.org/10.1029/2019ja027619

Tenfjord, P., Østgaard, N., Haaland, S. E., Snekvik, K., Laundal, K. M., Reistad, J. P., et al. (2018). How the IMF By induces a local By component during northward IMF Bz and characteristic timescales. *Journal of Geophysical Research: Space Physics*, *123*(5), 3333–3348. https://doi.org/10.1002/2018JA025186

Thorne, R. M. (2010). Radiation belt dynamics: The importance of wave-particle interactions. *Geophysical Research Letters*, *37*(22). https://doi.org/10.1029/2010gl044990

Toledo-Redondo, S., André, M., Khotyaintsev, Y. V., Lavraud, B., Vaivads, A., Graham, D. B., et al. (2017). Energy budget and mechanisms of cold ion heating in asymmetric magnetic reconnection. *Journal of Geophysical Research: Space Physics*, *122*(9), 9396–9413. https://doi.org/10.1002/2017ja024553

Toledo-Redondo, S., André, M., Khotyaintsev, Y. V., Vaivads, A., Walsh, A., Li, W., et al. (2016). Cold ion demagnetization near the X-line of magnetic reconnection. *Geophysical Research Letters*, *43*(13), 6759–6767. https://doi.org/10.1002/2016gl069877

Toledo-Redondo, S., André, M., Vaivads, A., Khotyaintsev, Y. V., Lavraud, B., Graham, D. B., et al. (2016). Cold ion heating at the dayside magnetopause during magnetic reconnection. *Geophysical Research Letters*, *43*(1), 58–66.



19449208, 2021, 3, Downloaded from https://agupubs.onlinelibrary.wiley.com/doi/10.1029/2020RG000707 by Cochrane France, Wiley Online Library on [07/11/2022]. See the Terms and Conditions (https://onlinelibrary.wiley.com/terms-and-conditions) on Wiley Online Library for rules of use; OA articles are governed by the applicable Creative Commons License

Toledo-Redondo, S., Dargent, J., Aunai, N., Lavraud, B., André, M., Li, W., et al. (2018). Perpendicular current reduction caused by cold ions of ionospheric origin in magnetic reconnection at the magnetopause: Particle-in-cell simulations and spacecraft observations. *Geophysical Research Letters*, *45*(19), 10–033.

Toledo-Redondo, S., Lavraud, B., Fuselier, S. A., André, M., Khotyaintsev, Y. V., Nakamura, N., et al. (2019). Electrostatic spacecraft potential structure and wake formation effects for characterization of cold ion beams in the Earth's magnetosphere. *Journal of Geophysical Research: Space Physics*, *124*, 10048–10062. https://doi.org/10.1029/2019JA027145

Toledo-Redondo, S., Vaivads, A., André, M., & Khotyaintsev, Y. V. (2015). Modification of the Hall physics in magnetic reconnection due to cold ions at the Earth's magnetopause. *Geophysical Research Letters*, *42*(15), 6146–6154. https://doi.org/10.1002/2015GL065129

Torkar, K., Nakamura, R., Tajmar, M., Scharlemann, C., Jeszenszky, H., Laky, G., et al. (2016). Active spacecraft potential control investigation. *Space Science Reviews*, *199*, 515–544. https://doi.org/10.1007/s11214-014-0049-3

Varney, R. H., Wiltberger, M., Zhang, B., Lotko, W., & Lyon, J. (2016a). Influence of ion outflow in coupled geospace simulations: 1. Physics-based ion outflow model development and sensitivity study. *Journal of Geophysical Research: Space Physics*, *121*, 9671–9687. https://doi.org/10.1002/2016ja022777

Varney, R. H., Wiltberger, M., Zhang, B., Lotko, W., & Lyon, J. (2016b). Influence of ion outflow in coupled geospace simulations: 2. Sawtooth oscillations driven by physics-based ion outflow. *Journal of Geophysical Research: Space Physics*, *121*, 9688–9700. https://doi.org/10.1002/2016ja022778

Vasyliunas, V. M. (1975). Theoretical models of magnetic field line merging. *Reviews of Geophysics*, *13*(1), 303–336. https://doi.org/10.1029/rg013i001p00303

Vasyliunas, V. M. (1983). Plasma distribution and flow. In A. J. Dessler (Ed.), *Physics of the Jovian magnetosphere* (pp. 395–453). Cambridge University Press. https://doi.org/10.1017/cbo9780511564574.013

Vernisse, Y., Lavraud, B., Faganello, M., Fadanelli, S., Sisti, M., Califano, F., et al. (2020). Latitudinal dependence of the Kelvin-Helmholtz instability and beta dependence of vortex-induced high-guide field magnetic reconnection. *Journal of Geophysical Research: Space Physics*, *125*(5), e2019JA027333. https://doi.org/10.1029/2019ja027333

Vines, S. K., Fuselier, S. A., Trattner, K. J., Burch, J. L., Allen, R. C., Petrinec, S. M., et al. (2017). Magnetospheric ion evolution across the low-latitude boundary layer separatrix. *Journal of Geophysical Research: Space Physics*, *122*(10), 10–247. https://doi.org/10.1002/2017ja024061

Walsh, B. M., Phan, T. D., Sibeck, D. G., & Souza, V. M. (2014). The plasmaspheric plume and magnetopause reconnection. *Geophysical Research Letters*, *41*(2), 223–228. https://doi.org/10.1002/2013gl058802

Walsh, B. M., Sibeck, D. G., Nishimura, Y., & Angelopoulos, V. (2013). Statistical analysis of the plasmaspheric plume at the magnetopause. *Journal of Geophysical Research: Space Physics*, *118*(8), 4844–4851. https://doi.org/10.1002/jgra.50458

Wang, S., Kistler, L. M., Mouikis, C. G., Liu, Y., & Genestreti, K. J. (2014). Hot magnetospheric O+ and cold ion behavior in magnetopause reconnection: Cluster observations. *Journal of Geophysical Research: Space Physics*, *119*(12), 9601–9623. https://doi.org/10.1002/2014ja020402

Wang, S., Kistler, L. M., Mouikis, C. G., & Petrinec, S. M. (2015). Dependence of the dayside magnetopause reconnection rate on local conditions. *Journal of Geophysical Research: Space Physics*, *120*(8), 6386–6408. https://doi.org/10.1002/2015ja021524

Welling, D. T., André, M., Dandouras, I., Delcourt, D., Fazakerley, A., Fontaine, D., et al. (2015). The Earth: Plasma sources, losses, and transport processes. *Space Science Reviews*, *192*(1–4), 145–208. https://doi.org/10.1007/s11214-015-0187-2

Welling, D. T., Barakat, A. R., Eccles, J. V., Schunk, R. W. & Chappell, C. R. (2016). Coupling the generalized polar wind model to global magnetohydrodynamics: Initial results. *AGU Monograph Series*. https://doi.org/10.1002/9781119066880.ch14

Welling, D. T., Jordanova, V. K., Zaharia, S. G., Glocer, A., & Toth, G. (2011). The effects of dynamic ionospheric outflow on the ring current. *Journal of Geophysical Research*, *116*(A2). https://doi.org/10.1029/2010ja015642

Welling, D. T., & Liemohn, M. W. (2014). Outflow in global magnetohydrodynamics as a function of a passive inner boundary source. *Journal of Geophysical Research: Space Physics*, *119*(4), 2691–2705. https://doi.org/10.1002/2013ja019374

Welling, D. T., & Zaharia, S. G. (2012). Ionospheric outflow and cross polar cap potential: What is the role of magnetospheric inflation? *Geophysical Research Letters*, *39*(23). https://doi.org/10.1029/2012gl054228

Westerberg, L.-G. (2019). Earth atmospheric loss through the plasma mantle and its dependence on solar wind parameters. *Earth Planets and Space*, *71*(1). https://doi.org/10.1186/s40623-019-1048-0

Whipple, E. C. (1981). Potentials of surfaces in space. *Reports on Progress in Physics*, *44*, 1197–1250. https://doi.org/10.1088/0034-4885/44/11/002

Wiltberger, M., Lotko, W., Lyon, J. G., Damiano, P., & Merkin, V. (2010). Influence of cusp O+ outflow on magnetotail dynamics in a multifluid MHD model of the magnetosphere. *Journal of Geophysical Research*, *115*(A10). https://doi.org/10.1029/2010ja015579

Winglee, R. M. (1998). Multi-fluid simulations of the magnetosphere: The identification of the geopause and its variation with IMF. *Geophysical Research Letters*, *25*(24), 4441–4444. https://doi.org/10.1029/1998gl900217

Winglee, R. M., Chua, D., Brittnacher, M., Parks, G. K., & Lu, G. (2002). Global impact of ionospheric outflows on the dynamics of the magnetosphere and cross-polar cap potential. *Journal of Geophysical Research*, *107*. https://doi.org/10.1029/2001ja000214

Winglee, R. M., & Harnett, E. (2011). Influence of heavy ionospheric ions on substorm onset. *Journal of Geophysical Research*, *116*. https://doi.org/10.1029/2011ja016447

Wygant, J. R., Cattell, C. A., Lysak, R., Song, Y., Dombeck, J., McFadden, J., et al. (2005). Cluster observations of an intense normal component of the electric field at a thin reconnecting current sheet in the tail and its role in the shock-like acceleration of the ion fluid into the separatrix region. *Journal of Geophysical Research*, *110*(A9). https://doi.org/10.1029/2004ja010708

Xu, Y., Fu, H. S., Norgren, C., Toledo-Redondo, S., Liu, C. M., & Dong, X. C. (2019). Ionospheric cold ions detected by MMS behind dipolarization fronts. *Geophysical Research Letters*, *46*(14), 7883–7892. https://doi.org/10.1029/2019gl083885

Yamada, M., Kulsrud, R., & Ji, H. (2010). Magnetic reconnection. *Reviews of Modern Physics*, *82*(1), 603–664. https://doi.org/10.1103/RevModPhys.82.603

Yamauchi, M. (2019). Terrestrial ion escape and relevant circulation in space. *Annales Geophysicae*, *37*, 1197–1222.

Yau, A. W., Abe, T., André, M., Howart, A. D., & Peterson, W. K. (2020). Ionospheric ion acceleration and transport. In *Space physics and aeronomy collection volume 2: Magnetospheres in the solar system, geophysical monograph*. John Wiley & Sons. https://doi.org/10.1002/9781119507512

Yau, A. W., Abe, T., & Peterson, W. K. (2007). The polar wind: Recent observations. *Journal of Atmospheric and Solar-Terrestrial Physics*, *69*, 1936–1983. https://doi.org/10.1016/j.jastp.2007.08.010

Yau, A. W., & André, M. (1997). Sources of ion outflow in the high latitude ionosphere. *Space Science Reviews*, *80*, 1–25. https://doi.org/10.1023/A:1004947203046



19449208, 2021, 3, Downloaded from https://agupubs.onlinelibrary.wiley.com/doi/10.1029/2020RG000707 by Cochrane France, Wiley Online Library on [07/11/2022]. See the Terms and Conditions (https://onlinelibrary.wiley.com/terms-and-conditions) on Wiley Online Library for rules of use; OA articles are governed by the applicable Creative Commons License

Yau, A. W., Peterson, W. K., & Abe, T. (2017). Measurements of ion outflows from the Earth's ionosphere. In *Magnetosphere-ionosphere coupling in the solar system, geophysical monograph 222* (1st ed.). John Wiley & Sons, Inc.

Yau, A. W., Whalen, B. A., Goodenough, C., Sagawa, E., & Mukai, T. (1993). EXOS D (Akebono) observations of molecular $NO^+$ and $N^{2+}$ upflowing ions in the high-altitude auroral ionosphere. *Journal of Geophysical Research*, *98*(A7), 11205–11224. https://doi.org/10.1029/92ja02019

Young, D. T., Balsiger, H., & Geiss, J. (1982). Correlations of magnetospheric ion composition with geomagnetic and solar activity. *Journal of Geophysical Research*, *87*(A11), 9077–9096. https://doi.org/10.1029/ja087ia11p09077

Young, D. T., Burch, J. L., Gomez, R. G., De Los Santos, A., Miller, G. P., Wilson, P., & Pollock, C. J. (2016). Hot plasma composition analyzer for the magnetospheric multiscale mission. *Space Science Reviews*, *199*(1–4), 407–470. https://doi.org/10.1007/s11214-014-0119-6

Zhang, B., Brambles, O. J., Cassak, P. A., Ouellette, J. E., Wiltberger, M., Lotko, W., & Lyon, J. G. (2017). Transition from global to local control of dayside reconnection from ionospheric-sourced mass loading. *Journal of Geophysical Research: Space Physics*, *122*(9), 9474–9488. https://doi.org/10.1002/2016ja023646

Zhang, B., Brambles, O. J., Lotko, W., & Lyon, J. G. (2020). Is nightside outflow required to induce magnetospheric sawtooth oscillations. *Geophysical Research Letters*, *47*, e2019GL086419. https://doi.org/10.1029/2019GL086419

Zhang, B., Brambles, O. J., Wiltberger, M., Lotko, W., Ouellette, J. E., & Lyon, J. G. (2016). How does mass loading impact local versus global control on dayside reconnection? *Geophysical Research Letters*, *43*(5), 1837–1844. https://doi.org/10.1002/2016gl068005

Zheng, Y., Moore, T. E., Mozer, F. S., Russell, C. T., & Strangeway, R. J. (2005). Polar study of ionospheric ion outflow versus energy input. *Journal of Geophysical Research*, *110*(A7). https://doi.org/10.1029/2004ja010995



19449208, 2021, 3, Downloaded from https://agupubs.onlinelibrary.wiley.com/doi/10.1029/2020RG000707 by Cochrane France, Wiley Online Library on [07/11/2022]. See the Terms and Conditions (https://onlinelibrary.wiley.com/terms-and-conditions) on Wiley Online Library for rules of use; OA articles are governed by the applicable Creative Commons License